1991

High resolution fluorescence studies of metabolic pathways of DNA and oligonucleotide adducts from polycyclic aromatic compounds

Hyuk Jeong
Iowa State University

Order Number 9207247

High resolution fluorescence studies of metabolic pathways of DNA and oligonucleotide adducts from polycyclic aromatic compounds

Jeong, Hyuk, Ph.D.

Iowa State University, 1991

U·M·I
300 N. Zeeb Rd.
Ann Arbor, MI 48106

High resolution fluorescence studies of metabolic pathways of DNA and oligonucleotide adducts from polycyclic aromatic compounds

by

Hyuk Jeong

A Dissertation Submitted to the
Graduate Faculty in Partial Fulfillment of the
Requirements for the Degree of
DOCTOR OF PHILOSOPHY

Department: Chemistry
Major: Analytical Chemistry

Approved:

Signature was redacted for privacy.
In Charge of Major Work

Signature was redacted for privacy.
For the Major Department

Signature was redacted for privacy.
For the Graduate College

Iowa State University
Ames, Iowa
1991

TABLE OF CONTENTS

		Page
I.	INTRODUCTION	1
	A. Cancer and Carcinogens	1
	B. Metabolic Pathways	7
	1. Monooxygenation mechanism and metabolites	9
	2. One-electron oxidation and metabolites	11
	C. Analytical Methods	13
II.	THEORETICAL BACKGROUND OF HIGH RESOLUTION SPECTROSCOPY	19
	A. Optical Line Shape in Solid State Spectroscopy	19
	B. Principles of Fluorescence Line Narrowing	22
	C. Principles of Spectral Hole Burning	31
III.	EXPERIMENTAL	37
	A. Materials and Reagents	37
	B. Instrumentation	38
IV.	RESULTS AND DISCUSSION	46
	A. Spectral Library	46
	1. Model compounds from B[a]P	47
	2. Model compounds from BPDE	62
	3. FLN spectra of isomeric BPTs	68
	4. Model compounds from 7,12-DMBA	73
	B. Identification of BP-6-N7Gua in the Urine and Feces of Rat Treated with B[a]P	83

C. Identification of B[a]P-DNA Adduct Formed by Rat Liver Microsomes *in vitro* 86

D. Identification of Depurinated Adducts from Mouse Skin DNA 102

E. Identification of 7,12-DMBA-DNA Adducts Formed by Rat Liver Microsomes *in vitro* 105

F. Interaction Between BPT and DNA in Solid Water and Glass Host 113

G. Spatial Conformations of the Stereoisomeric Oligonucleotide Adducts from (±)-*anti*-BPDE 123

1. General remarks of adduct conformations 126
2. Adducts from (+)-*trans*-BPDE 136
3. Adducts from (+)-*cis*-BPDE 143
4. Adducts from (-)-*trans*-BPDE 150
5. Adducts from (-)-*cis*-BPDE 153

V. CONCLUSIONS 156

VI. LITERATURE CITED 159

VII. ACKNOWLEDGEMENTS 174

I. INTRODUCTION

A. Cancer and Carcinogens

Cancer, produced by exposure to UV radiation, viruses, or chemicals has been known for at least 200 years and it has probably existed as long as human history [1]. Under normal conditions, cells of multicellular animals control their proliferation rate through all productive approaches and growth control mechanisms. In the mature body some cell types divide rarely or never at all, while others, like skin and circulating blood cells, must divide throughout life in order to replace the billions of cells that die every day. Clearly a very carefully controlled program must determine the growth of every type of cell in the body, since a few extra-doublings or insufficient divisions would cause chaos. Tumors arise when a cell loses its sense of these controls [2-4]. In other words, tumor-cells have greater potential to yield unlimited growth which is avoided by typical block points which regulate the initiation of the cellular growth in a normal cell.

When a cell divides, the two progeny cells are usually morphologically identical to the parental cell. The factors which endow a cancer cell with the distinct property of unrestricted growth are thus regularly passed on from parent to progeny cells. The heritability of the changes allowing unrestricted growth suggests that genetic changes within chromosomal DNA may underlie the cancerous phenotype. The evidences that genetic damage might be responsible for cancer growth are diverse: the recognition of hereditary predispositions to cancer [5-7], the detection of damaged chromosomes in cancer cells [8-10], the apparent connection between susceptibility to cancer and impaired

ability of cells to repair damaged DNA [11,12], and evidence that relates the mutagenic potential of substances to their carcinogenicity [13]. Now all these findings have been connected by the discovery of cellular genes (proto-oncogenes) and its damaged forms (oncogenes) that can cause neoplastic growth. Transformation is the process by which normal cells acquire many of the morphological as well as growth properties of cancer cells. A certain group of agents have been implicated in this unlimited DNA replication, and are known as carcinogens which include electromagnetic radiation, viruses, and organic and inorganic compounds.

Viruses can cause cancers in susceptible animals [14,15]. The cancer producing potential of RNA and DNA tumor viruses comes from a single cancer-inducing gene, an oncogene. All known oncogenes are altered forms of normal cellular genes (proto-oncogene) which can be transformed to oncogenes. Rous sarcoma virus (RSV), for example, develops highly malignant tumors in chickens. The most striking change is that transformed cells grow continuously and chaotically, without regard for their neighbors. Furthermore, transformed cells contains viral-specific DNA that is integrated into the host genome, which accounts for the fact that transformation is a heritable alteration. The abnormal characteristics of transformed cells are perpetuated in cultures derived from transformed colonies. In addition, some transformed cells from tissue culture grow into a cancer when they are injected in sufficient number into an appropriate host.

The viruses that can cause cancer and also transform cells in culture include several groups with DNA genome-papoviruses, adenoviruses, and herpesviruses as well as

the RNA containing retroviruses. In general, the oncogenes of DNA viruses are virus-coded gene products that are also required for the normal replication of the virus. In contrast, most of the retrovirus oncogenes that have been studied are not required for replication. Rather they are cellular genes which were transduced by chance onto the viral genome. Although the first known tumor virus (RSV) was found as early as 1911, examples of additional viruses which could induce tumors in animals appeared so infrequently that it is generally believed that viruses cannot be a major cause of cancer. So far, about 30 different tumor viruses have been identified and their cancer-inducing mechanisms studied.

Ultraviolet and X-ray light have long beeHxknown to be highly cancer-causing and mutagenic agents [16]. For example, exposure of skin to UV light can induce skin cancer, while X-ray exposure to the thyroid induces thyroid cancer. Electromagnetic radiation, however, may not be assumed to cause all the cells in an exposed population to become cancerous since radiation can also produce many other deleterious changes leading to cell death. A radiation dose sufficient to induce cancer in all cells will virtually kill every cell. Not only can radiation induce simple mutation, it can also produce chromosome fragmentation, resulting in large deletions of genetic material. Thus radiation causes a variety of genetic changes, many of which might contribute to the cancerous state. A well known deleterious effect, xeroderma pigmentosum, is magnified in certain individuals. These people are homozygous for a recessive mutation that inactivates a gene involved in repairing thymine dimers, the major damage caused by UV

radiation, and so such individuals develop multiple skin cancers. Presumably sufferers of xeroderma pigmentosum are unable to repair somatic mutations, some of which cause a cell to develop cancer. The increased incidence of skin cancers in people with xeroderma pigmentosum provides further support for the mutational origin of cancer.

Various classes of organic and inorganic compounds (known as chemical carcinogens) have long been known to be potential carcinogens. Among the most potent chemical carcinogens are the polycyclic aromatic hydrocarbons (PAHs) which are mutagenic as well. PAHs are found in various petroleum and combustion products derived from heat and power generation and motor vehicle exhausts [17]. Since PAHs are produced in large quantity from the pyrolysis of daily organic compounds, our bodies are continuously exposed to chemical carcinogens from the environment [18,19]. However, the first investigation for the tumorigenic property of PAH occured about 200 years ago, with the report that scrotal cancer in chimney sweepers originating from their occupational exposure to soot [20-21]. Later [22], the compound responsible for the scrotal cancer was identified as benzo[a]pyrene (B[a]P) which is now known as one of the most potent carcinogens. Subsequently, the mutagenic and tumorigenic properties of PAH have been the subjects of numerous investigation and have been the subject of several reviews [23-25].

PAH can induce diverse tumors, including mammary carcinoma, leukemia, sarcoma, etc. [26]. Chemical carcinogenesis is generally believed to be a multi-steps process emanating from a single somatic cell. The concepts of tumor initiation,

promotion, conversion, and progression have been developed from studies in experimental carcinogenesis. Recent data strongly indicate that the initial event in cancer production is adduct formation between cellular DNA and carcinogens [23-25,27,28]. PAHs are, however, chemically inert compounds toward DNA. Therefore, metabolic activation of PAHs to reactive electrophiles is a necessary initial step for chemical carcinogenesis. Certain chemical carcinogens have been widely investigated due to their high genotoxicity and/or abundance. These include B[a]P and 7,12-dimethylbenz[a]anthracene (DMBA). These two molecules are the compounds of primary focus in this dissertation.

A schematic representation of the principal events in chemical carcinogenesis is shown in Figure 1. PAHs (carcinogens) are not reactive towards biological macromolecules such as DNA, RNA, and/or globin, and must be enzymatically activated to reactive electrophiles (ultimate carcinogens) which can covalently bind to macromolecules. Most of the metabolized hydrocarbons are detoxified by forming hydrophilic compounds, but a small portion of the metabolized carcinogens are converted to ultimate carcinogens which become adducted to DNA. Although globin adducts are not considered to be pathobiological lesions, they provide useful complementary data to DNA adduct levels, serving as dosimeters for carcinogen exposure [29,30]. The characterization and determination of labile adducts which undergo elimination (into urine and/or feces) is also very important, since it can not be assumed the "nick" produced in DNA by depurination of the adduct is less effective than a stable DNA adduct in initiation of carcinogenesis. Under the assumption that DNA-carcinogen adducts lead to

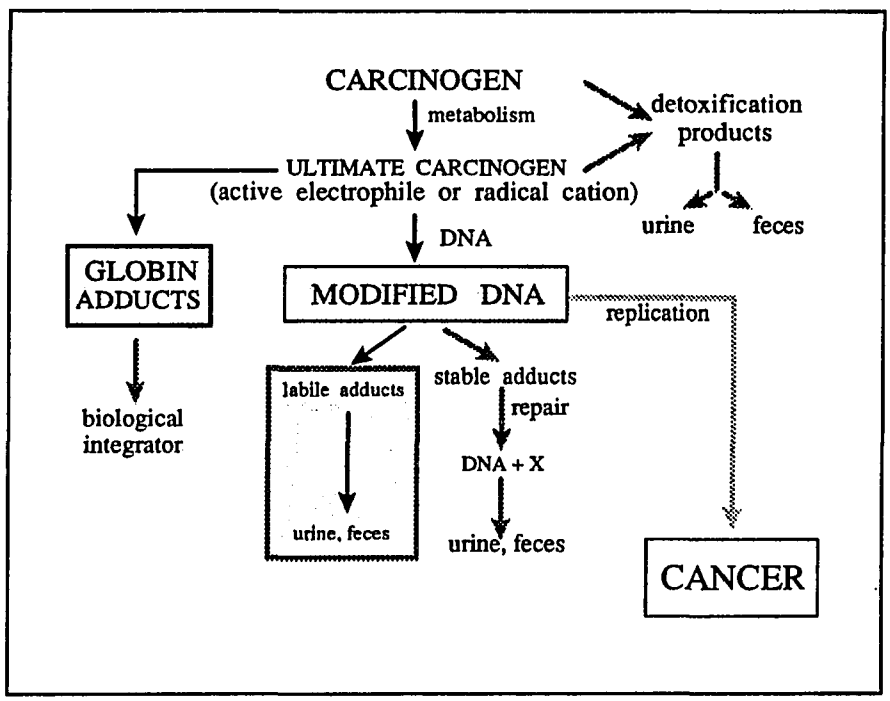

Figure 1. Schematic representation of the principal events in chemical carcinogenesis

genetic lesions, including mutations, adduct formation is deserving of intense study. The current view of metabolic activation in the initiation process is that there are two major pathways: monooxygenation to yield diol epoxides [23-25,27,28,31-33] and one-electron oxidation to produce radical cations [34-36]. The nature of these pathways will be discussed in more detail in the next section.

B. Metabolic Pathways

Covalent binding of PAH to target cell DNA is thought to be the first event in the tumor-initiating process. The physico-chemical properties of PAH and the catalytic properties of cytochrome P-450 suggest that PAH are generally activated by two major mechanisms, monooxygenation to yield bay-region diol epoxides [23-25,27,28,31-33] and one-electron-oxidation to yield radical cations [34-36]. Some PAHs are believed to be metabolized by the diol epoxide pathway alone, others by one-electron oxidation alone, and some by a combination of both pathways. This overall view of PAH activation is based on several different types of results, including tumorigenicity data and the structure of PAH-DNA adducts. Schematic representations of B[a]P and DMBA adduct formation with DNA by two important pathways are given in Figure 2. B[a]P is enzymatically activated to the ultimate carcinogens, the diol epoxide and radical cation, which lead to several adducts, only two of which are shown.

The discovery that carcinogenic activityHxs a property of specific PAH stimulated extensive investigations to determine the molecular structural requirements for maximum biological activity. At the beginning, it was believed that the K-region (typified by the

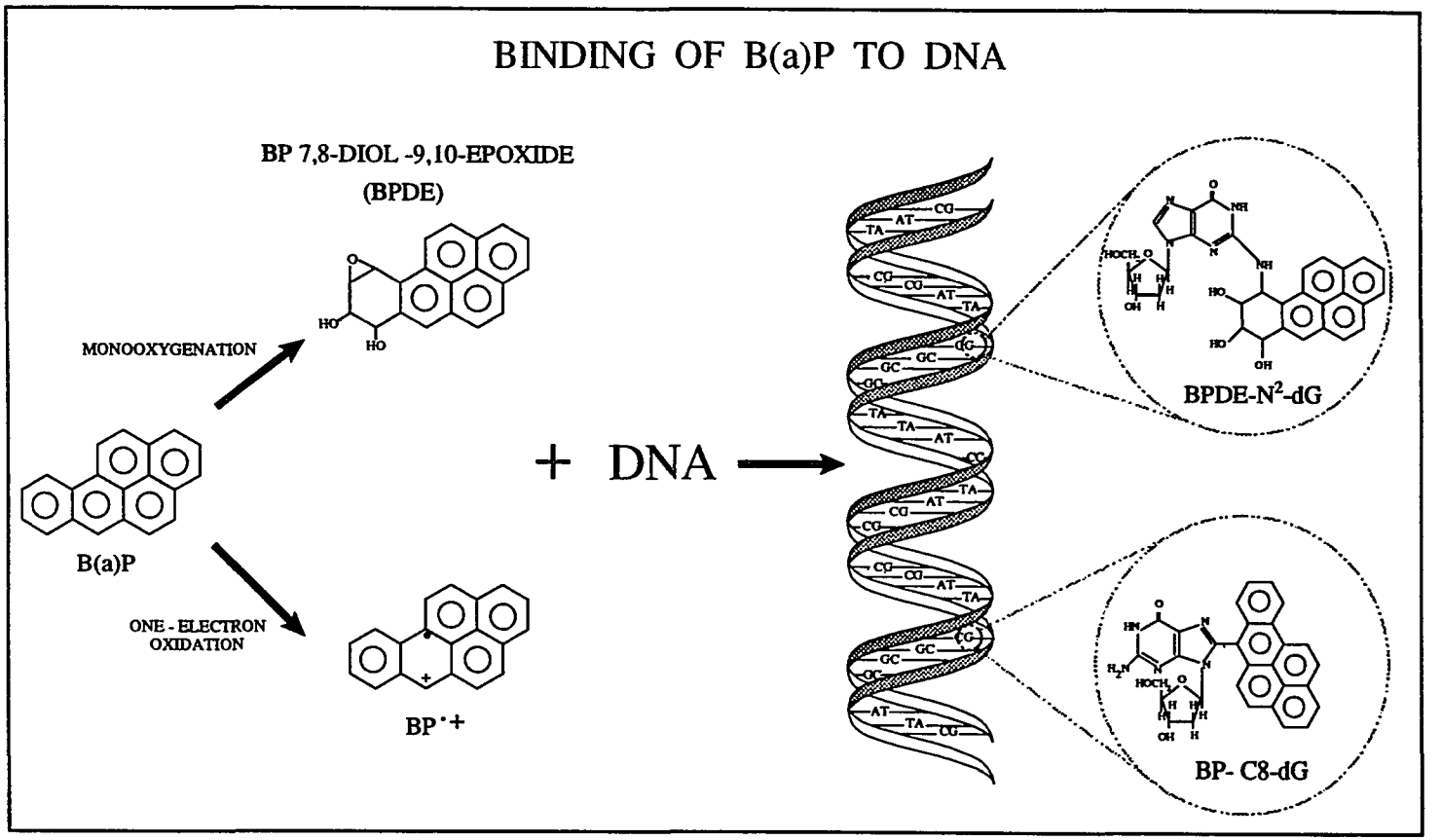

Figure 2. Schematic representation of B[a]P adducts formation with DNA by monooxygenation and one-electron oxidation

5,6-bond of DMBA) and methyl group(s) in the L-region as well as 4-6 fused rings were required for the maximum activity [37]. The new era of PAH carcinogenesis started in 1974 with a proposal by Peter Sims that the active metabolite of B[a]P was bay-region (sterically hindered region between C-10 and C-11 of B[a]P, see Figure 3) diol epoxide formed by microsomal oxidation [38].

1. Monooxygenation mechanism and metabolites

As with other PAHs, B[a]P undergoes metabolic activations. A schematic of the monooxygenation mechanism and the possible four structural isomers of the 7,8-dihydroxy-9,10-epoxy-7,8,9,10-tetrahydrobenzo[a]pyrene (BPDE) is shown in Figure 3. Upon introduction to certain cells, B[a]P is readily oxidized to a 7,8-oxide [39] by a microsomal system which includes cytochrome p-450 and epoxide hydrolase. The resulting racemic arene oxides are then transformed to corresponding (±)-*trans*-7,8-dihydrodiols [40,41] which might be transformed further to various metabolites. B[a]P 7,8-dihydrodiol is further metabolized by rat liver microsomes to a reactive metabolite, 7.8-diol 9,10-epoxide (BPDE), which is known to bind to DNA [38,42]. Among the four different isomeric BPDEs, (+)-anti-BPDE is believed to be the predominant isomer produced metabolically (90%), but minor amounts of (-)-*anti*-BPDE and (±)-*syn*-BPDE are also formed [31]. While all four BPDE isomers are reactive towards DNA, (+)-*anti*-BPDE has strong tendency to react with 2-NH_2 of guanosine base in DNA, yielding ~90% N2-dG adducts [43] along with lesser amounts of N6-dA, O6-dG, and N7-dG adducts (see Figure 13 for numbering). The (-)-*anti*-BPDE is less regiospecific, yielding

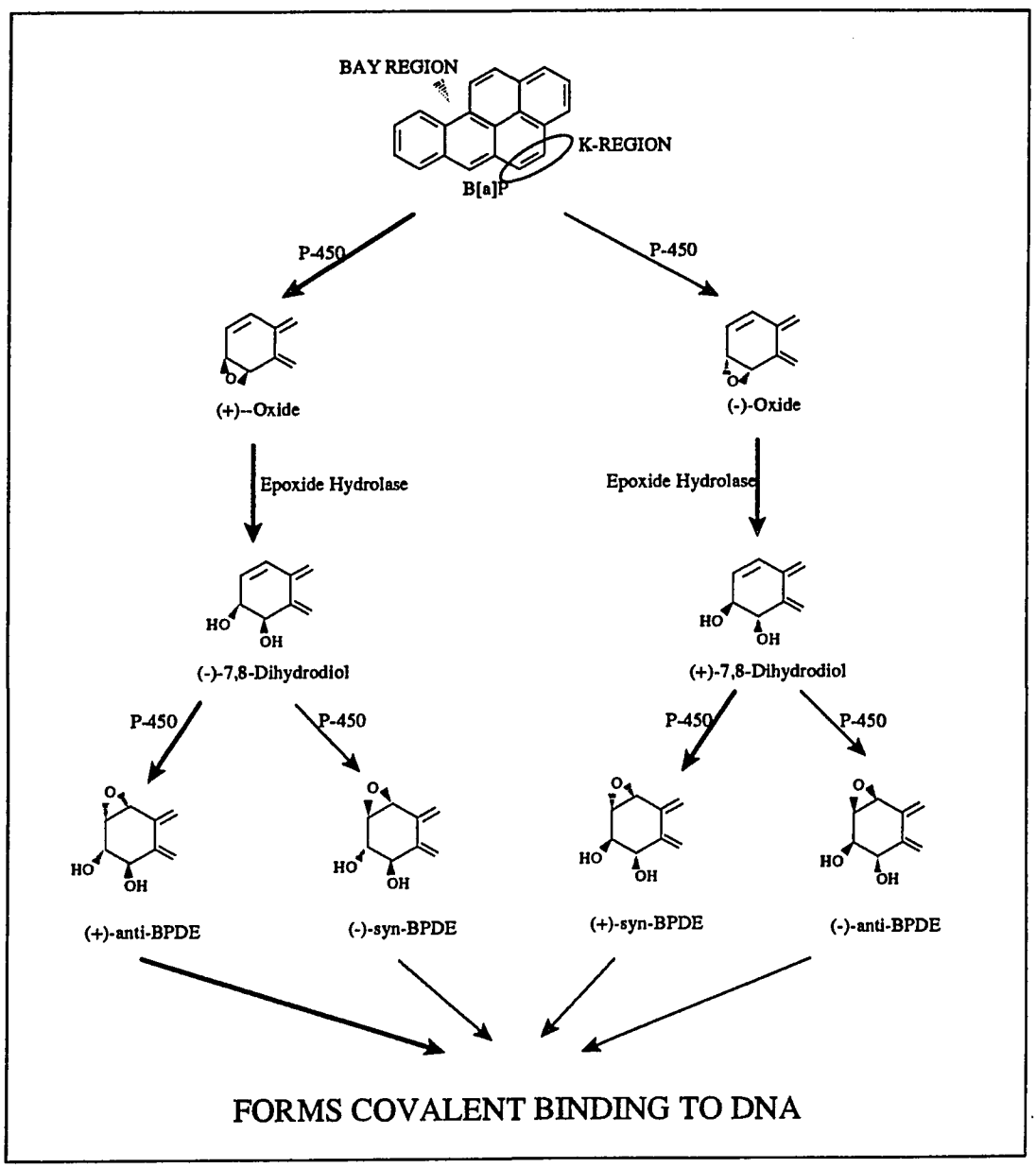

Figure 3. Step mechanism of monooxygenation of B[a]P and the structures of isomeric BPDEs

only 50 % of the N2-dG product along with substantial amounts of other adducts. The major adduct which accounts for about 80~85 % of the alkylated product , was shown to be a guanosine derivative covalently linked between the 2-NH_2 group and the 10-position of the principal reactive metabolite of B[a]P, (+)-*anti*-BPDE. In *vitro* studies with rat liver microsomes have shown that B[a]P is metabolized to 4,5- and 9,10-dihydrodiols as well as 7,8-dihydrodiol, to 1-, 3-, 7-, and 9-hydroxy-B[a]P, and to 1,6-, 3,6-, and 3,12-quinones [44-48]. Many of these metabolites are also formed by other mammalian and nonmammalian tissues and organs, including rat lung [49,50], rat intestinal microsomes [51], rat liver nuclei [52-54], hamster embryo cell [55]. Analogous diol epoxide metabolites have been implicated subsequently as the active forms of other PAHs: 7-methylbenz[a]anthracene, DMBA [56-58], 9-fluoro- and 10-fluoro-DMBA [56], 5-methyl-crysene [59], dibenz[ah]pyrene, dibenzo[ai]pyrene, and dibenzo[ae]fluoranthene [60]. The major active isomer has been identified in all cases as the bay region *anti*-diol epoxide. Similar studies have shown that relatively weak carcinogens are also metabolized by monooxgenation mechanism. In most cases, however, the evidence is much less complete than in the case of B[a]P and rests primarily on comparison of the relative mutagenicities and tumorigenicities of the isomeric dihydrodiols or the corresponding diol epoxides obtained through synthesis.

2. One-electron oxidation and metabolites

The monooxygenation mechanism, which emphasizes the important role of the bay-region diol epoxide, has been widely accepted during last 15 years. There are,

however, observations which cannot be explained by the bay-region diol epoxide mechanism [61-64]. Among fluorinated derivatives, which block the formation of the bay-region diol epoxide, only 9-fluoroB[a]P was inactive in both mouse skin and rat mammary gland targets. B[a]P 7,8-dihydrodiol, which is the precursor of B[a]P diol epoxide, showed only similar activity to the parent compound in mouse skin but was much less active than B[a]P in rat mammary gland. 1,2,3,4-Tetrahydro-7,12-dimethylbenz[a]anthracene, in which formation of the bay-region diol epoxide is impossible, due to saturation of the angular benzo ring, was extremely active as a mammary carcinogen and relatively potent in mouse skin. The results from these experiments in mouse skin and rat mammary gland support the proposal that multiple mechanisms of activation are involved in initiation of chemical carcinogenesis.

The one-electron oxidation mechanism provides an explanation of the above observations. This mechanism is one that produces radical cations by removal of a π-electron. Radical cations of unsubstituted and methyl substituted PAHs have been successfully generated by iodine [65,66] and manganic acetate [67,68] oxidations with subsequent trapping by a nucleophiles. In biological systems, mammalian peroxidases, including prostaglandin H synthase (PHS) [69-72], horseradish peroxidase [69,70,72,73], and cytochrome P-450 [73-76] catalyze one-electron oxidation.

However, only PAHs with certain characteristic features can be activated by this mechanism. Firstly, a relatively low ionization potential (IP, below ~7.35 eV) is required, which allows metabolic removal of one electron with formation of a relatively

stable radical cation [77-78]. Secondly, charge localization in the produced PAH radical cation is critical to render this intermediate specifically and efficiently reactive toward nucleophiles [36,65-68]. Finally, an optimal spatial configuration is required to facilitate formation of appropriate physical complexes with macromolecules [79]. All those characteristics are common in the most potent PAH including B[a]P, DMBA, and 3-methylcholanthrene (MC).

A schematic one-electron oxidation mechanism for DMBA is outlined in Figure 4. Removal of one electron from the π-system generates a radical cation in which the positive charge can be localized mainly at C12 atom (upper path) or C7 atom (lower). In both cases, radical cations lose a proton and an electron to yield benzylic carbenium ions. Both rapidly attack nucleophilic site(s) of bases in DNA to form permanent covalent bonds with C8 or N7 guanine, or N7 of adenine [80]. N7 adducts of guanine and adenine are unstable so that they are lost by depurination from DNA. However, the C8 adduct is relatively stable (see Figure 15 for numbering). A similar study of BP-DNA adducts shows that the major depurinated adduct contains BP bound at C6 to the N7 of adenine [81]. BP- and DMBA-DNA adducts formed by the one-electron oxidation mechanism have been studied or are currently being characterized [34,80,81].

C. Analytical Methods

Although the carcinogenic properties of PAHs have been known for over a hundred years, the absence of adequate analytical technique prevented extensive studies of chemical carcinogenesis until about 15 years ago. Accordingly, except for B[a]P

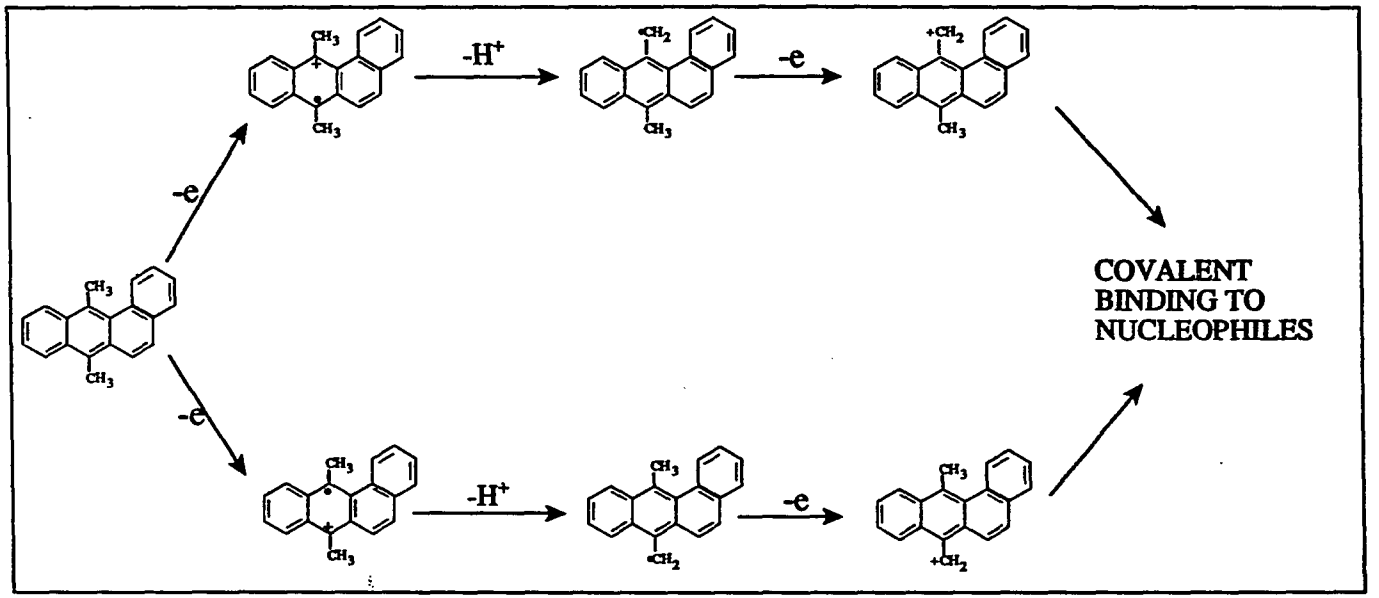

Figure 4. Activation of 7,12-dimethylbenz[a]anthracene by one-electron oxidation

adducts, only limited data related to DNA adduct structures are available. The level of *in vivo* DNA modification from exposure to chemical carcinogens is very low, in the range of one adduct per 10^8 to 10^{10} bases in the DNA helix. As discussed earlier, a metabolite, BPDE for example, can also generate a wide variety of adducts with cellular macromolecules including DNA, RNA, and globin. Consequently, bioanalytical methods used to detect and characterize cellular macromolecular damages must have high sensitivity and a selectivity sufficient to distinguish between structurally similar adducts. Since most of the biological techniques [82-86] and spectroscopic techniques [82-85,87] used for the study of chemical carcinogenesis have been reviewed, only those that are not discussed will be discussed in this dissertation.

High sensitivity to the cellular macromolecular damages can be achieved indirectly by employing some methods in which the effect of damage is amplified to a certain measurable level. An example of indirect tool is the Ames assay [88-90]. With this method, a thin layer of agar containing about 10^9 bacteria, Salmonella, which are unable to grow without histidine due to mutation, is placed in a petri dish. The addition of PAHs produce revertant which can produce histidine by reverse mutation induced by PAHs. These revertant multiply in the absence of exogenous histidine and appear as discrete colonies after the plate is incubated at 37°C for two days. Mutational events occurring even with very low frequencies can be detected with this method, since a large number of bacteria can be exposed to the active metabolites of PAHs. This type of assay, while sensitive, rapid, and relatively simple to perform, has serious limitation to

expand to human cancer research because of the lack of simple quantitative relationship between carcinogenesis and mutagenesis [91]. Although it is possible to obtain simple correlation for certain experimental system, human are normally exposed to a complex mixture of chemicals in which synergistic and antagonistic effect should be taken into account.

Bioanalytical methods with direct detection including radioactive labeling [82], enzyme-linked immunosorbent assay (ELISA) [92-95], ^{32}P post-labeling [92,96-98], have been widely utilized in chemical carcinogenesis. Electrophoresis is, however, worth to be noticed, because it is relatively new technique. A molecule with a net charge will move in an electric field. This phenomenon, termed electrophoresis, offers powerful means of separation of biological macromolecules, such as DNA, RNA, and proteins as well as small molecules. Qualitatively, the migration velocity (v) of molecules in electric field is proportional is proportional to the net charge on the analytes (z) and electric field strength (E), and inversely proportional to the frictional coefficient (f) [99,100]. The frictional coefficient depends on the mass and shape of the migrating molecule and the viscosity of the medium. Samples of PAH adducts are injected to the previously generated polyacrylamide gel [83] and then electrophoresced under the electric field. Generally, small molecules move rapidly through the gel, whereas large ones stay at the top of the thin vertical slab, near the point of injection of the mixture. The mobility of most analytes under these conditions is linearly proportional to the logarithm of their mass [101]. Finally the adducts in the gel can be visualized by staining them with silver

or a dye solution, which reveals a series of bands. Radioactive labeled bands can be detected by placing a sheet of x-ray film over the gel (autoradiography). Polyacrylamide gel electrophoresis is sensitive, capable of a high degree of resolution, and relatively rapid. As little as femtomol range of adducts can be detected using radiolabeling technique. Electrphoresis can be utilized for the separation of a full spectrum of adducts. Electrophoresis of carcinogen-modified DNA oligomers showed that (+)-*anti*-BPDE forms more stable adducts than (-)-*anti*-BPDE [101]. Conformational heterogeneity of (±)-*anti*-BPDE is currently being performed by the separation of reaction mixtures from these metabolites with 10-bases double-stranded oligomers. Previous conclusion that adducts from (-)-*anti*-BPDE are more heterogeneous, is seemingly confirmed, although more studies are necessary to draw a firm conclusions [102].

Analytical spectroscopy utilized in chemical carcinogenesis have been extensively studied [82-85,87]. These include synchronous fluorescence spectroscopy [82,86,92,103-105] and low temperature laser-based high resolution spectroscopy such as matrix isolation [106-109], supersonic jet [107,109-111], and Shpol'skii [107,109,112]. A number of serious limitations are implicated in the techniques described above. The synchronous fluorescence spectroscopy, like normal broad fluorescence spectroscopy, is severely limited when attempts are made to analyze exposure to complex mixtures of PAHs, because this methods does not have selectivity enough to distinguish among those mixture due to the relatively broad excitation and emission spectra. In the laser excited Shpol'skii spectroscopy (LESS), the materials generally employed for the matrix,such as

nitrogen, hexane, or n-paraffins are quite unsuited to PAH-modified DNA samples because of the limited solubility. Samples are evaporated first to be mixed with matrix gas and then deposited on the cold trap in matrix isolation spectroscopy. Therefore thermally unstable molecules and molecules with low vapor pressure can not be employed in this technique.

A superior laser-based solid state spectroscopy, termed as fluorescence line narrowing spectroscopy (FLNS), employs glass forming mixture in which DNA samples can be embedded. In such glasses, only isochromat resonating with laser frequency may be excited and subsequent fluorescence is composed of very narrow lines which offer excellent distinction between structurally similar adducts. It is the intent of this dissertation to show that FLNS is rapid, broadly applicable, sensitive, and selective technique for the study of chemical carcinogenesis. Nevertheless, even though excellent resolution can be obtained from FLNS, this technique needs standard spectrum with which "finger print" modes matching can be compared. Thus, a serious of standards of DNA-adducts are prepared and identified with mass spectrometry and NMR throughout the studies explained in this dissertation.

II. THEORETICAL BACKGROUND OF HIGH RESOLUTION SPECTROSCOPY

A. Optical Line Shape in Solid State Spectroscopy

A solid state optical spectrum is determined by properties of both guest (sample) and host matrix. The excited states of host matrix are usually band shape and dispersed (delocalized) over many molecules [113,114], where the excited states of the guest molecules are localized in much lower energy level and referred to as matrix isolated since they are decoupled from the host matrix.

If an optical spectrum is generated from molecules doped in a more or less ideal crystal lattice (Shpol'skii), or by monochromatic laser excitation (FLNS), *inhomogeneous* broadening in the spectrum of the solid state sample is dramatically removed. The resulting appearance of the spectrum is determined by two factors, the vibronic structure of the molecule and the interaction between the electron of the molecule and the lattice vibronic modes (phonons). In the spectrum, the vibronic structures of the molecule are manifested as vibrational progression in addition to the pure electronic transition, whereas electron-phonon coupling are shown as rather broad phonon side band (PSB) adjacent to sharp zero-phonon line (ZPL) [115].

For the discussion of the coupling between electron and lattice vibrational modes (phonons), it is worth to note that similar principles used for intermolecular vibronic coupling are valid in electron-phonon coupling. Typical phonon energies lies in the range of 10 to 150 cm^{-1} and they have a continuum character. The theoretical background of electron-phonon coupling have been extensively reviewed in the literature

[115,116-119] which will be briefly reviewed in this section. In order to introduce quantitative description for electron-phonon coupling, the hypothetical transition between two electronic states with energies of E_0 and E_1 is shown in Figure 5. This transition accompany the equilibrium distance from change $\xi_i = 0$ to $\xi_i = \Delta\xi_i$ for the given phonon mode i. On each state on can build up phonon harmonic oscillators with energies of $\hbar\omega_i$. By similar reason explained in intramolecular vib transition, the electronic transitions precede so fast that the nuclear position will remain fixed (Franck-Condon principle). In other words, the electronic transition between two states can be depicted as straight lines as drawn. The corresponding energy change by added phonons is proportional to the force constant $K_i = m_i\omega_i^2$ of the harmonic oscillator with mass m_i and frequency ω_i, *i.e.*,

$$E_{ph,i} = \frac{1}{2}K_i(\Delta q_i)^2 = \frac{1}{2}m_i\omega_i^2(\Delta q_i)^2 \qquad \text{(B-1)}$$

where the subscripts *ph*, *i*, and *n* denote phonon, i^{th} phonon mode and number of phonon quanta involved in the transition. The energy $E_{ph,i}$ correspond to half the Stokes-shift between the two maxima of the PSB in the absorption or emission spectrum. Depending on the magnitude of $\Delta\xi_1$, one of the electron phonon transition will be predominant as two phonon transition in Figure 5. For the overall transition, however, one has to sum over many phonon modes (phonon mode = *i*, *j*, *k* · · ·). An important quantity is the Lorentzian zero-phonon line $z(\omega)$ with its integrated area α as well as the phonon side band $p(\omega)$ with its area $1-\alpha$, where α is referred to as Debye-Waller factor, and is

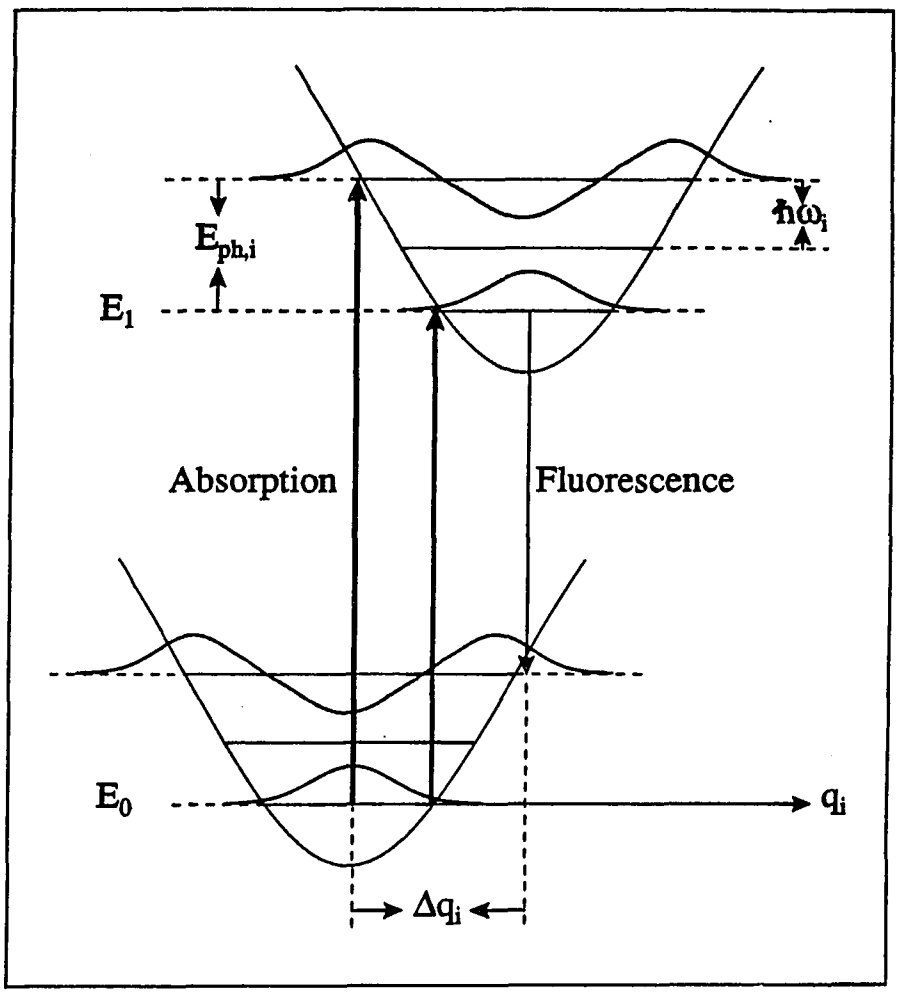

Figure 5. Energy diagram for interpreting the phonon sideband spectra in terms of configurational coordinates: q_i represents a normal mode of the lattice. The arrows correspond to zero-phonon and two-phonon transitions in absorption (thick solid arrows) and emission (solid arrow), respectively

extremely important quantity of the high resolution spectroscopy. The overlap integral between two harmonic oscillators has been derived by Keil [120]. As an extreme case where T → 0, Debye-Waller factor α is readily calculated [116] as follow

$$\alpha(T=0) = \exp(-\frac{1}{2}\sum_i \frac{m_i \omega_i}{\hbar}(\Delta q_i)^2) = \exp(-S) \qquad \text{(B-2)}$$

The physical interpretation of the symbolic S, which is called as Huang-Rhys parameter, is the strength of the electron-phonon coupling for a particular guest-host system, and is the number of vibronic (phonon) quanta excited in the maximum in single phonon mode. At very low temperature, but non-zero temperature, the temperature dependence of the ZPL intensity can be expressed as;

$$I_{ZPL} \sim \exp(-S)\exp[-8S(\frac{\kappa T}{h\nu_D})^2] \qquad \text{(B-3)}$$

where ν_D is th Debye Frequency for the matrix which is relevant to the distribution of the density of the phonon states. Consequently, at very low temperature, the ZPL intensity decreases approximately quadratically with increasing temperature. As a result, the spectral line will be broadened and the intensity of PSB will be increased.

B. Principles of Fluorescence Line Narrowing

It was discussed in previous section that the molecular spectra in condensed phase systems are suffered band broadening by several mechanisms. In addition to the band broadening due to relaxation phenomena, the electronic transitions in solid state are also changed by "solvent shift" [117] due to electronic and van der Waals' interaction, which

introduce further band broadening. However, all broadening mechanisms can be categorized as *homogeneous* or *inhomogeneous*. In the case of perfect crystalline lattice the solvent shift should be identical to all impurity molecules in the sample. Thus, their optical transition overlap each other at fixed position as shown in Figure 6A. The resulting line has Lorentzian shape and line (This line width is referred to as *homogeneous* line width, Γ_{hom}). If considering amorphous lattice such as glassy matrix, the microscopic environment of the solvent is random. As shown in Figure 6B, each guest molecule will occupy a variety of energetically inequivalent site in the matrix due to different local field environment. As a result, the electronic transition energies of the molecules will be shifted relative to each other, and distributed statistically under the Gaussian curve as shown in Figure 6B. The FWHM of the gaussian distribution is referred to as *inhomogeneous* line width and termed as Γ_{inh}. In low temperature, the contribution of the *homogeneous* broadening is typically less than 1 cm^{-1}. The *inhomogeneous* broadening due to heterogeneous solvent effects is 100 ~ 300 cm^{-1} in amorphous hosts, such as glasses and polymers. For crystalline hosts, Γ_{inh} is reduced by about 2 orders of magnitude.

Fluorescence line narrowing is a low temperature solid state technique that can eliminate or greatly reduce the contribution of site *inhomogeneous* line broadening (Γ_{inh}) to vibronic fluorescence bandwidths. In FLNS , narrow line laser excitation into the inhomogeneously broadened vibronic absorption bands of the $S_1 \leftarrow S_0$ absorption system leads to *site excitation energy selectivity*. Fluorescence vibronic bandwidths of 1-5 cm^{-1}

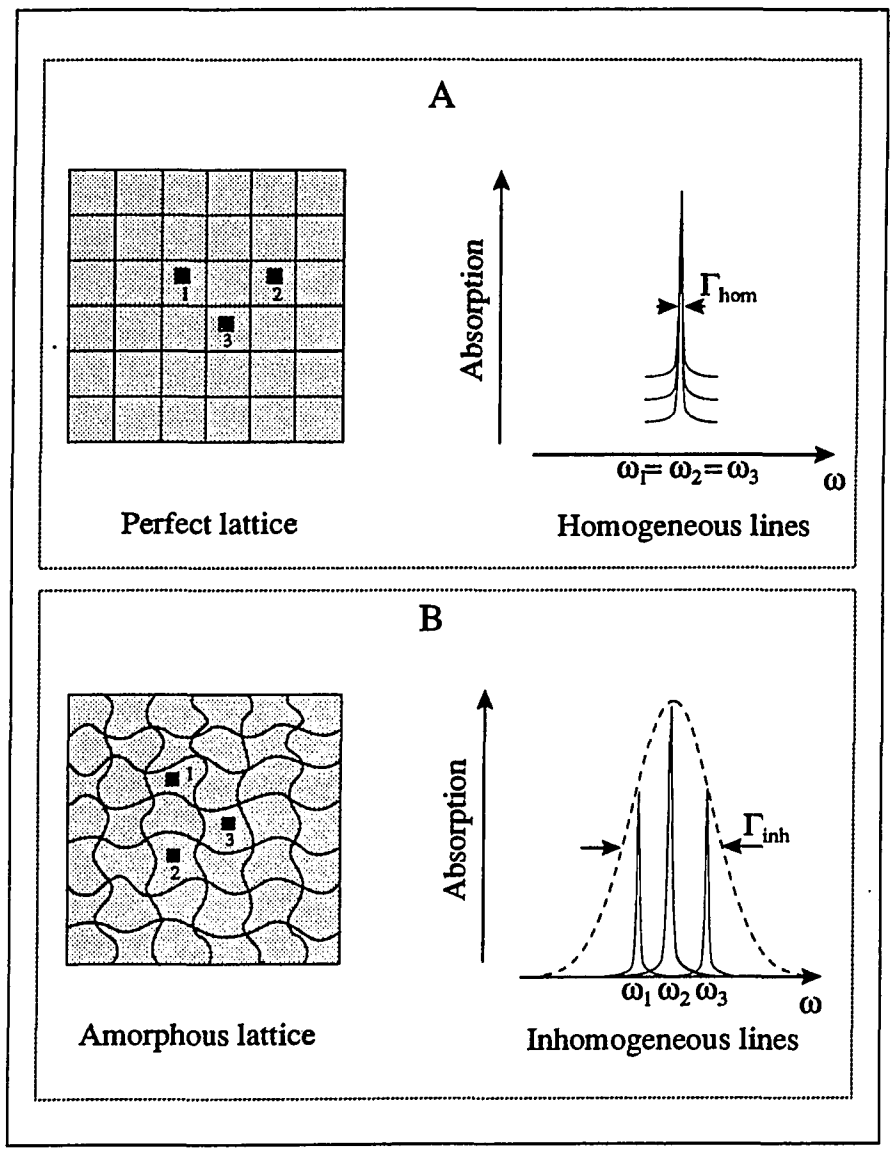

Figure 6. Schematic view of the optical absorption lines of three (identical) guest molecules in a perfect crystal (A) and an amorphous host (B)

are readily achievable (low temperature near 4 K are required to eliminate the thermal broadening contribution to the bandwidth). This represents an improvement in spectral resolution of about two orders of magnitude (measured relative to Γ_{inh} of the vibronic absorption widths in amorphous hosts). Site *inhomogeneous* line broadening of PAH in crystalline and amorphous hosts has been extensively studied. In crystalline hosts Γ_{inh} is about orders of magnitude smaller than in glasses. Thus, one could say that in the application of FLNS to molecules embedded in amorphous hosts, a narrow line laser is used to "trick" an amorphous host into behaving like a well ordered crystalline host, albeit at a loss of about two orders of magnitude in sensitivity.

Fluorescence line narrowing technique was first applied to gases by Feld and Javan in 1969 [118] and subsequently to ionic solids by Szabo [119] and to molecular solids by Personov *et al.* [120,121]. Since then it has been studied from a variety points of view [122-127]. Figure 7 is a schematic representation of an inhomogeneously broadened electronic absorption origin band, (0,0), at low temperature. As mentioned earlier, the relatively sharp dashed bands depicting the (0,0) transitions of the "guest" molecule occupying inequivalent sites are referred to as zero-phonon line (ZPL). Building to higher energy on each ZPL in Figure 7 is a broader phonon wing referred to as phonon side band (PSB). The basic principles of FLNS can be understood from Figure 7. First we note that if a broad band classical excitation source is used to excite the (0,0) band, all sites (ZPL) will be excited and excited sites will fluoresce, resulting in a broad fluorescence spectrum characterized by vibronic bandwidths equal to Γ_{inh}. If

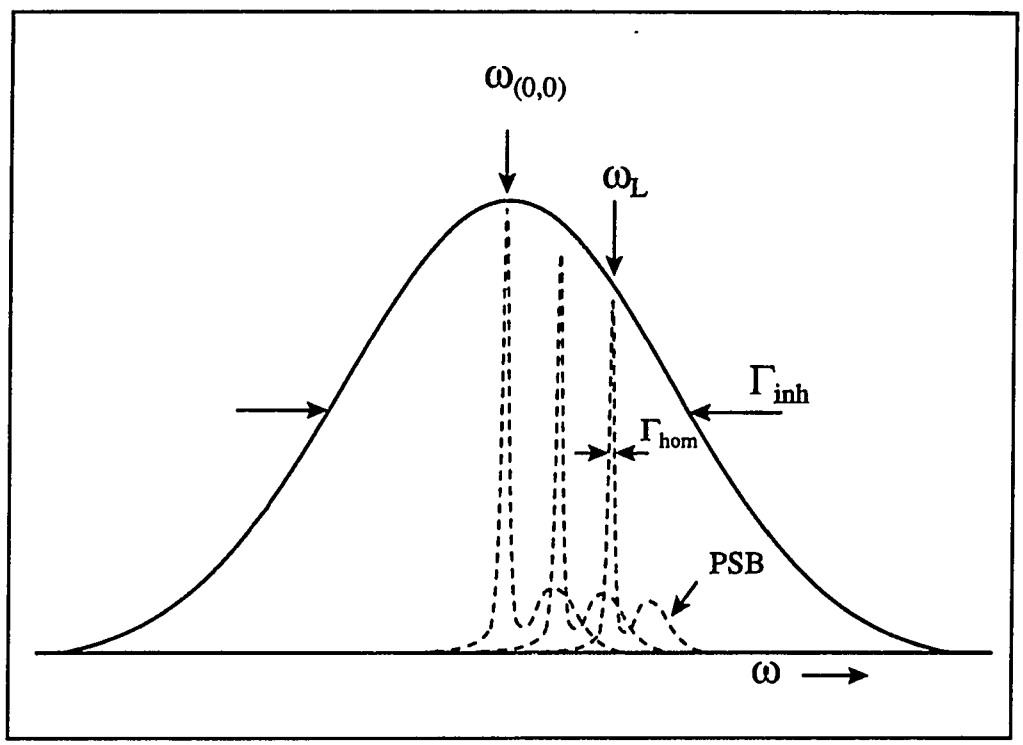

Figure 7. Schematic resentation of homogeneous (Γ_{hom}) and inhomogeneous (Γ_{inh}) broadening. Profiles of the zero-phonon lines (ZPL) and their associated phonon side bands (PSB) for specific sites at different frequencies have been enlarged compared to the inhomogeneous line to provide more detail. ω_L is the laser frequency which selectively excites a narrow isochromat of an inhomogeneously broadened absorption band

instead a laser of frequency ω_L and linewidth $\Delta\omega_L << \Gamma_{inh}$ is used , only ZPL (sites) whose transition frequency overlaps the laser profile will be excited. In the absence of intermolecular energy transfer only this "isochromat" will fluoresce, resulting in a "line-narrowed" fluorescence spectrum. The spectrum consists of an origin ZPL coincident with ω_L and, to lower energy, numerous ZPL corresponding to transitions to intramolecular vibrational sublevels of the ground electronic states. Note that as ω_L is tuned across the inhomogeneously broadened absorption, the origin ZPL and, therefore, the entire fluorescence spectrum will "track" ω_L. More important and interesting is the dependence of the fluorescence spectrum on ω_L. Upon excitation to not particularly high vibronic levels (up to 2000 cm^{-1}), the detailed structure of the spectrum essentially depends on the wavelength of the laser excitation. When the excitation is performed in the (0,0) transition region, the fluorescence spectrum consists of single vibronic lines. For this origin band excitation, however, the origin ZPL is not a useful analytical line due to interference from scattered laser light. On the other hand, with excitation to the vibronic levels, the fluorescence spectrum becomes more complicated and consists of groups of lines: "multiplets". An essential property of these multiplets is that they are independent of the solvent. For this reason and others related to selectivity, it proves advantageous to excite into vibronic bands (vibronically excited FLN).

To understand multiplicity of the spectra, let us turn to Figure 8A where the electronic ground and excited states are labeled as S_0 and S_1. For simplicity, the vibrational energy levels (including zero-point level) of S_0 is depicted as isoenergetic for

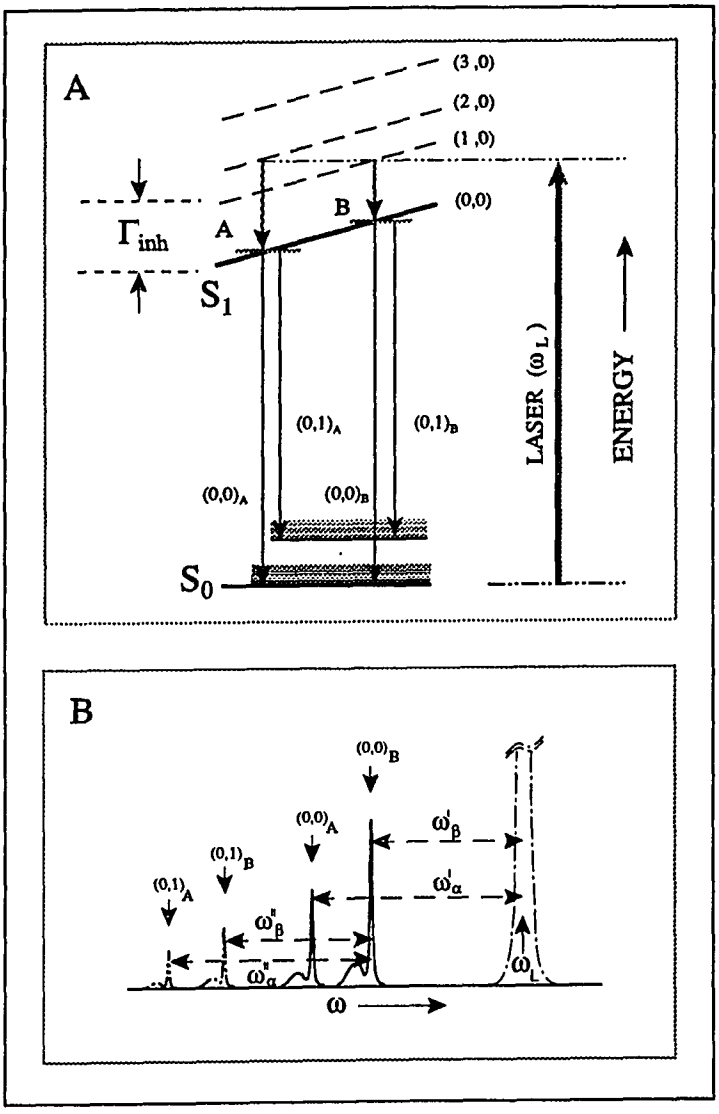

Figure 8. Schematic for vibronically excited fluorescence line narrowing. A: The slope of excited-state levels represents the variation of their energies as a function of site. Γ_{inh} denotes the inhomogeneous broadening of the (0,0) transition. Using the laser excitation, ω_L, two subsets of molecules within Γ_{inh} are selectively excited. B: Schematic of the resulting fluorescence spectrum. Fluorescence from two isochromats results in a boubling of the origin or (0,0) transitions as well as the (0,1) vibronic transitions

all sites. The site *inhomogeneous* broadening for the (0,0) absorption transition is indicated by the "slanted" solid line for S_1. The magnitude of Γ_{inh} is indicated to the left of the S_1 state. The slated dashed lines for the S_1 state denote vibrational; sublevels 1,2,3. The absorption transition to the vibrational levels of the excited state are labeled as (1,0), etc., where the zero indicates that the absorption originates from the zero-point level of S_0 (We assume that all molecules reside in zero-point energy level of the ground at low temperature). Since the Γ_{inh} for these transition to the vibronic region is essentially the same as for the pure electronic transition, (0,0), they will not be resolved in absorption spectrum even at very low temperature. The thick solid vertical arrow is the laser excitation frequency (ω_L) chosen to excite isochromats A and B belonging to (1,0) and (2,0) transitions, respectively. The intersections of the horizontal dash-dot line with the dashed lines are the locations of the isochromats in the site excitation energy distributions for the two vibronic transitions (for the two same type of molecule in two different site). After vibrational relaxation to their respective and correlated zero-point distribution in the S_1 state (A and B) (squiggly downward arrows), these molecules emit quantum of fluorescence shown as solid arrows. The resulting line narrowed flurrescence spectrum is given in Figure 8B. Note that the pure electronic transition (0,0) and transition to the first vibronic level (in S_0) (0,1) are doublets. If, in the excited state, the dissolved molecules have not two, but several closely spaced vibronic levels close to the laser frequency (ω_L) , the corresponding more complex "multiplet" appears in the (0,0) transition region of the fluorescence spectrum. More importantly, the spectrum has the

information of both the ground and excited state vibrational frequencies. For example, the displacements of $(0,0)_A$ and $(0,0)_B$ from ω_L yield the excited state vibrational frequencies (ω_α' and ω_β') and the displacement of $(0,1)_A$ and $(0,1)_B$ from corresponding $(0,0)_A$ and $(0,0)_B$ yield the ground state vibrational frequencies (ω_α'' and ω_β''). By varying the excitation frequency ω_L we can "prove" various regions of the vibronic states and determine all the vibrational frequencies (that are active in the given electronic transition) up to 2000 cm^{-1}.

The $(0,0)_A$ and $(0,0)_B$ lines comprise what will be referred to as *multiplet origin structure*. It is because $\Gamma_{inh} >> \Gamma_{hom}$ at low T that one can observe such structure and, therefore, determine excited state vibrational frequencies. The intramolecular vibrational sublevels of S_1 have a lifetime of ~1 psec due to rapid relaxation to the zero-point level in S_1. Therefore, the multiplet origin bands will generally be not sharper than ~5 cm^{-1}. For reasons not completely understood [128], excited state vibrational structure is often far more sensitive to minor structural perturbations than ground state vibrational structure. The validity of the above "multiplet structure" on the excitation frequency of the laser and interpretation of "multiplet" was experimentally confirmed on a number of molecules, for which the vibrational frequencies in the excited electronic state were determined by independent methods. With Figure 8A one can see that for (0,0) band excitation, the FLN spectrum generates "single" vibronic lines and provides information on ground state vibrations only. As mentioned earlier, the (0,0) fluorescence band is not generally useful as an analytical line due to laser light scattering.

Now let us turn to the relatively broad PSB that builds on the ZPL in absorption and fluorescence as shown in Figures 7 and 8B. The PSB is contributed to by 1-, 2-, ··· phonon transitions. As discussed before, however, the PSB profiles depend on the phonon density of state and electron-phonon coupling constant. For PAH in glass, the 1-phonon density profile has a maximum at $\omega_m \sim 25$ cm^{-1} and a width of $\Gamma \sim 40$ cm^{-1}. The r-phonon profile has a maximum at $r\omega$ and a width of $\sim r^{1/2}\Gamma$ [127,129]. From the Debye-Waller factor given by Eq. (B-2), it is easy to show that for $S<1$ (weak coupling) the ZPL is dominant while for $S>1$ (strong coupling), the PSB is dominant. For large S, the ZPL becomes Franck-Condon forbidden and FLN will not be possible. Except for intercalated DNA-PAH adducts, we have found that carcinogen-adduct spectra are characterized by weak coupling.

D. Principles of Spectral Hole Burning

Solid state spectral hole burning [115,121,123,130-132] is another example of a line narrowing technique which can be applied to biomolecular systems. Since this thesis is dedicated to mainly FLNS, only a brief and quantitative description will be given here. There are two types of hole burning (HB): photochemical hole burning (PHB) and non-photochemical hole burning (NPHB). With an understanding of site inhomogeneous broadening and isochromat selection by a narrow linewidth laser, HB mechanism is easy to follow. Irradiation into an inhomogeneously broadened line with a narrow-band laser of frequency ω_L can induce resonant molecules either to undergo a photochemical transformation such that the product absorbs at different frequency, or to pass over

temporarily to a metastable state.

PHB can be observed for amorphous and crystalline hosts. As the name implies, photochemical hole burning typically involves a reversible or irreversible photochemical reaction such as the electron transfer in RC of photosynthetic bacteria [133,134], PS II [135-137]. Within PHB one can distinguish between intramolecular photochemical reactions, taking place inside the guest molecule [138-141], or intermolecular ones occurring between the guest and the host [142-144]. In the former group, photochemistry may be reversible in the sense that irradiation into the photoproduct fills the hole and reconstitutes the original spectrum, or may be irreversible.

NPHB is characteristic for only amorphous systems. Unlike photochemical hole burning, non-photochemical hole burning only involves the modification of the microscopic environment of the impurity molecules. On excitation, a reorientation of the guest molecule with respect to its environment takes place [145-147]. A tunneling mechanism has been proposed in the literature [145-147] which is schematically represented in Figure 9: after selective excitation in the left hand conformation, tunneling takes place in the excited state, and reorientation occurs. In this way, a non-photochemical "hole" is burnt in the absorption band. The products created through this process are typically located very close to the burn frequency ($<< 100\ cm^{-1}$) where as in the case of photochemical hole burning, the product are located quite further away from the absorption [115,131] (typically greater than several hundred cm^{-1}). The generated "hole" represents a negative replica of the homogeneous spectral transition and the

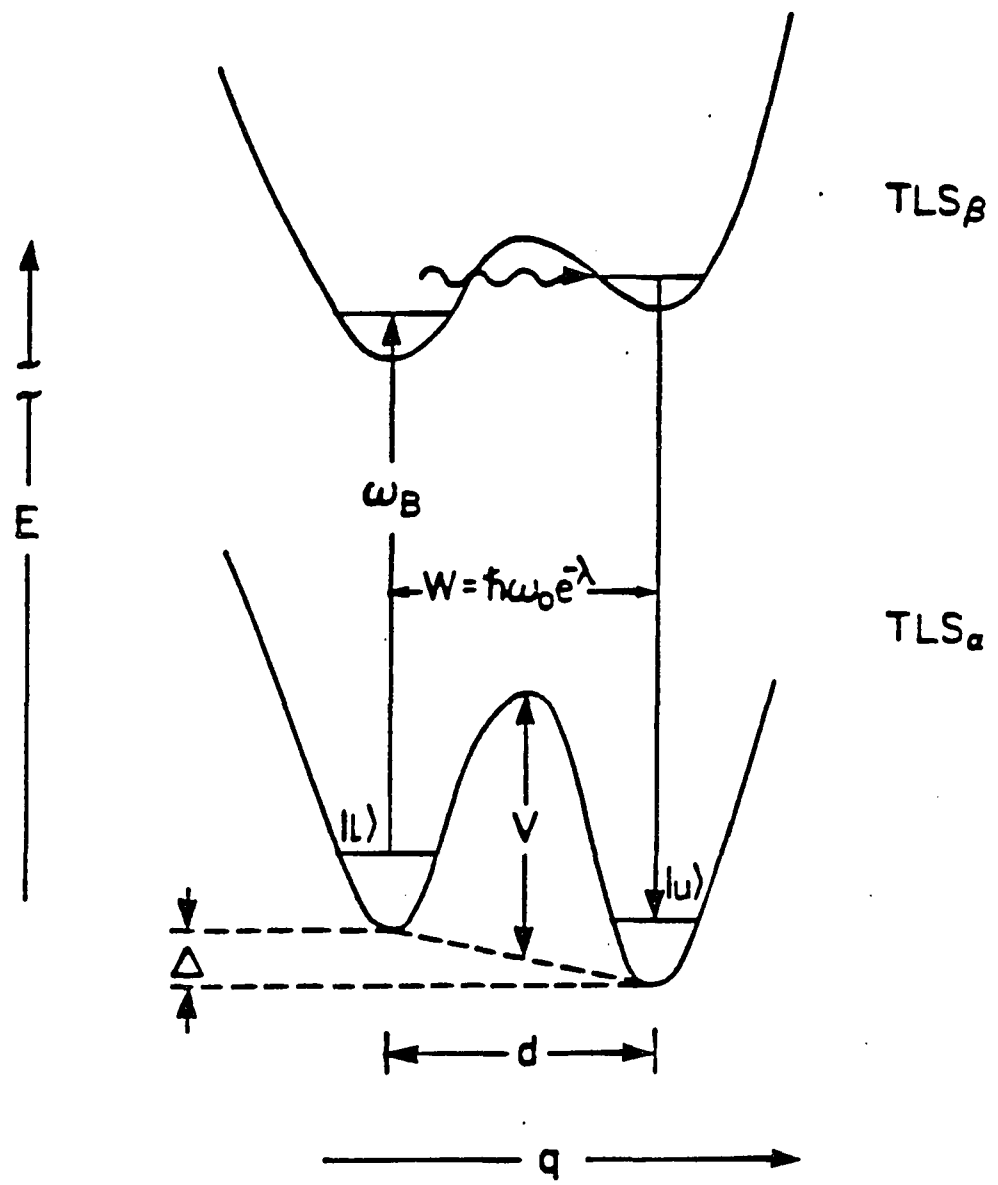

Figure 9. The two-level system (TLS) model for nonphotochemical hole burning. The subscripts α and β label the TLS that interact with the impurity in its ground and excited electronic states. The tunnel frequency, W, depends on the tunnel parameter λ which is defined as $d(2mV)^{1/2}/h$, where m is the tunneling mass. The frequency ω_B is that of the burn laser

holewidth if carefully measured, yields the unknown quantity Γ_{hom}. A schematic diagram of hole burning spectrum is presented in Figure10. In the absorption spectrum of Figure 10A laser with frequency ω_L (burn frequency) is irradiated on an isochromat in the (0,0) band. The molecule(s) in given isochromat, however, also contribute to the $(1_\alpha,0)$ and $(1_\beta,0)$ vibronic bands. Therefore, a zero-phonon hole (ZPH) burnt at ω_L will be accompanied by higher energy vibronic satellite holes, as indicated in the Δ-absorbance spectrum. Because the ZPL in absorption is accompanied by a PSB, the ZPH is accompanied by phonon sideband holes (PSBH). The PSBH to higher energy side of the ZPH is readily understood and is referred to as the real-PSBH. That a pseudo-PSBH to lower energy of the ZPH should appear is not so obvious. The pseudo-PSBH is due to sites whose ZPL frequencies lie to lower energy of ω_L and which absorb the laser light by virtue of their PSB. The phonons excited rapidly relax to the zero point level after which NPHB ensues [127].

In the same manner that pseudo-PSBH can be observed, pseudo-vibronic hole structure can be generated. The basic idea is very similar to that involved in vibronically excited FLN. In Figure 10B the laser (ω_L) excites two isochromats (α and β) belonging to first and second vibrations, respectively. Since the inverse of the average rate constant for NPHB is no larger than ~10^{-6} sec, the vibrational isochromats relax to their respective zero point positions in the (0,0) band prior to hole burning. Two ZPH, $(0,0)_A$ and $(0,0)_B$, are produced, which lead to a hole at ω_L. The relative intensities of the former two and latter hoe depend, in part, on the Franc-Condon factors for two vibrations. What

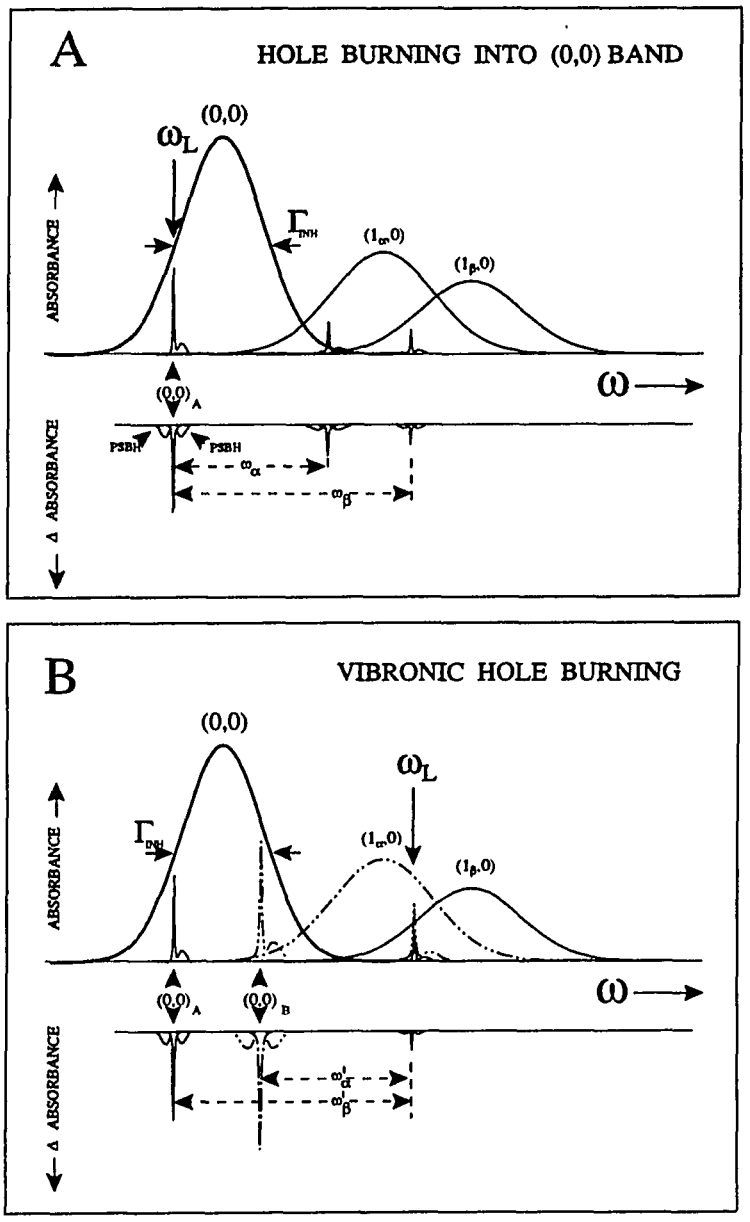

Figure 10. Schematic hole burning (selective photobleaching) into origin band (A) and into vibronic region (B) (see explanation in text)

importance is that the displacements of the vibronic "satellite" holes from the burn frequency yield the excited state vibrational frequencies.

HB effect appearing as hole in the absorption spectrum can be detrimental in FLNS. That is, the intensity of the sharp ZPL in fluorescence might be reduced due to photobleaching, and will be disappeared in the limit of saturation by intense laser light. By this reason and possible photochemical reaction, the samples were degassed to remove oxygen. In the absence of oxygen gas, the spectral degradation is less significant. It is, however, interesting to note that NPHB can be used improve the selectivity in combination with FLNS [86]. To obtain better selectivity, one has to measure FLN spectrum (spectrum A) and then measure another FLN spectrum (spectrum B) after irradiation (hole burning) to the sample with high power of laser light for certain period of time (~3 min). The latter spectrum B is dominated by PSBs From various sources, while the former spectrum is a convolution of given PSBs and sharp ZPLs from resonant isochromats. Then the new spectrum from the difference of the two spectra (A-B) is simply predominated by extremely sharp ZPLs, thus better selectivity may be obtained.

III. EXPERIMENTAL

A. Materials and Reagents

Samples to be analyzed by spectroscopy were dissolved in a glycerol/water/ ethanol mixture (0.5: 0.4: 0.1 by volume) that forms an optically transparent medium at low temperature. Reagent grade glycerol from Fisher Scientific and 100% ethanol from Iowa State University store room were used for the glassy mixture. Doubly distilled deionized water was obtained and routinely used for the glass forming solvent and clean up procedure. Solid samples were dissolved first in minimal amounts of dimethyl sulfoxide (DMSO) from Fisher Scientific. Spectroscopic grade 1,4-dioxane was also purchased from Fisher Scientific and used to dissolve laser dyes such as QUI, DMQ, and p-terphenyl. Electrophoretic purity grade (>99.9%) acrylamide used for fluorescence quenching experiments was purchased from Bio-Rad Laboratories.

Approximately 20 μl of each sample in DMSO was contained in a 1 cm long quartz tube (3 mm o.d. x 2mm i.d.) with sealed one end. For a given amount of sample, smaller volume provided better detection limits. For most of the experiments performed, the were degased and then rapidly cooled (~2 min) to liquid He temperature (4.2K) for FLNS or liquid nitrogen temperature (77K) for non-line narrowed fluorescence spectroscopy. Many standards, metabolites, nucleoside adducts, globin adducts, and DNA adducts were used throughout this research. However, names and acronyms, suppliers, and preparation of all samples will be presented with spectral analyses in the following section IV.

B. Instrumentation

The instrumentation applied to low temperature FLNS has previously been described in detail [86], so only a brief description will be given here. The equipment needed to perform FLNS can be divided into four major components: a spectrally narrow excitation source, an optically accessible low-temperature sample chamber, a dispersion device, and a detection system. A block diagram of the FLNS apparatus is shown in Figure 11.

The excitation source used for FLNS experiment is a Lambda-Physik EMG 102 MSC excimer (*XeCl*) pumped tunable dye laser (Lambda Physik FL-2002) system. The excimer laser system is operated with 80 parts of Xe, 100 parts of HCl, and 2420s part of Ne gases and provides high energy (130 mJ/pulse) pulses with a repetition rate of up to 100 Hz at 308 nm. Although the laser firing is synchronized to the electronic output pulse with temporal width of 10 ns, it may slowly drift with time and thyratron temperature relative to the electronically synchronized output pulse. For gated mode detection, therefore, a Lambda Physik EMG-97 zero-drift controller (ZDC) is required to trigger a high voltage gate pulse generator (Princeton Instruments FG-100), which controls both the adjustable delay times and the width of the temporal detection window. The ZDC uses a photodiode (PD) pulse to monitor the laser firing time and electronically synchronized pulse from the triggering circuit, and compares them in an electronic comparator which corrects the long term temporal drift. Since the excimer laser has an inherent shot to shot instability of ±7 ns due to the thyratron, a minimal 7 ns delay time

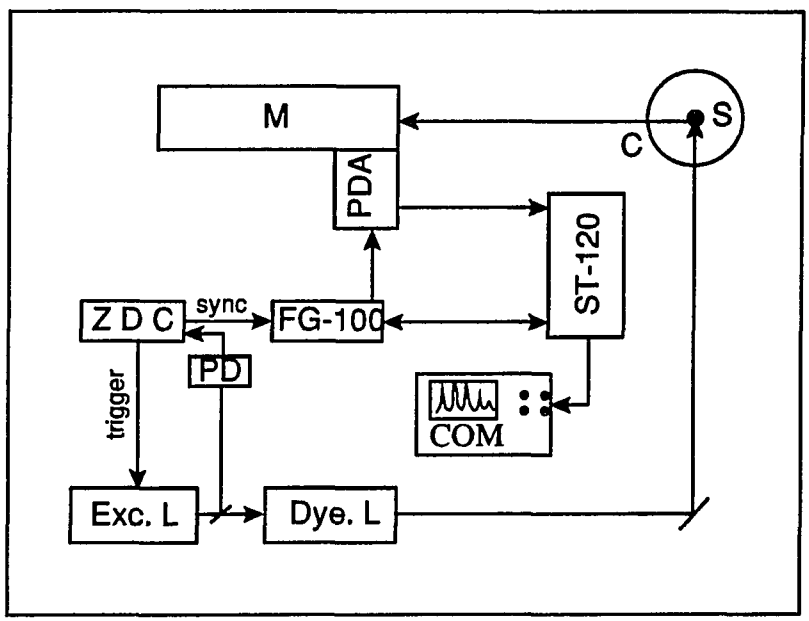

Figure 11. Block diagram of present FLNS instrumentation: excimer laser (Exc. L), dye laser (Dye L), photodiode (PD), zero-drift control (ZDC), cryostat (C), sample (S), photodiode array (PDA), monochromator (M), multichannel analyzer (ST-120), and computer (COM)

is suggested for complete elimination of laser scattering. The corresponding dye laser uses a grating in a Littrow geometry for wavelength selection. With this oscillator, a moderate grating angle (typically less than 75°) can be used to allow lower frequency jittering, higher grating efficiency and less sensitive operation. With the described grating, the laser has a 0.22 cm^{-1} spectral line width which can be reduced to 0.04 cm^{-1} by inserting an etalon type selector.

Because most PAHs absorb in the 340 ~ 420 nm range, p-terphenyl (332-350 nm, λ_{max} = 343 nm), DMQ (346-377 nm, λ_{max} = 360 nm), QUI (368-402 nm, λ_{max} = 390 nm), and PBBO (386-420 nm, λ_{max} = 396 nm) dyes from Lamda Physik were employed to select the excitation wavelength. Based on the typical conversion efficiency of 5%, the output laser power is ~7 mJ/pulse which corresponds to ~100 mW/cm^2. The laser beam has a symmetrical trapezoidal shape with an approximate dimension of 2 mm x 2mm. The laser is then shaped into a 10 mm x 2 mm beam by using a quartz biconvex cylindrical lens combination for complete irradiation of the sample.

A 3L double-nested glass low temperature cryostat manufactured by H. S. Martin Inc. was used for both 4.2 K and 77 K optical experiments. The outer layer is evacuated with typical pressure of $5x10^{-6}$ torr, while the next two layers contain liquid nitrogen and liquid He. When a 77 K experiment was performed, the inner container was filled with liquid nitrogen. A sample in a quartz tube was directly immersed in liquid He (or liquid nitrogen) to obtain optical spectra at 4.2 K (or 77 K). The cryostat is designed to exclude liquid nitrogen from the optical pathway in order to eliminate laser scattering

from the liquid nitrogen bubbles and is equipped with 3 quartz windows for the proper UV excitation of samples. The temperature was measured with a silicon diode thermometer (Lake Shore Cryogenics model DT-500K) and then calibrated over the range of 1.4 K to 300 K; thereafter the temperature was assumed to be the same for subsequent experiments. Fluorescence was collected at the right angle at the excitation and focused to the monochromator by two 50 mm lenses to give 0.2 % collecting efficiency [86]. Collected fluorescence was dispersed by a 1-meter McPherson 2061 monochromator (F/7) equipped with a 140 mm x 120 mm (136 mm x 116 mm of ruled area) grating with 2400 grooves/mm, providing a linear dispersion of 0.416 nm/mm at first order. The McPherson 2061 monochromator is in a Czerny Turner geometry and is designed to reduce the scattered light to less than 1 part in 10^6 in the 200 to 800 nm range. This system can provide a resolution of 0.085 nm at 200 μm slit width. The monochromator has aspherical mirrors for collimating and focusing, and slits in a fixed position, while the grating is rotated for wavelength selection. Entrance and exit slits may be the bilateral opening type, turret-mounted fixed slits, or dovetail mounting fixed width slits. Fixed width slits require user selection from 5 μm to 2 mm. The bilateral feature at the exit slit, especially, enables the user to access a second detector merely by switching the mirror in place. The monochromator is scanned by a McPherson Digital Drive (Model 787) which controls wavelength output through a stepping motor coupled to the drive screw.

Two kinds of optical detectors were employed for current spectroscopic analyses

of chemical carcinogenesis in this research: a photomultiplier tube (PMT) and a photodiode array (PDA). The PDA detector was used for FLNS study while the PMT was used for 77 K non-line narrowed fluorescence experiments and provided supplemental spectra for the present research. The PMT system shown in Figure 12 is utilized mainly to perfom both the broad fluorescence experiments at 77 K and the fluorescence excitation experiments. The Amperex XP-2232 photomultiplier tube is specially wired for fast signal response. The fluorescence signal from the PMT is sent to an SRS Model SR250 boxcar averager (BXC. I). The SR250 boxcar consists of a gate generator, a fast gated integrator, and exponential averaging circuitry. The synchronous output pulse of the ZDC triggers the gate generator, which provides both an adjustable delay from a few nanoseconds to 0.1 seconds and a continuously adjustable gate from 2 nsec to 15 msec. The fast gated integrator integrates the input signal acquired during the gate operation. The output from the integrator is then normalized by the gate width to provide a voltage which is proportional to the average of the input signal during the sampling gate opration. The averager circuitry makes a moving exponential average over 1 to 10,000 samples available to pull small signals from noisy backgrounds. The laser beam intensity is monitored by a reference photodiode, and the signal is input to the second channel of the boxcar averager. The signals from the PMT and the reference photodiode is input to an SRS Model SR235 analog processor, where they are ratioed in order to compensate for pulse-to-pulse jitter from the laser. The analog signal from the analog processor is then converted into a digital signal through the SRS Model SR245

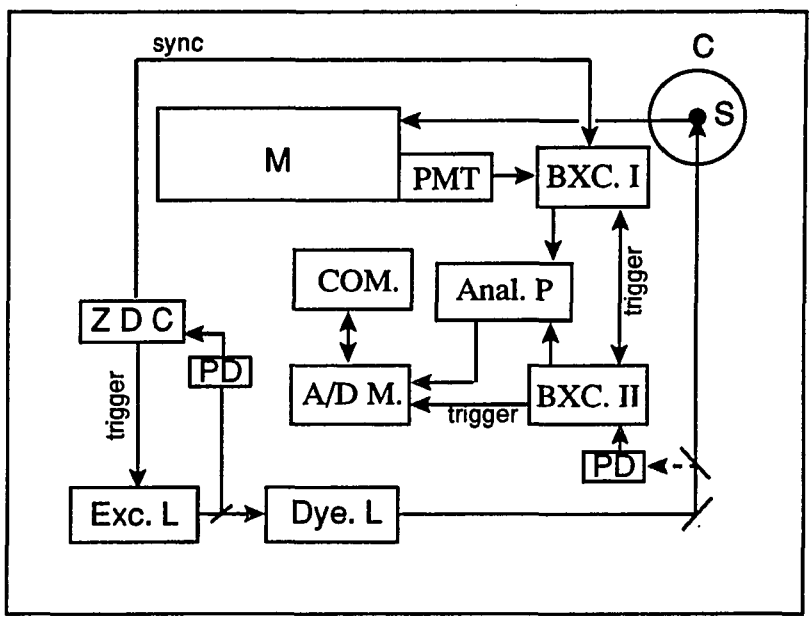

Figure 12. Block diagram of the fluorescence instrumentation using an Amperex XP-2232 photomultiplier tube as the detector: excimer laser (Exc. L), dye laser (Dye L.), cryostat (C), sample (S), photomultiplier tube (PMT), monochromator (M), SRS Model SR250 boxcar averager (BOX I and II), SRS Model SR 235 analog processor (Anal. P), SRS Model SR245 computer interfacing module (A/D M.), zero-drift control (ZDC), photodiode (PD), and computer (COM)

computer interfacing module, and the data acquisition is accomplished by an accompanying computer program, SR265. All spectra obtained from PDA and PMT systems can be transformed into files of "Spectra Calc" and "MASS11-DRAW" commercial computer graphics programs, which greatly facilitate the spectral analysis process.

The second detector, the PDA system used a Princeton Instruments IRY-1024/G/R/B intensified blue enhanced gatable photodiode array (optical multichannel analyzer, OMA) which is able to detect a 9-nm segment of the spectrum simultaneously. This model consists of 1024 photodiodes optically interfaced to a microchannel plate (MCP) image intensifier through an optical-fiber coupler. The combined high gain (more than 10^6 electron multiplier) of the MCP image intensifier and the low readout noise of the diode array resulted in a very sensitive detector capable of responding to a single photoelectron. Moreover, the detector is able to detect, measure, and manipulate spectra at a high acquisition rate (33 msec) with an excellect dynamic range, high resolution, and excellect overall accuracy and performance. A block diagram of the OMA system (illustrated in Figure 11) consists of the computer console, an ST-120 Detector Controller, an FG-100 Gate Pulse Generator, and an IRY-1024 Detector. The synchronous output pulse from the ZDC is used to trigger the FG-100 Gate Pulse Generator, which is primarily designed to provide high speed gating with pulse delay control. A low voltage pulse (200 V) is used to gate the detector on and off. Combined with Princeton Instruments high conductivity photocathodes, it is possible to obtain gating times as short

as 5 nsec. The time interval between the trigger pulse and the output pulse is continuously adjustable from 20 to 1700 μsec. Considering that the synchronous output pulse of the ZDC precedes the laser light pulse, the actual delay time from 0 to 1500 nsec can be set by timing signals to the detector head, coordinates data gathering with experiments, sets exposure time, digitizes and averages data, temporarily stores data, and transmits it to an IBM/AT computer. A combination of the ST-120 controller and the FG-100 pulse generator provides versatile trigger modes which can meet a variety of experimental requirements. The mode shown in Figure 11 is used to monitor a free-running pulsing laser which operates asynchronously with the ST-120.

IV. RESULTS AND DISCUSSION

A. Spectral Library

Elucidation of the mechanisms of activation of polycyclic aromatic hydrocarbons (PAH) is essential for understanding the process of tumor initiation and the design of preventive strategies. The identification of PAH-DNA adduct structures is, therefore, very important. As mentioned earlier, studies thus far point to two major mechanisms of activation: one-electron oxidation to form intermediate radical cations [34-36] and monooxygenation to produce bay-region diol epoxides [23-25,27,28,31-33]. In biological experiments, in which modification levels are extremely low, it is essential to develop a very sensitive and selective analytical techniques for the structural characterization and elucidation. As discussed in the Introduction, FLNS is very promising in this regard. In this subsection we present the standard FLN spectra of synthesized adducts from B[a]P and 7,12-DMBA expected from the radical cation pathway as well as the monooxygenation pathway. The structures of the synthesized adducts were determined by FAB MS/MS and NMR. Pertinent metabolite spectra are also presented. The FLN spectra are constitute a library of reference spectra which is essential for *in vivo* and *in vitro* studies of chemical carcinogenesis.

The FLNS characterization of a number of the expected metabolites of B[a]P, including *racemic* BP tetrol, 7-hydroxy-7,8,9,10-tetrahydrobenzo[a]pyrene, 10-hydroxy-7,8,9,10-tetrahydrobenzo[a]pyrene, and 9-methoxybenzo[a]pyrene-4,5-dihydrodiol, and the major adduct formed by monooxygenation between BPDE and DNA has been

accomplished previously [86,148,149]. In this dissertation, therefore, only the model monooxygenated adducts not previously studied and one-electron oxidation adducts from B[a]P, 7,12-DMBA, and standard H_4DMBA will be discussed. The structures and acronyms of all PAH model compounds studied are shown in Figures 13-15. The sources for those adducts and their synthesis are presented later.

1. Model compounds from B[a]P

B[a]P is one of the most extensively studied chemical carcinogens due to its potent mutagenic and carcinogenic properties. To date most of the results in chemical carcinogenesis research have been derived from *in vivo* and *in vitro* experiments usnig B[a]P as the parent carcinogen. It was very important, therefore, to generate a FLN spectral library for B[a]P and its adducts expected from both the one-electron oxidation and monooxygenation metabolic pathways. The standard model compounds discussed in this section, including B[a]P, 6-methylB[a]P, 6-fluoroB[a]P, BP-6-N3dG, BP-6-NHdG, BP-C8dG, BP-6-C8Gua, BP-6-N7Gua, and BP-6-N7Ade, were prepared [161,170] by Dr. E. Cavalieri and his group at Eppley Institute for Research in Cancer and Allied Diseases, University of Nebraska Medical Center.

The FLN spectrum of B[a]P in a glycerol/ethanol/water glass at 4.2 K is shown in Figure 16. Figure 16 shows that the 0-0 origin band of the $S_1 \leftarrow S_0$ is centered at ~403 nm, in agreement with the position determined from 77 K non-line narrowed fluorescence spectra ($S_2 \leftarrow S_0$ excitation). Two excitation wavelengths, 393.8 (spectrum A) and 392.0 nm (spectrum B), were selected for vibronic excitation at ~580 cm^{-1} and ~700 cm^{-1}

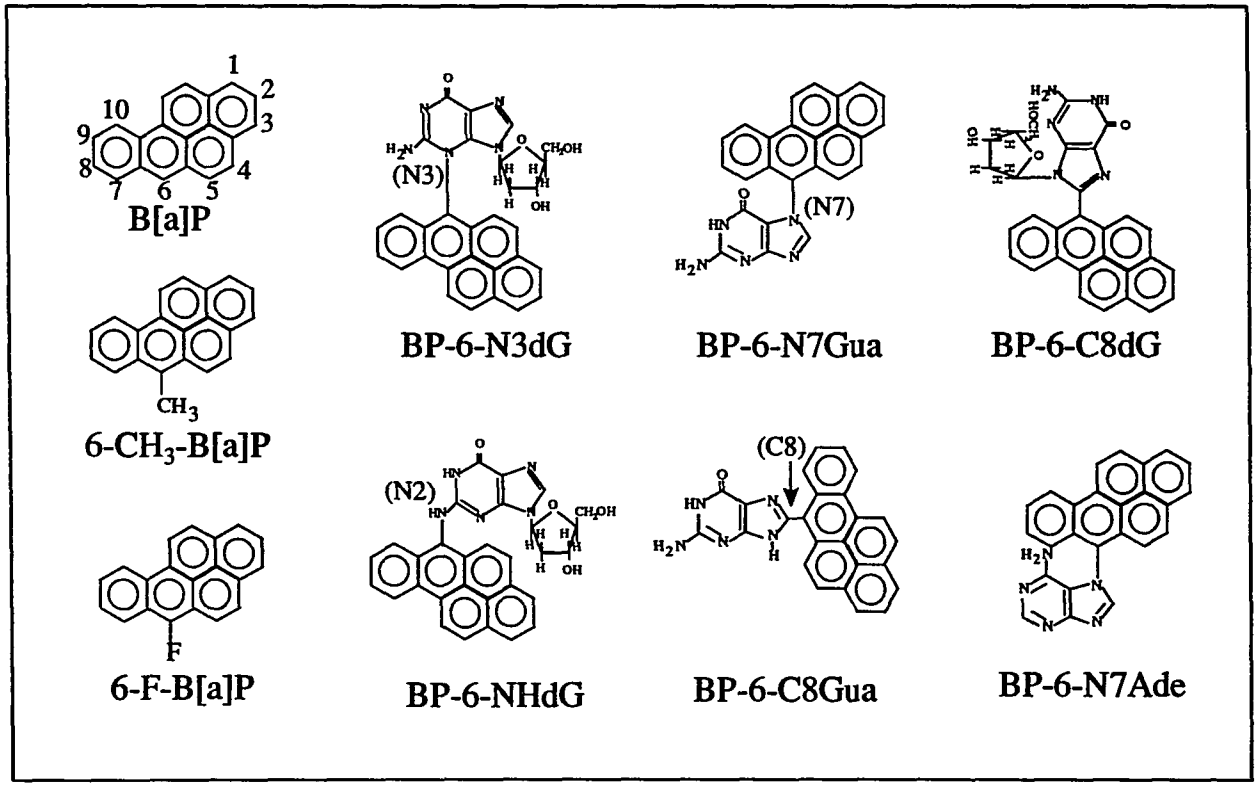

Figure 13. Structures and acronyms of B[a]P and its model adducts expected from one-electron oxidation

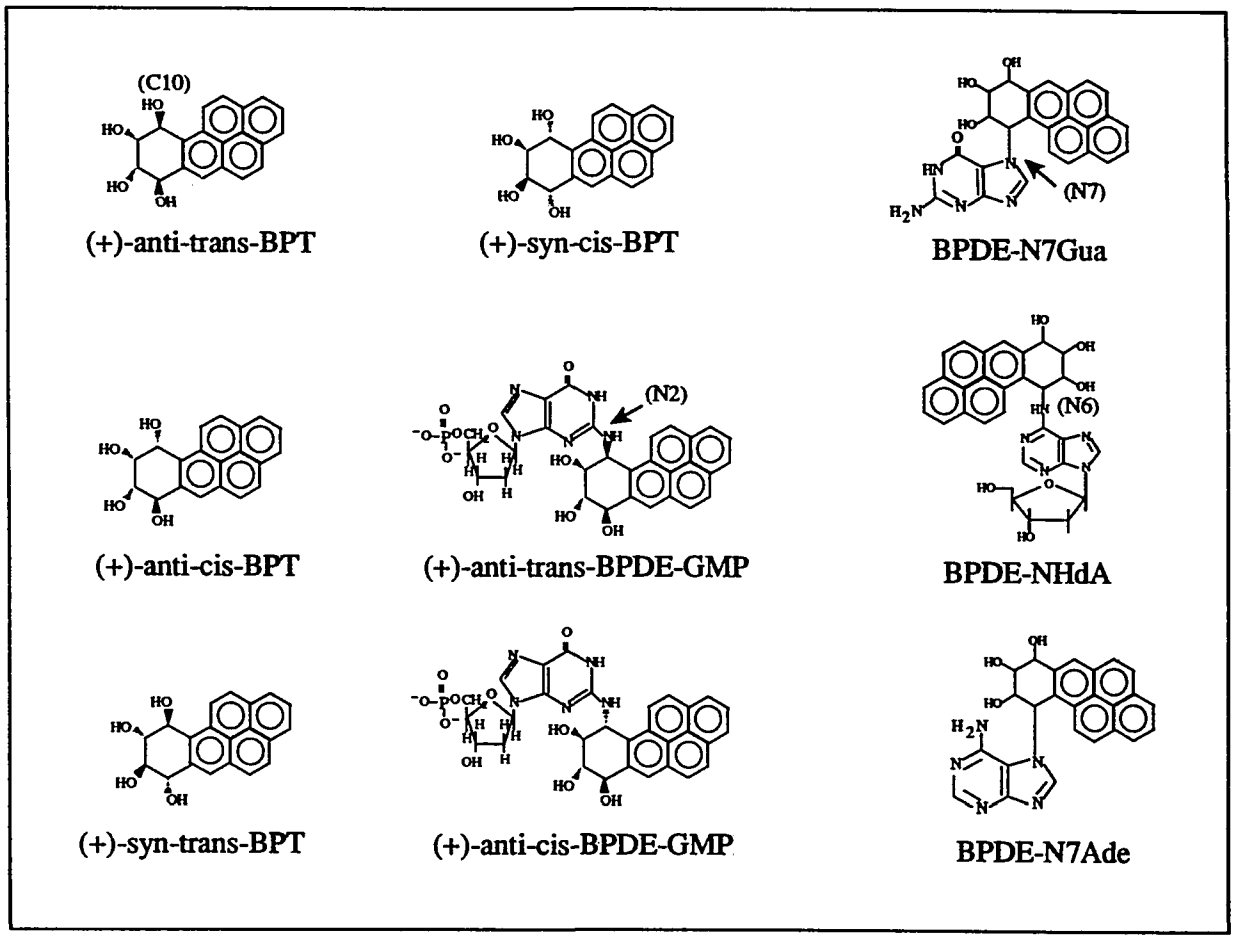

Figure 14. Structures and acronyms of BPT and model BPDE-adducts expected from monooxygenation

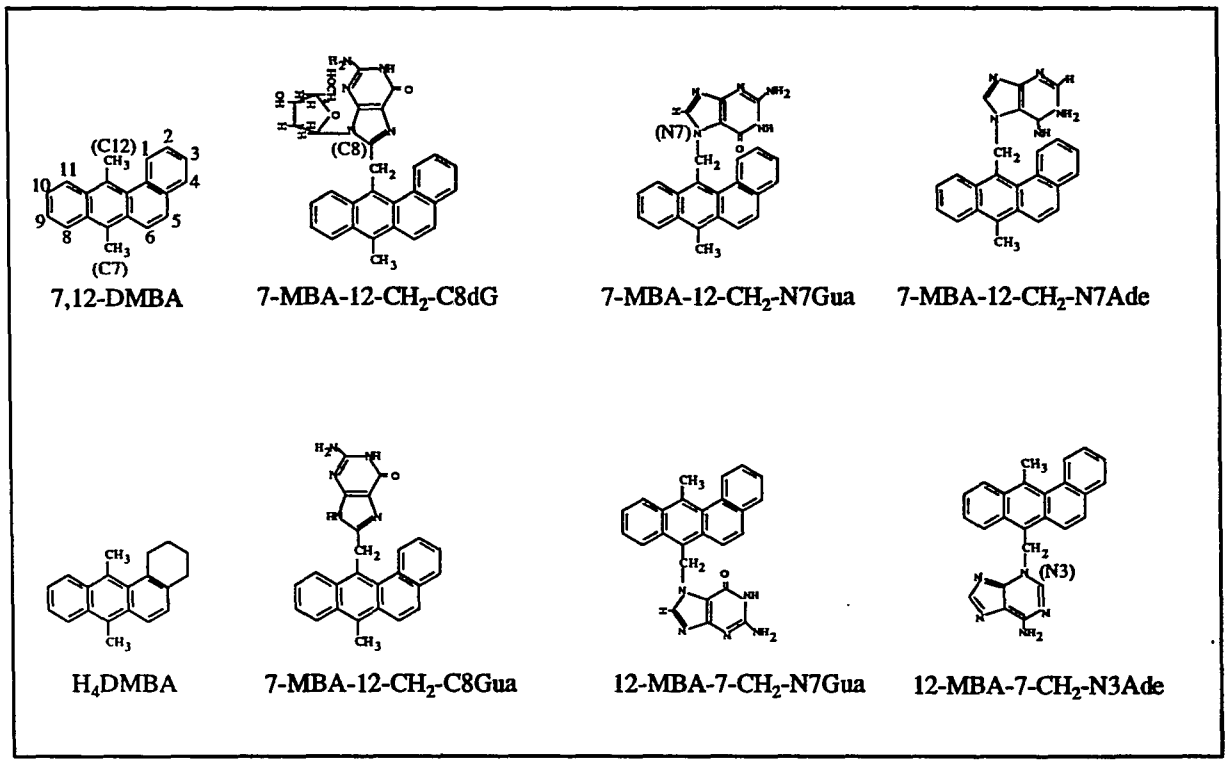

Figure 15. Structures and acronyms of 7,12-DMBA, and its model adducts expected from one-electron oxidation

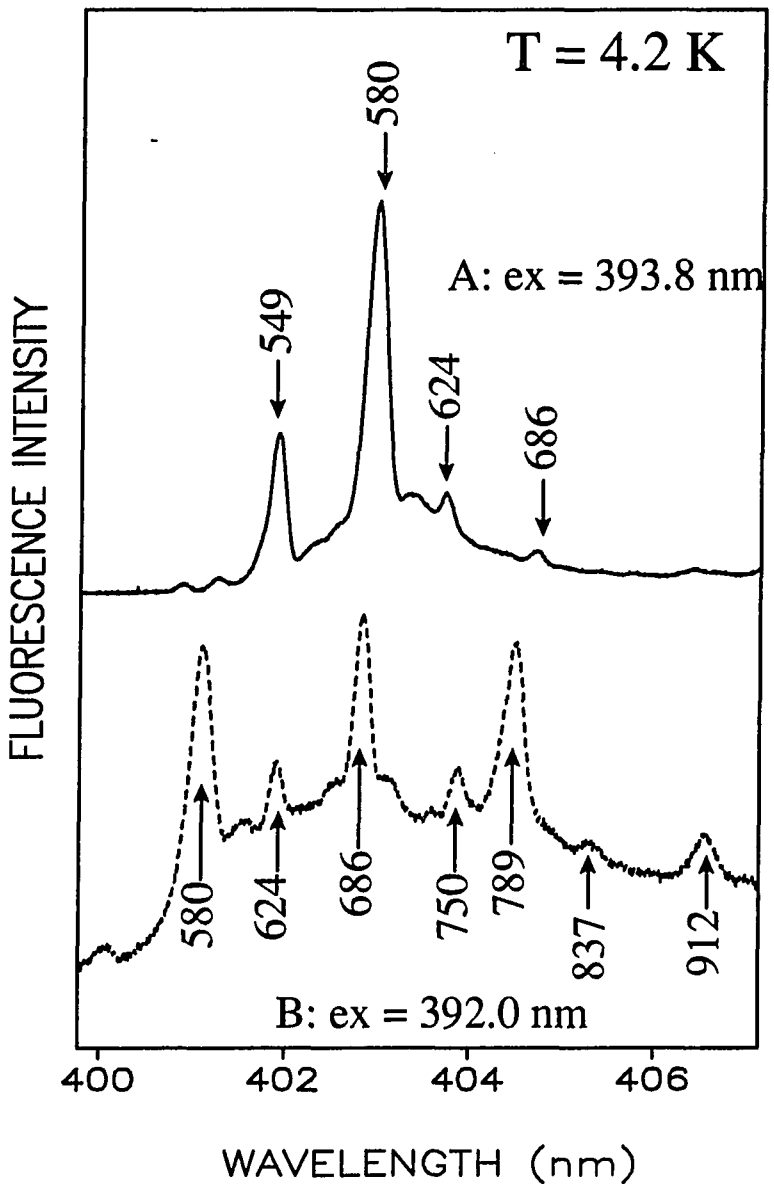

Figure 16. FLN spectra of B[a]P at 4.2 K, obtained with λ_{ex} = 393.8 nm (spectrum A) and 392 nm (spectrum B). The peaks are labeled with their excited state vibrational frequencies in cm^{-1}

above the zero-point vibrational level of the S_1 state, respectively. The prominent zero-phonon bands are labeled with their excited state vibrational frequency in cm^{-1} and closely resemble those previously presented [150]. The FLN spectra are characterized by weak electron-phonon coupling or strong ZPLs. As discussed in section II-B, the vibronic intensity distributions but not the mode frequencies depend on the excitation wavelength. Comparison of spectra A and B reveals that as the excitation is tuned to higher energy, modes with higher frequencies become more intense. By tuning the excitation wavelength over a sufficiently wide range one can map out the frequencies of all modes active in the $S_1 \leftarrow S_0$ absorption system. A partial list of excited state vibrational frequencies for B[a]P is given in the first column of Table 1.

The study of the effects on the FLN spectra of substitutents at the C6-position of B[a]P is very important because the positive charge rendering electrophilicity of B[a]P-carbenium ion generated by one-electron oxidation is mainly localized on C6-position of this metabolite. It has been shown that alkyl substitution effect at C6 of B[a]P leads to an increase in the electron-phonon coupling strength, the strength increasing as the size of alkyl group is increased [87]. We have obtained the FLN spectra for 6-fluoro- and 6-methyl-B[a]P. The 0-0 origin bands of both substituted compounds are red-shifted relative to that of B[a]P, ~5 nm for the former and ~6 nm for the latter. As a result 77 K non-line narrowed fluorescence spectra can be used to distinguish these compounds from B[a]P. It has also been shown that FLNS can directly resolve mixtures of methyl-substituted pyrene, anthracene [87], and naphthalene [151] from their corresponding

Table 1. Excited-state (S_1) vibrational frequencies (cm^{-1}) of B[a]P and its derivatives expected from one-electron oxidation[a]

B[a]P		6-CH_3-B[a]P	6-F-B[a]P	BP-6-C8dG	BP-6-N7Gua	BP-6-C8Gua	BP-6-N7Ade	BP-6-NHdG	BP-6-N3dG
327	954	437	370	469	465	469	-	-	-
376	973	510	428	498	498	498	496	497	497
427	1009	550	454	538	538	538	-	536	536
449	1032	575	510	566	569	563	554	560	569
471	1063	614	546	586	588	586	587	588	588
512	1119	676	570	-[b]	-	-	612	606	606
549	1133	770	589	-	633	-	634	634	634
580	1179	1128	617	-	671	-	-	673	673
624		1177	641	1126	1132	1126	1132	1131	1131
686		1222	670	1164	1164	1164	1164	1168	1168
750		1249	752	1219	1218	1219	1220	1219	1219
789		1282	772	1247	1250	1247	1252	1251	1252
837		1314		-	1296	-	-	1293	1292
912				1314	1316	1314	1316	1318	1319
933				-	1398	-	1396	1400	1400

a. excitation wavelengths used: for B[a]P 386.5, 392, and 393.8 nm; for 6-CH_3-B[a]P 390, 398.7 nm; for 6-F-B[a]P 398.7 nm; for model adducts from one-electron oxidation 386.5 and 395.7 nm.

b. not observed or very weak.

unsubstituted parents. A vibronically excited FLN spectra in glass mixture at 4.2 K are shown in Figure 17 for 6-fluoro-B[a]P (spectrum A) and 6-methyl-B[a]P (spectrum B). Differences in the frequencies of certain modes and vibronic intensity distributions are quite significant. Certian modes in the FLN spectrum of 6-fluoro-B[a]P, for example 454 and 752 cm^{-1}, are absent in the 6-methyl-B[a]P spectrum. For both compounds the electron-phonon coupling is sufficiently weak to result in pronounced ZPLs. Figure 17 indicates that the 0-0 origin is centered at ~408 for 6-fluoro-B[a]P and ~409 nm for 6-methyl-B[a]P. At comparable concentrations, therefore, these two compounds could be resolved in a binary mixture. The excited state vibrational frequencies for both compounds are also listed in Table 1.

Because it is generally believed that DNA is a cellular macromolecule of critical importance to the initiation of carcinogenesis, detailed studies of covalent adducts between DNA bases and PAH electrophilic metabolites are clearly mandated. Many studies have shown that the major nucleophilic binding sites in DNA are exocyclic NH_2 group (N2) and oxygen (O6) of guanine, the exocyclic NH_2 group (N6) in adenine [27,152], the 7-position (N7) of adenine and guanine, and the 8-position (C8) of guanine [34-36] (see Figures 13-15 for numbering). The first three binding sites are particularily important to the monooxygenation mechanism, while the latter two are important to the one-electron oxidation mechanism. Therefore, the following model adducts were analyzed: BP-6-N3dG, BP-6-NHdG, BP-6-C8dG, BP-6-C8Gua, BP-6-N7Gua, and BP-6-N7Ade. These adducts are linked through the 6-position of B[a]P to the 3-position (N3)

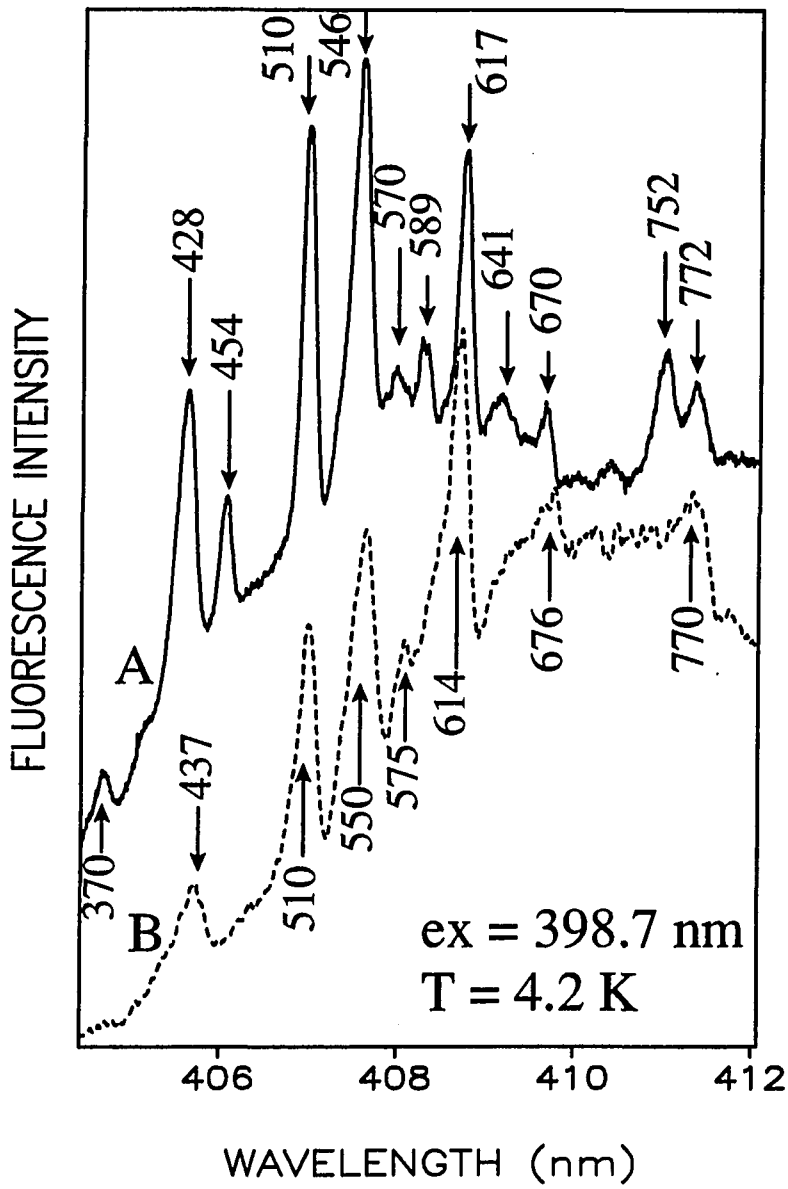

Figure 17. A comparison of the FLN spectra of 6-fluorobenzo[a]pyrene (spectrum A) and 6-methylbenzo[a]pyrene (spectrum B) obtained with λ_{ex} = 398.7 nm at 4.2 K

of guanine, the exocyclic NH_2 (NH) of deoxyguanosine, 8-position (C8) of deoxyguanosine and guanine, and 7-position (N7) of guanine and adenine (see Figure 13). These adducts are expected from the one-electron oxidation pathway. The model one-electron oxidation adducts are structurally very similar and their FLN spectra are, likewise, quite similar. As will be discussed later, however, these adducts can be readily distinguished from B[a]P, 6-methyl-B[a]P, and 6-fluoro-B[a]P on the basis of their FLN spectra.

Figure 18 shows the vibronically excited FLN spectra of BP-6-N3dG (spectrum A) and BP-6-NHdG (spectrum B) at 4.2 K, λ_{ex} = 395.7 nm. The mode frequency range is 400-700 cm^{-1}, the region of greatest activity. Their FLN spectra are very similar due to the structural similarity. Most strong modes of BP-6-N3dG (spectrum A), especially the 497, 536, 588, and 634 cm^{-1} modes, have identical counterparts in the FLN spectrum (B) of BP-6-NHdG. An exception is the 569 cm^{-1} which is shifted from the 560 cm^{-1} mode by 9 cm^{-1}. Nevertheless, distinction between these two compounds in a mixture would generally not be possible. Consequently a chromatographic pre-separation is required for resloution. The electron-phonon coupling strength of the above two compounds (as well as other model adducts, *vide infra*), are different from that of B[a]P. The FLN spectrum of B[a]P is basically dominated by narrow ZPLs which are well resolved. The ZPLs of the above adducts and BP-6-C8dG, BP-6-C8Gua, BP-6-N7Gua, and BP-6-N7Ade, are superimposed on a much broader fluorescence profile. The difference can be explained by the increased electron-phonon coupling of all model

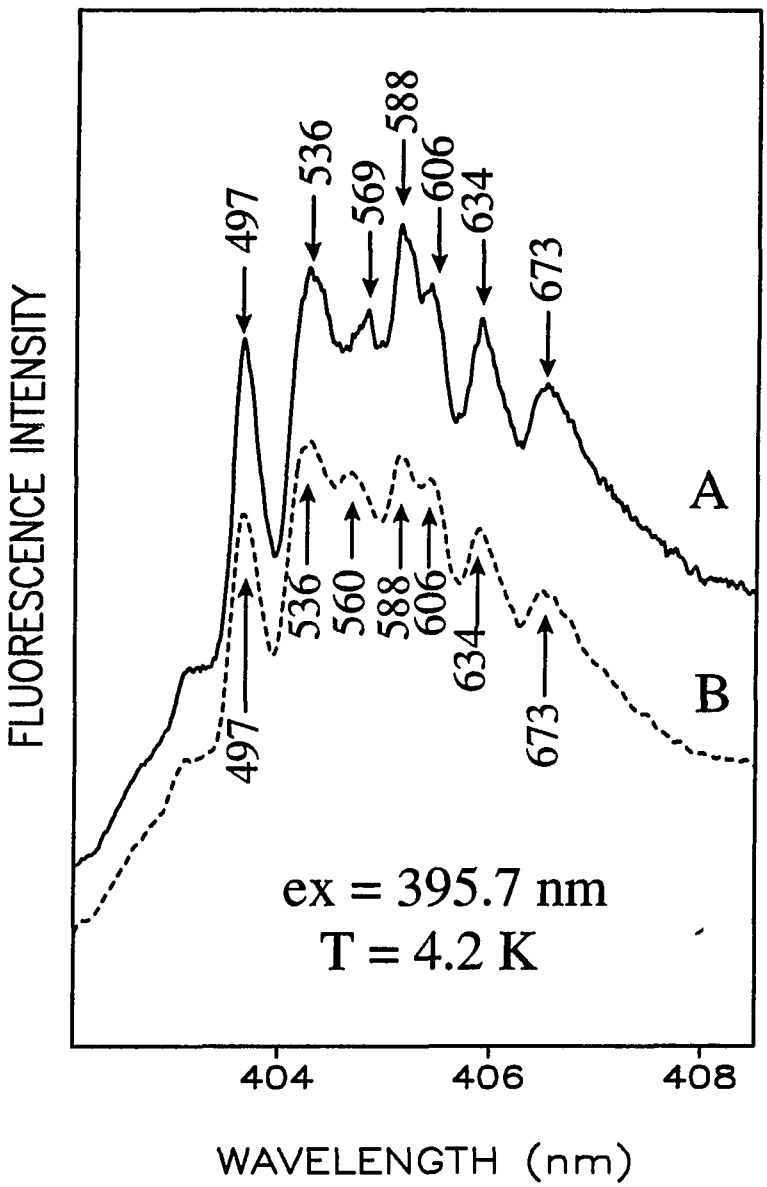

Figure 18. A comparison of FLN spectra of BP-6-N3dG (spectrum A) and BP-6-NHdG (spectrum B) obtained with λ_{ex} = 375.7 nm at 4.2 K. The excited state vibrational frequencies of two compounds are extremely similar

adducts compared to those of B[a]P, 6-methyl-B[a]P and 6-fluoro-B[a]P. This finding is in accord with the previous results [87] which show that the coupling strength increases with the size of the substituent at C6 of B[a]P. The excited state vibronic frequencies for both model adducts are listed in Table 1.

The FLN spectra of BP-6-C8dG, BP-6-C8Gua, and BP-N7Gua have previously been reported [150]. While B[a]P and these three model adducts were distinguishable, the resolution among three model adducts was not as straightforward, not only because of the structural similarity of the adducts but also because the spectra were broader and less well-resolved due to the increased linear electron-phonon coupling. The selectivity was, however, improved by the application of double spectral selection [150] which was discussed in the section II-C. The line-narrowed double selection FLN spectra of the above three adducts exhibited minor differences which were used to prove that a major depurination adduct from the binding of B[a]P to DNA in rat liver nuclei was BP-6-N7Gua [153]. The major adduct from metabolic activation of B[a]P by one-electron oxidation in the horseradish peroxidase catalyzed reaction of B[a]P with DNA (*in vitro*) was also identified as BP-6-C8Gua [153].

Quite recently the detection system of the prototype FLNS instrument has been improved by employing an OMA system from Princeton Instruments (see section III, experimental). The resulting improvement in the quality (S/N ratio) of the FLN spectra enable us to distinguish BP-6-C8Gua from BP-6-N7Gua. A comparison of the vibronically excited (λ_{ex} = 395.7 nm) FLN spectra of BP-6-N7Gua (spectrum A) and BP-

6-C8Gua (spectrum B) is presented in Figure 19. Portions of the FLN spectra from the two adducts obtained with λ_{ex} = 386.5 nm are also shown in the inset to this figure. Although the spectra are quite similar, there are important differences. For example, the 633, 671, and 1296 (inset) cm^{-1} modes are absent from the spectrum of BP-6-C8Gua. The relatively broad and weak band at ~406.5 nm in the spectrum B may be correspond to the 671 cm^{-1} mode, but it is relatively weak. Furthermore the 569 cm^{-1} mode of BP-6-N7gua shifts to 563 cm^{-1} for BP-6-C8Gua. Non-line narrowed 77 K spectra (not shown) indicate that the 0-0 origin band of BP-6-N7Gua is red-shifted by ~50 cm^{-1} relative to that of BP-6-C8Gua. This is consistent with the results of Figure 19 which show more intensity for the ZPL of BP-6-N7Gua corresponding to the higher frequency modes. The above differences are sufficient to allow for structure assignment of the two adducts when they are isolated by HPLC. However, the resolution of BP-6-C8Gua and BP-6-C8dG by FLNS is not possible due to the fact that deoxyribose group in the dG moiety is remote from the binding site (C6-position) of the B[a]P chromophore. On the other hand, the distinction between BP-6-C8Gua and BP-6-C8dG is rather straightforward by FAB MS/MS analysis [161].

A vibronically excited FLN spectrum of BP-6-C8dG (spectrum A) is shown in Figure 20. As mentioned above, the vibrational frequencies (determined with λ_{ex} = 386.5 nm) of BP-6-C8dG are extremely similar to those of BP-6-C8Gua shown in the inset (spectrum C) of the Figure 19. Specific regions of the standard FLN spectra for BP-6-N7Ade, obtained with laser excitation at 386.5 nm (spectrum B) and 395.7 nm (inset) are

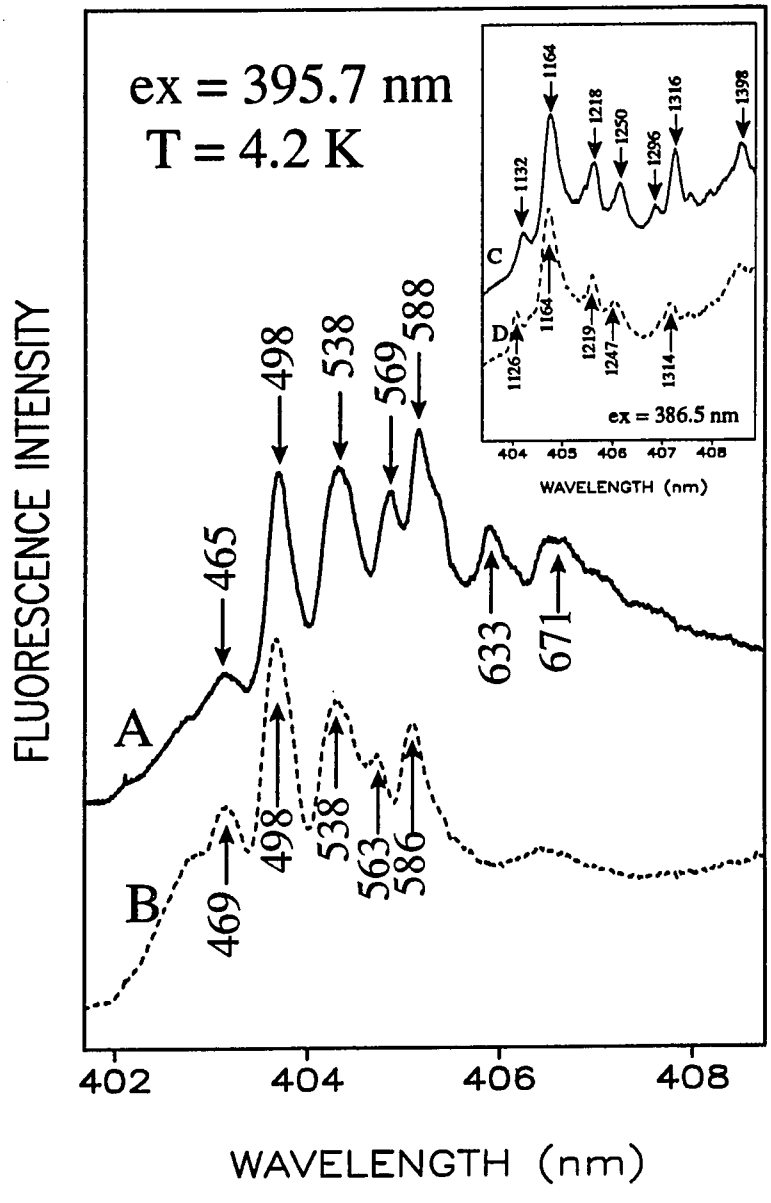

Figure 19. FLN spectra of BP-6-N7Gua (spectra A and C) and BP-6-C8Gua (spectra B and D). Spectra A and B were obtained with λ_{ex} = 395.7 nm, whereas spectra C and D were obtained with λ_{ex} = 386.5 nm

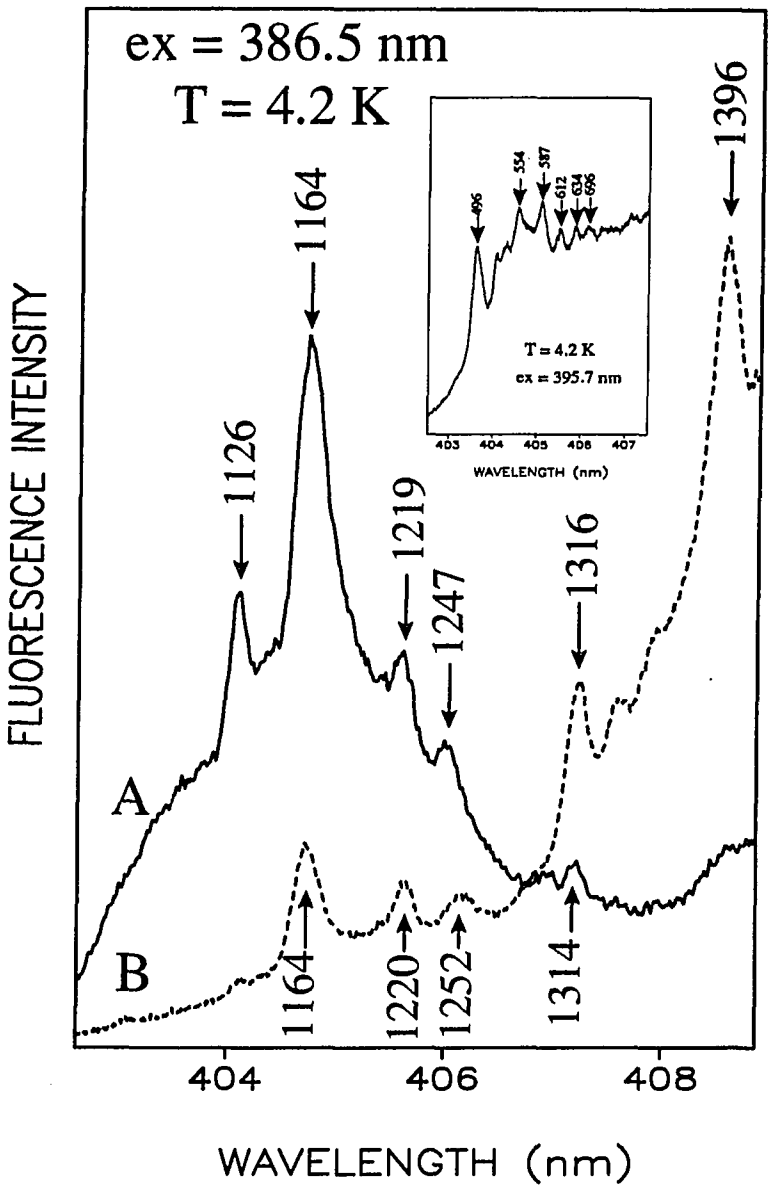

Figure 20. A comparison of the FLN spectra of BP-6-C8dG (spectrum A) and BP-6-N7Ade (spectrum B) obtained with λ_{ex} = 386.5 nm at 4.2 K. FLN spectrum for BP-6-N7Ade obtained with λ_{ex} = 395.7 nm is shown in the inset

also presented in Figure 20. A comparison of the vibrational frequencies (in the 1100 ~ 1400 cm^{-1} region) of BP-6-N7Ade (Table 1) shows that they are essentially identical to those of BP-C8Gua and/or BP-6-N7Gua. The ability of FLNS to distinguish convincingly between BP-N7Ade and Gua adducts rests on the fact that the 0-0 origin band of BP-6-N7Ade is red-shifted ~200 cm^{-1} compared to that of BP-6-N7Gua which, in turn, lies ~50 cm^{-1} to the red of the C8Gua analogue. This shift is clearly indicated in Figure 20 where the 0-0 origin band of BP-6-N7Ade is centered at 408~409 nm at the right edge of the frame. The S_1-state energy shifts are responsible for the distinct vibronic intensity distribution observed for each adduct for every vibronic excitation wavelength used [154].

2. Model compounds from BPDE

B[a]P is believed to be metabolically activated to ultimate carcinogens which induce the initial step of chemical carcinogenesis. In contrast to the carbenium ion formed by one-electron oxidation, B[a]P is metabolized to 7,8-dihydroxy-9,10-epoxy-7,8,9,10-tetrahydrobenzo[a]pyrene (BPDE) by enzymatic epoxydation and hydrolysis by cytochrome p-450 [38,42]. The structures of isomeric BPDEs are presented in Figure 3 with their acronyms. Each BPDE can undergo covalent bond formation with specific binding sites in macromolecular DNA, such as the exocyclic NH_2 of guanine and/or adenine and oxygen in guanine [27,152].

The vibronically excited FLN spectra of (+)-*anti-trans*- and (+)-*anti-cis*-BPDE-GMP (guanine monophosphate) in which BPDEs are bound at their C10-position to

exocyclic NH_2 of deoxyguanosine-5′-monophosphate (see Figure 14), are presented in Figure 21. These model adducts were supplied by Dr. N. Geacintov at Department of Chemistry, New York University. Laser excitation at 363.4 and 369.6 nm provide for optimum resolution between the *trans* and *cis* isomers. Since (+)-*anti*-BPDE is believed to be the most potent carcinogen of the four isomers and has strong tendency to react with exocyclic NH_2 of deoxygunosine base in DNA, BPDE-GMP model adducts are important for the study of the mutagenesis and carcinogenesis. Furthermore, the ability of FLNS to distinguish between interested adduct isomers can supply additional information on the configuration (e. g., *trans*- or *cis*-structure) of adducts formed in intact DNA.

Because the chromophores in both GMP-adducts are pyrenes formed by saturation of a bay-region ring of B[a]P, the 0-0 origin bands of BPDE-GMP (or DNA) adducts are centered at ~378 nm, far removed from ~405 nm, the location of the 0-0 origin band of B[a]P. The differences in vibronic frequencies and intensity distributions displayed in the 400-700 cm^{-1} region (Figure 21A), λ_{ex} = 369.6 nm, are quite spectacular. For the *trans* isomer, the relatively weak 453, 466, and 503 cm^{-1} modes are followed by a strong 578 cm^{-1} mode. On the other hand, the FLN spectrum of the *cis* isomer is dominated by three ZPLs. The 579 cm^{-1} mode of the *cis* isomer probably correlates with the 578 cm^{-1} mode of the *trans* isomer, but the *trans* isomer does not exhibit the pronounced 546 and 613 cm^{-1} modes. The *cis* adduct also exhibits modes at 891, 950, and 1027 cm^{-1} which are significantly different from the 957, 1005, and 1043 cm^{-1} modes of the *trans* adduct.

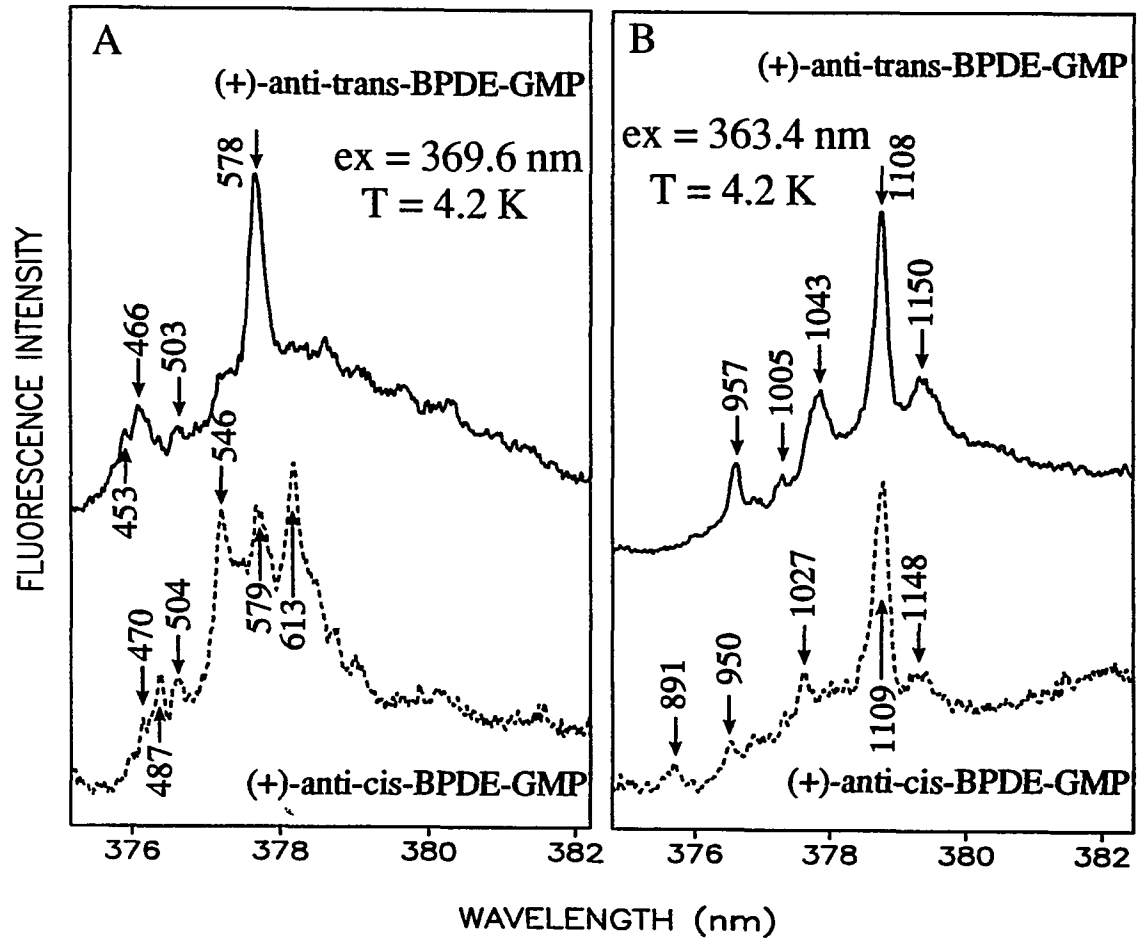

Figure 21. FLN spectra of (+)-*anti-trans*-BPDE-GMP (solid line) and (+)-*anti-cis*-BPDE-GMP (dashed line) obtained at 4.2 K with λ_{ex} = 369.6 nm (A) and 363.4 nm (B)

The more complete listing of excited state vibrational frequencies in Table 2 demonstate that modes at >1100 cm^{-1} are very similar for the two isomers. We note that FLNS cannot distinguish between enatiomers, as expected.

Other BPDE-type adducts expected from monooxygenation mechanism are BPDE-N7Gua, BPDE-N7Ade, and BPDE-NHdA for which the BPDEs are bound at their C10-position to the 7-position (N7) of guanine and adenine, and exocyclic NH_2 of deoxyadenine, respectively. These model adducts were prepared [170] and supplied by Dr. E. Cavalieri and coworkers at Eppley Institute for Research in Cancer and Allied Diseases, University of Nebraska Medical Center. In Figure 22, FLN spectra of these three model adducts obtained with laser excitation at 356.9 and 369.6 nm are shown. All model adducts of Figure 22 are a unknown composition of isomeric *trans*- and *cis*-configurations from covalent binding of specific binding sites in the nucleoside to the C10-position of *anti*- and *syn*-BPDE. The spectra are dominated by ZPLs for both excitations indicating that electron-phonon coupling is weak. We contrast first the FLN spectrum of BPDE-NHdA (spectrum c) with those of N7Ade (spectrum a) and N7Gua (spectrum b). The strong excited state vibrational frequencies of BPDE-NHdA at 482, 498, 540, 612, and 1533 cm^{-1} are either absent or relatively weak in the spectra of the other two adducts. Thus, BPDE-NHdA is readily distinguishable from BPDE-N7Ade and BPDE-N7Gua. Resolution between the latter two is more difficult presumably because of the structural similarity of their substituents and bacause binding is at N7 for both. Unlabeled ZPLs in spectrum b for BPDE-N7Gua have frequencies identical to those of

Table 2. Excited-state (S_1) vibrational frequencies (cm^{-1}) of BPT and BPDE model adducts expected from monooxigenation[a]

(+)-*anti*-*trans*-BPT	(+)-*anti*-*cis*-BPT	(±)-*syn*-*trans*-BPT	(±)-*syn*-*cis*-BPT	(+)-*anti*-*trans*-BPDE-GMP	(+)-*anti*-*cis*-BPDE-GMP	BPDE-N7Gua	BPDE-N7Ade	BPDE-NHdA
-	-	395	421	453	470	-	330	316
-	-	432	444	466	487	394	394	348
450	-	453	462	503	504	470	470	381
468	464	-	-	578	546	-	495	423
-	481	481	-	957	579	506	504	465
503	497	498	498	1005	613	541	543	482
-	540	516	560	1043	891	578	580	498
577	561	552	570	1108	950	608	606	540
-	578	-	865	1150	1027	957	957	558
-	-	-	-	1388	1109	1005	1009	581
-	894	909	-	1444	1148	1044	1045	612
-	-	-	-	1521	1392	-	1079	862
956	934	952	954	1561	1452	1110	1110	892
-	955	1034	1034	1602	1528	1385	1385	950
1109	1029	1110-	1110		1561	1442	1442	976
1385	1112	1382	1379		1609	1464	1466	1025
1406	1387	1401	1404			1504	-	1108
1440	1406	1440	1440			1518	1518	1385
1500	1443	1499	1499			1561	1561	1442
1559	1518	1518	1523			1603	1603	1521
	1560	1558	1558					1553

a. excitation wavelengths used: for BPT and isomeric (+)-*anti*-BPDE-GMP 356.9, 363.4, and 369.6 nm; for model adducts from monooxigenation 356.9, 363.4, 369.6, and 371.4 nm.

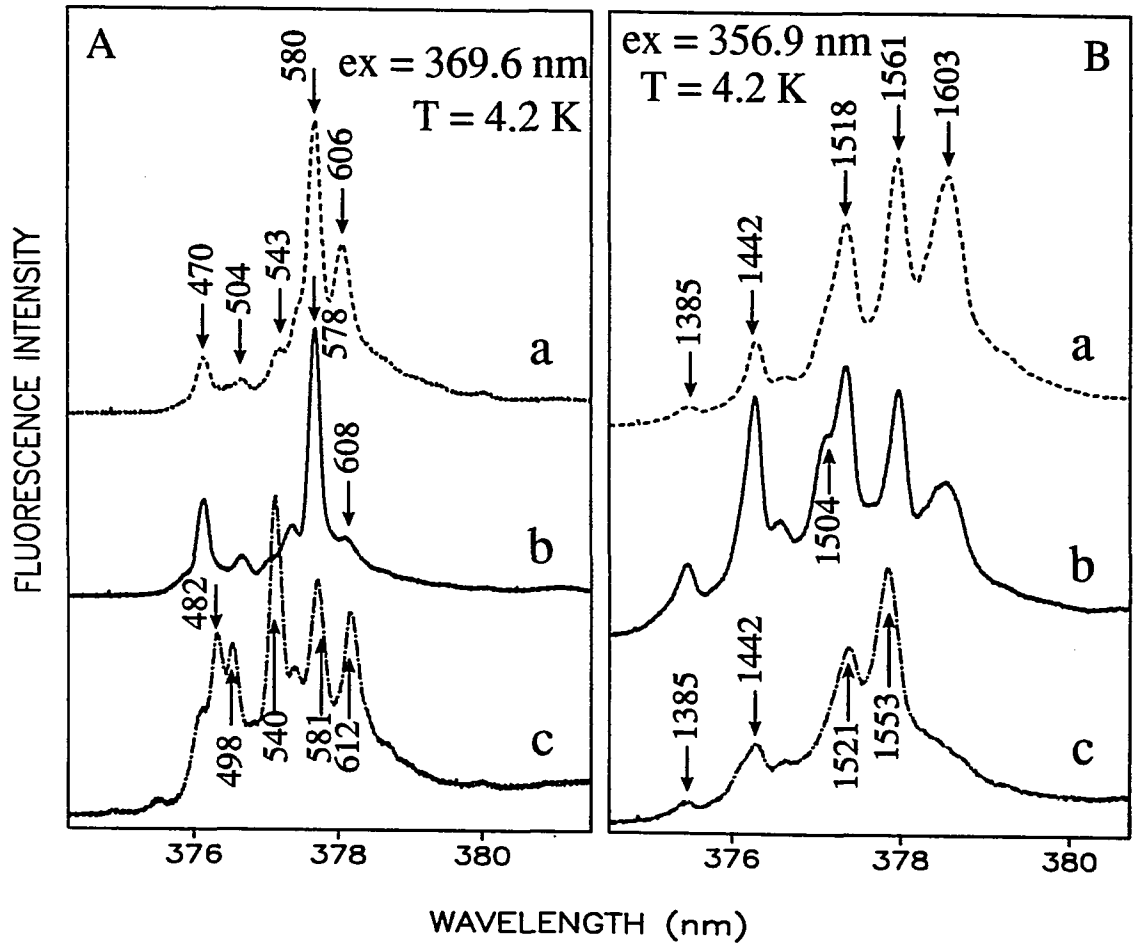

Figure 22. FLN spectra of synthesized BPDE-N7Ade (spectrum a), BPDE-N7Gua (spectrum b), and BPDE-NHdA (spectrum c) obtained with λ_{ex} = 369.6 (A) and 356.9 nm (B). Unlabeled peaks in spectrum b have frequencies identical to those of the corresponding bands in spectrum a

the corresponding labeled bands of spectra a. The 606 cm^{-1} mode of BPDE-N7Ade (spectrum a) is noteworthy because it is considerably stronger than the 608 cm^{-1} mode of N7Gua. Turning to the spectra in Figure 22B, one can observe a shoulder at 1504 cm^{-1} for BPDE-N7Gua which is far more pronounced than for BPDE-N7Ade. These slight differences suffice for distinction between the two adducts.

3. FLN spectra of isomeric BPTs

As discussed previously, isomeric BPDEs from the monooxygenation pathway are believed to be important electrophiles for the initiation of tumor induction. However, the diol epoxides are generally not isolable due to the facile reactions with water and other nucleophiles in biological systems. Consequently, the implication of BPDEs in tumor initiation step is evidenced only by the covalent DNA adducts they form and, less convincingly, by their hydrolysis products, 7,8,9,10-tetrahydro-7,8,9,10-tetrahydroxybenzo[a]pyrene (BPT). Spectroscopic studies of the reaction of *anti*-BPDE with calf thymus DNA have demonstrated that BPDE is rapidly intercalated into the base pairs of DNA [28,155]. The intercalated complex is characterized by a 10 nm red-shift in its UV absoption maximum and its negative linear dichroism spectrum. The intercalated BPDE is then subjected under rate-determining protonation to yield an intercalated triol carbonium ion intermediate which undergoes decomposition into two different products. The major process, which accounts for >90% of BPDE products, is hydrolysis to yield tetrols which can still remain in the DNA double helix. The second process, which is biologically more important is covalent binding to specific sites of

DNA bases. Since the BPTs are major decomposition products from BPDE, it is extremely important to be able to distinguish between the FLN spectra of physically adducted and "free" tetrols from those of BPDE-base covalent adducts. Two structural isomeric (*trans* and *cis*) tetrols may be formed from each BPDE; the structures of all the BPT isomers are shown in Figure 14. FLNS studies have been successfully performed on a racemic mixture of BPT (probably from *anti*-BPDE). It has also been demonstrated that FLNS is also operative for and can resolve the following compounds in a mixture: 1,2,3,4-tetrahydro-1,2,3,4-tetrahydroxybenz[a]anthracene, 8,9,10,11,tetrahydro-8,9,10,11-tetrahydroxybenz[a]anthracene, 1,2,3,4-tetrahydro-1,2,3,4-hydroxy-5-methylcrysene, 1,2,3,4-tetrahydro-1,2,3,4-tetrahydroxycrysene, 4,5-dihydro-4,5-dihydroxy-9-methoxybenzo[a]pyrene, and BPT [149]. The BPTs studied in this dissertation were supplied by Dr. N. Geacintov at Department of Chemistry, New York University.

High resolution FLN spectra of BPTs are now presented and discussed. Figure 23 presents FLN spectra of (+)-*anti-trans*-BPT and (+)-*anti-cis*-BPT imbedded in a glass matrix (devoid DNA), obtained with laser excitation at 363.4 (B) and 369.6 nm (A). As was the case for BPDE-GMP (*vide supra*), their enantiomeric (-)-*anti*-counterparts follow exactly identical FLN spectra, as expected. The 0-0 origin bands of the above tetrol isomers are centered at ~376.5 nm which is a significant blue shift relative to the 0-0 bands of the model BPDE adducts considered earlier, which are at ~378 - 378.5 nm (determined from 77 K non-line narrowed fluorescence spectra). Careful comparison of the FLN spectrum of (+)-*anti-trans*-BPT with that of (+)-*anti-trans*-BPDE-GMP (Fig. 21)

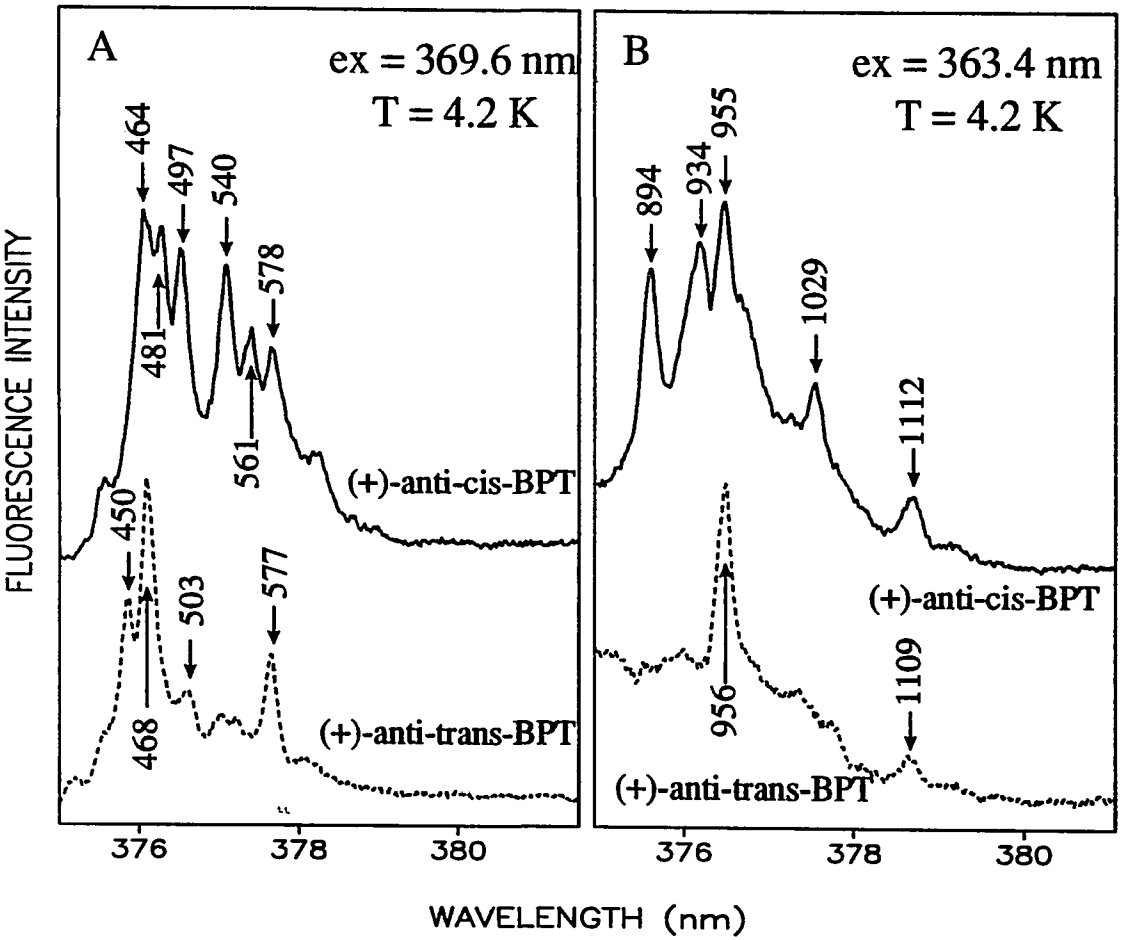

Figure 23. A comparison of the FLN spectra of (+)-*anti-cis*-BPT (solid line) and (+)-*anti-trans*-BPT (dashed line) obtained at 4.2 K with λ_{ex} = 369.6 (A) and 363.4 nm (B)

shows that excited state vibronic frequencies are essentially identical. Even though the vibronic frequencies of the most intense modes of (+)-*anti-trans*-BPT are 468 (spectrum in Fig. 23A) and 956 cm^{-1} (spectrum in Fig. 23B) compared to 578 and 1108 cm^{-1} for (+)-*anti*-BPDE-GMP, Figures 21A and 21B, most modes of the tetrol have a counterpart in GMP adduct, *e.g.*, 450, 468, 503, 577, 956, 1109 cm^{-1} modes for the former versus 453, 466, 503, 578, 957, and 1108 cm^{-1} bands for the latter. The two weak peaks between the 956 and 1109 cm^{-1} bands in Figure 23B may correlate with the 1005 and 1043 cm^{-1} modes of (+)-*anti-trans*-BPDE-GMP, cf. Figure 21B. Similar arguments are applicable to (+)-*anti-cis*-BPT and its corresponding GMP adduct. That is, the 0-0 origin band of *cis* tetrol is characterized by ~2 nm blue-shift compared to that of *trans*- and/or *cis*-GMP, and most vibrational frequencies of the former can be correlated with frequencies of the latter.

FLNS possesses the potential to distinguish between *anti-trans*-, *anti-cis*-, *syn-trans*-, and *syn-cis*-BPT. Vibronically excited FLN spectra of all four tetrols are given in Figures 23 and 24 for *anti*- and *syn*-BPT, respectively. All spectra are dominated by well-resolved narrow ZPLs which are labeled with their excited state vibrational frequencies in cm^{-1} (see Table 2). For these tetrols three different excitation wavelengths were employed. Only the results from 363.4 and 369.6 nm excitation, for which optimum differences are obtained, are presented in frames A and B of both figures. The spectra show that FLNS can be used to distinguish between all hydrolysis products (BPTs) of the BPDE.

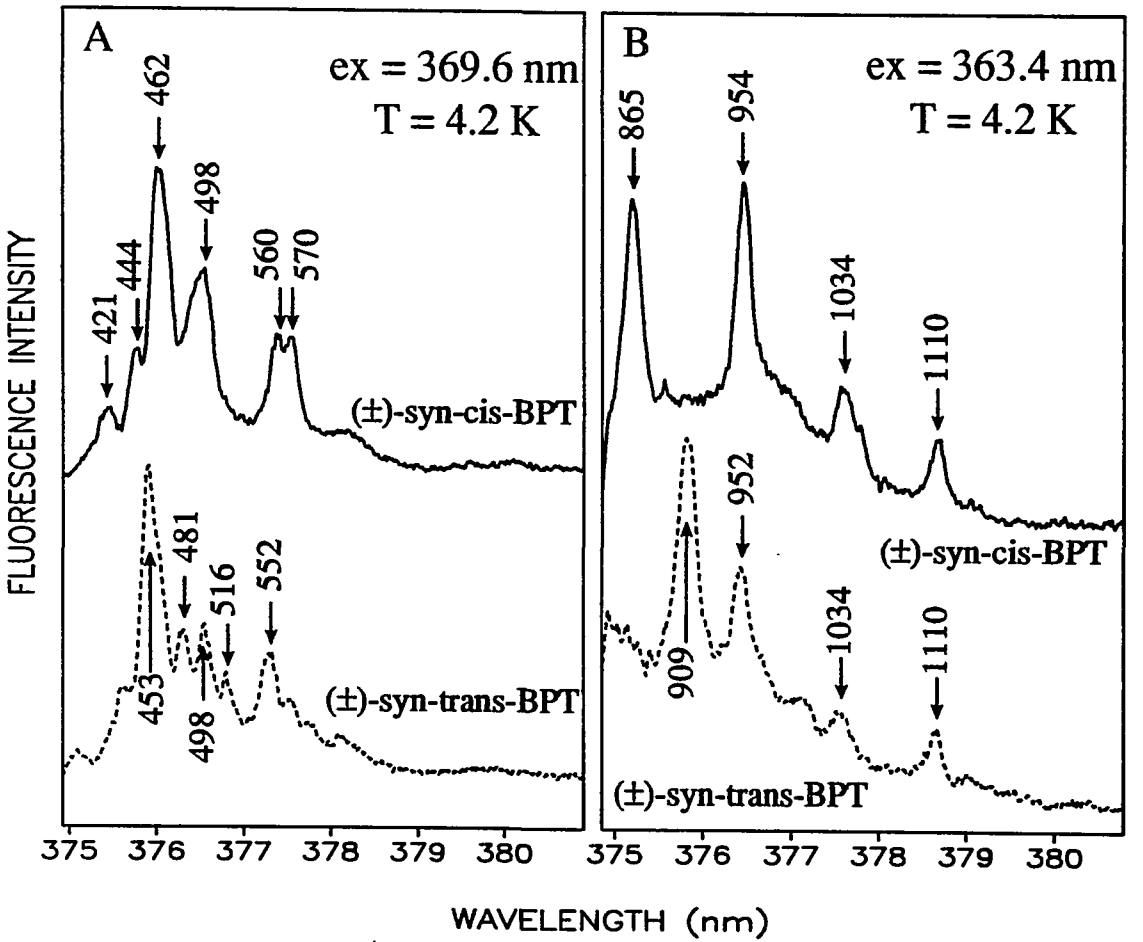

Figure 24. A comparison of the FLN spectra of (±)-*syn-cis*-BPT (solid line) and (±)-*syn-trans*-BPT (dashed line) obtained at 4.2 K with λ_{ex} = 369.6 (A) and 356.9 nm (B)

4. Model compounds from 7,12-DMBA

7,12-Dimethylbenz[a]anthracene (7,12-DMBA) which is being widely employed in animal model tumor studies, is one of the most potent chemical carcinogens ever examined [156]. It has been demonstrated that both monooxygenation [157,158] and one-electron oxidation [80] are involved in the enzymatic metabolism (depending on the experimental conditions) of 7,12-DMBA. Although data are much less complete than for B[a]P, resting primarily on comparison of the relative mutagenicities and tumorigenicities of the parent carcinogen and/or isomeric procarcinogens. The electrochemical synthesis [159] of 7,12-DMBA model adducts, therefore, provides not only a demonstration of the specific reactivity of nucleosides and 7,12-DMBA under oxidizing conditions, but is also a source of necessary reference materials for studying the 7,12-DMBA-DNA adducts formed in biological systems. Furthermore, the analytical application of FLNS to model adducts is essential for *in vivo* studies of 7,12-DMBA-DNA adducts. One-electron model adducts from 7,12-DMBA studied in this dissertation were prepared [159] and supplied by Dr. E. Cavalieri and coworkers at Eppley Institute for Research in Cancer and Allied Diseases, University of Nebraska Medical Center.

FLNS can be employed to distinguish between nucleoside adduction at the 7-CH_3 and 12-CH_3 groups of 7,12-DMBA and, furthermore, to determine whether attachment of 7,12-DMBA occurs at the C8- or N7-positions of guanine and to the N7- or N3-positions of adenine. All of the 7,12-DMBA-nucleoside adducts studied aggregate in the glass solvent at room temperature, as well as in the glass at low temperatures. Although

aggregate formation at room temperature can be eliminated by dilution, it was found that aggregates persisted in the glass for concentration as low as 10^{-8} M. Apparently, the stabilization energy of n-solvated monomers is less than that of a solvated aggregate of n-monomers near the glass transition temperature [160]. The fluorescence from aggregate for all adducts is substantially red-shifted and very broad relative to that of the monomer. Spectra A and B in Figure 25 present 77 K non-line narrowed fluorescence spectra of 7,12-DMBA at two different concentrations. The fluorescence origin bands for the monomer and aggregate are centered at ~403 and ~408 nm, respectively, and, thus some spectral discrimination is possible. At the higher concentration (spectrum A), however, the two origin bands are convolved with each other to form an unresolved broad single band. Therefore, one expects that FLN would be observed under excitation conditions that selects significant population of the S_1 state of the monomer. The FLN spectrum of 7,12-DMBA in the inset of the figure (obtained with λ_{ex} = 392.8 nm) shows relatively broad ZPLs in the vicinity of ~402 nm. Fortunately, the aggregate fluorescence lifetime is considerably shorter than the monomer fluorescence lifetime of ~130 nsec. For this reason, a 50-150 nsec delay time for observation window was employed to reduce further the interference from aggregate fluorescence to the structured FLN spectra of the monomer. Only the most highly resolved FLN spectra of the electrochemically synthesized 7,12-DMBA adducts are presented here. These standard FLN spectra are essential for *in vitro* and *in vivo* studies of 7,12-DMBA adducts formed by the one-electron oxidation pathway.

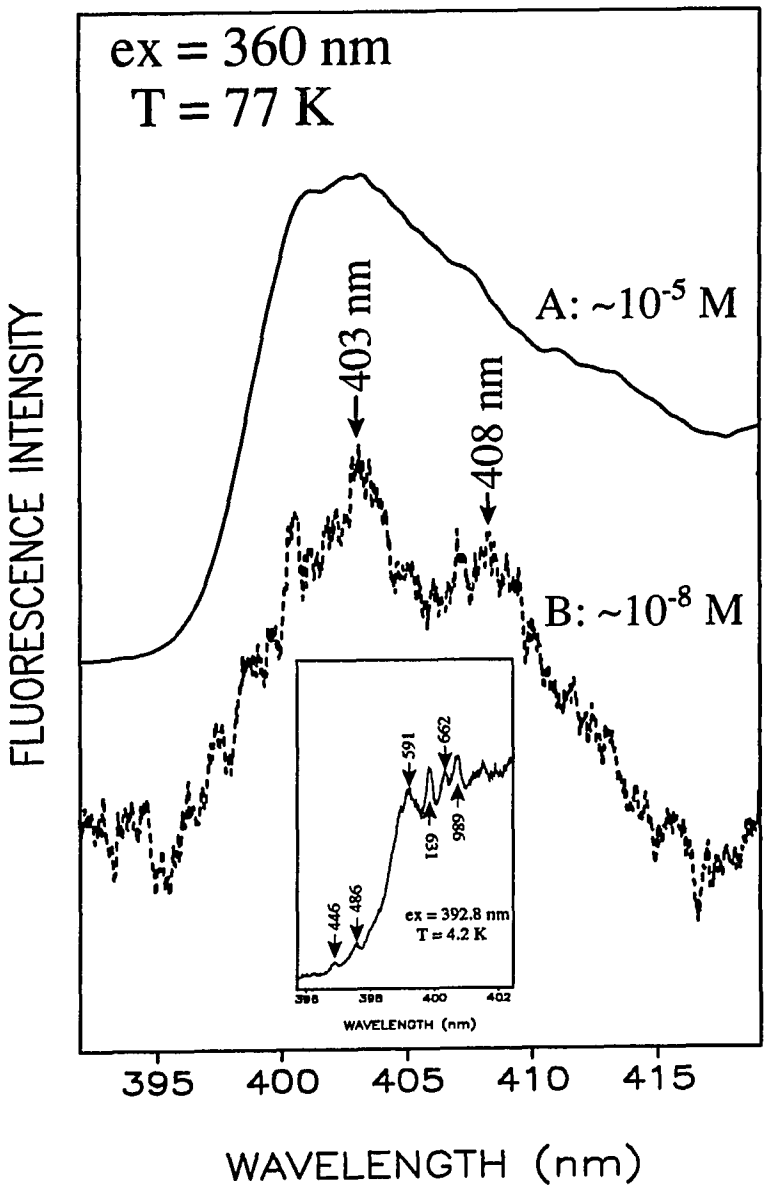

Figure 25. Origin bands of the 77 K laser-excited fluorescence spectra of 7,12-dimethylbenz[a]anthracene in concentration of ~$1x10^{-5}$ M (spectrum A) and ~$1x10^{-8}$ M (spectrum B). Spectrum B of lower concentrated 7,12-DMBA clearly shows distinct band from aggregate centered at ~408 nm

H_4DMBA for which a bay region ring is saturated, also forms aggregates in glass at low temperature. However, it seems that it does so to a greater degree than 7,12-DMBA, cf. Figure 26. At a concentration of ~10^{-6} M (spectrum B), only a small fraction of H_4DMBA exists as monomer which yields the ZPLs at ~409 nm. Thus, one can only generate FLN with laser excitation that lies to the blue of ~409 nm, consistent with the observation that the FLN spectrum in the inset exhibits partially resolved ZPLs superimposed on a broad band. However, the formation of aggregates can be avoided by employing $CDCl_3$ as the matrix. Figure 27 presents a series of highly resolved line-narrowed fluorescence spectra of H_4DMBA in $CDCl_3$, obtained with three different excitations. Rather than forming aggregates, H_4DMBA occupies as many as three distinct sites in the polycrystalline $CDCl_3$ matrix at low temperature. All sites are excited by the three excitation wavelengths employed, and, thus, identical spectra are observed. Nevertheless, the intensity distributions are different for the three spectra of Figure 27, providing that the excitation probabilities of the three sites depend on the excitation wavelength.

Segments of the FLN spectra of 12-MBA-7-CH_2-N7Gua (spectrum A) and of 7-MBA-12-CH_2-N7Gua (spectrum B) are presented in Figure 28. These vibronically excited spectra were obtained with λ_{ex} = 390 nm. The line-narrowed bands for both adducts (monomer), which are labeled according to their excited state (S_1) vibrational frequencies in cm^{-1}, are superimposed on the high energy tail of the broad aggregate fluorescence discussed above. Although the FLN spectra of 12-MBA-7-CH_2-N7Gua and

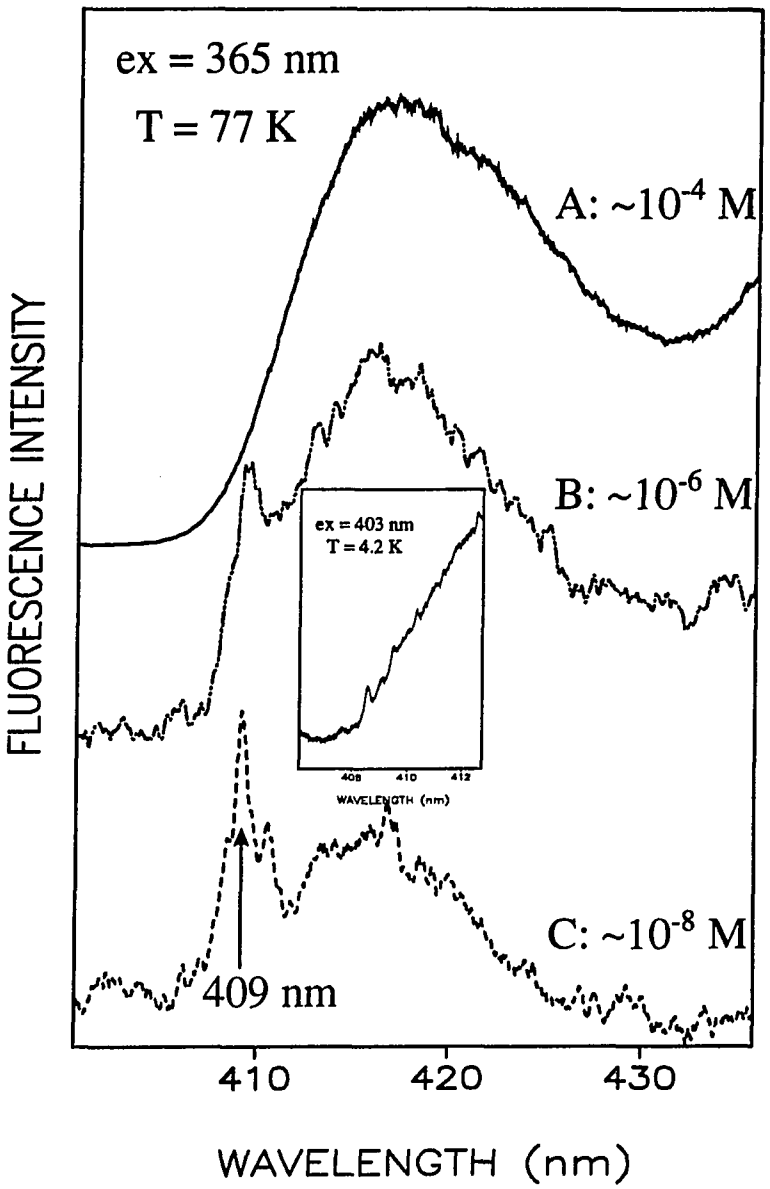

Figure 26. Origin bands of the 77K laser-excited fluorescence spectra of H_4DMBA at a concentration of ~1x10^{-4} M (spectrum A), ~1x10^{-6} M (spectrum B) and ~1x10^{-8} M (spectrum C). FLN spectrum obtained with λ_{ex} = 403 nm (inset) shows that line-narrowing is obtainable only ~409 nm where the origin band of the monomer is located

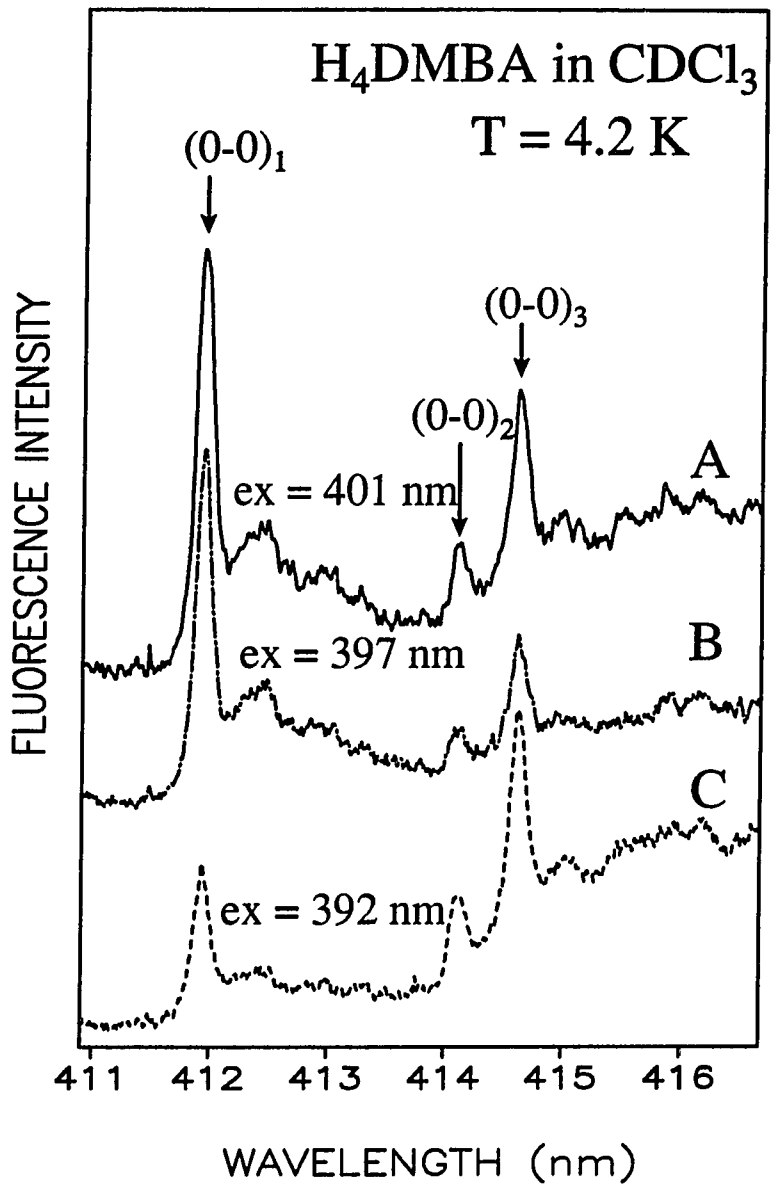

Figure 27. Low temperature fluorescence spectra of H_4DMBA in $CDCl_3$ obtained with λ_{ex} = 401 nm (spectrum A), 397 nm (spectrum B) and 392 nm (spectrum C). H_4DMBA is dispersed in at least three different sites of polycrystalline structure of $CDCl_3$ indicated by three well resolved (0-0) lines

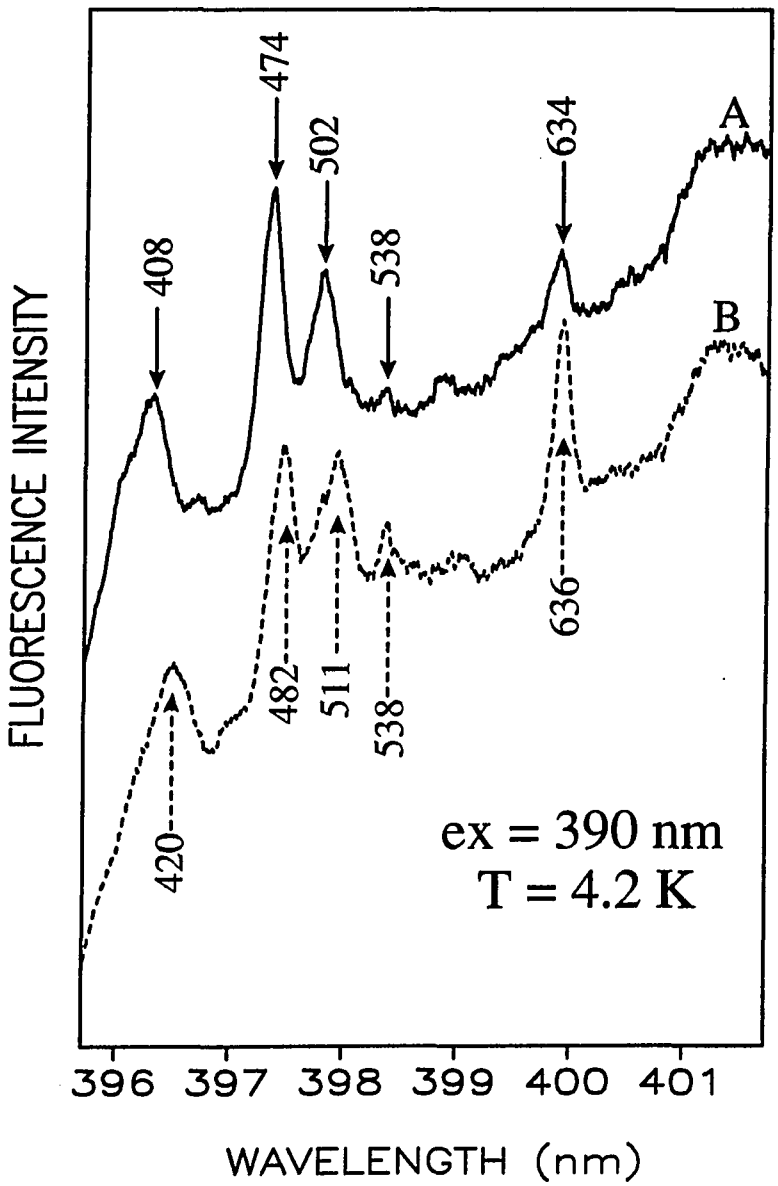

Figure 28. Vibronically excited FLN spectra of 12-MBA-7-CH_2-N7Gua (spectrum A) and 7-MBA-12-CH_2-N7Gua (spectrum B) obtained at T = 4.2 K with λ_{ex} = 390 nm

7-MBA-12-CH_2-N7Gua are quite similar, significant differences in vibrational frequencies are observed (*e.g*, 408, 474, 502 cm^{-1} for the former versus 420, 482, and 511 cm^{-1} for the latter). More complete listings of vibrational frequencies obtained from Figure 28 and other FLN spectra are given as the fifth and fourth columns of Table 3. For comparison, the corresponding frequencies for 7,12-DMBA are listed in the first column.

The spectra of Figure 28 and others obtained with different λ_{ex}-values indicate the S_1 state of 7-MBA-12-CH_2-N7Gua lies ~100 cm^{-1} lower in energy than that of 12-MBA-7-CH_2-N7Gua. This explains why the vibronic intensity distributions of spectra A and B of Figure 28 are significantly different (e. g., note that the 636 cm^{-1} signal is considerably more intense in spectrum B than in spectrum A). Thus, these two N7Gua adducts can be distinguished on the basis of vibronic frequencies and the intensity distribution. This is only possible for a binary mixture when the concentrations of the two adducts are comparable.

The FLN spectra for the 7-MBA-12-CH_2-N7Gua, 7-MBA-12-CH_2-C8Gua and 7-MBA12-CH_2-C8dG adducts obtained with λ_{ex} = 390 nm are shown in Figure 29, spectra A-C, respectively. Portions of the FLN spectra for the former two adducts obtained with λ_{ex} = 392.8 nm are shown in the inset to this figure. Comparison of the spectra for 7-MBA-12-CH_2-N7Gua and 7-MBA-12-CH_2-C8Gua reveals that these two adducts can be distinguished on the basis of the FLN spectral shifts of the 355 cm^{-1} (Fig. 29D) and 482 cm^{-1} (Fig. 29A) modes of the former adduct to 343 cm^{-1} (Fig. 29E) and 477 cm^{-1} (Fig.29B) for 7-MBA-12-CH_2-C8Gua. The 7-MBA-12-CH_2-C8Gua (Fig. 29B) cannot,

Table 3. Excited-state (S_1) vibrational frequencies (cm^{-1}) of 7,12-DMBA and its adducts formed with dG and dA by electrochemical oxidation [a]

7,12-DMBA	7-MBA-12-CH_2-C8dG	7-MBA-12-CH_2-C8Gua	7-MBA-12-CH_2-N7Gua	12-MBA-7-CH_2-N7Gua	7-MBA-12-CH_2-N7Ade	12-MBA-7-CH_2-N3Ade
-[b]	220	220	220	221	221	221
267	271	270	273	267	273	267
321	311	310	311	309	311	310
373	347	343	355	w	360	355
393	w[c]	w	w	w	398	w
446	421	420	420	408	426	409
486	477	475	482	474	478	472
515	513	511	511	502	510	499
591	538	538	538	538	537	w
631	636	632	636	634	634	638
662	-	-	-	-	710	-

a. excitation wavelengths used for 7,12-DMBA and all adducts 390 and 392,8 nm.

b. not observed

c. very weak

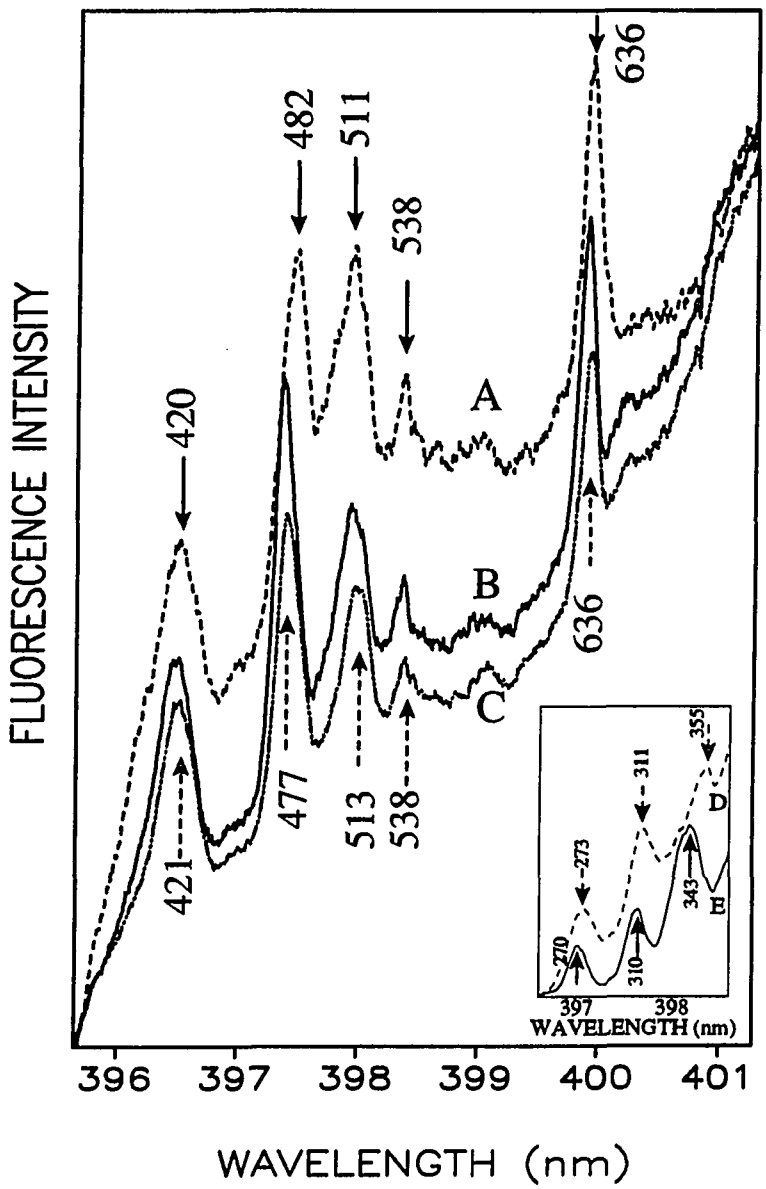

Figure 29. FLN spectra of 7-MBA-12-CH_2-N7Gua (spectrum A and insert D), 7-MBA-12-CH_2-C8Gua (spectrum B and inset E) and 7-MBA-12-CH_2-C8dG (spectrum C) obtained at 4.2 K with λ_{ex} = 390 nm

however, be differentiated from 7-MBA-12-CH_2-C8dG (Fig. 29C). This is also the case for the C8Gua and C8dG one-electron oxidation adducts of B[a]P [153]. The vibrational frequencies for 7-MBA-12-CH_2-C8Gua are listed in Table 3, column 3.

The FLN sepctra for the 12-MBA-7CH_2-N3Ade and 7-MBA-12-CH_2-N7Ade adducts are compared in Figure 30, spectra A and B, respectively. The vibrational mode frequencies for these two adducts are strikingly different, as are the vibronic intensity distributions. Thus, their differentiation by FLNS is straightforward. Their vibrational frequencies are given in the last two columns of Table 3. Therefore, all of these model adducts formed can be distinguished by FLNS.

B. Identification of BP-6-N7Gua in the Urine and Feces of Rat Treated with B[a]P

When B[a]P is activated by one-electron oxidation to its radical cation, B[a]P binds through its C6-position to the C8-position of dG, forming BP-6-C8dG. This adduct, which is relatively stable in DNA, has been identified *in vitro* [161]. B[a]P radical cation also forms an adduct with N7-position of guanine (BP-6-N7Gua). This adduct is rapidly lost from DNA by depurination. It represents at least 75% of the B[a]P adducts formed in the binding of B[a]P to DNA mediated by horseradish peroxidase [161]. It is also predominant in the cytochrome P-450 catalyzed binding of B[a]P to DNA with rat liver microsomes or nuclei [162].

Modification of the N7-position of guanine in DNA with a number of carcinogens results in products that depurinate spontaneously, leaving an apurinic site. The released

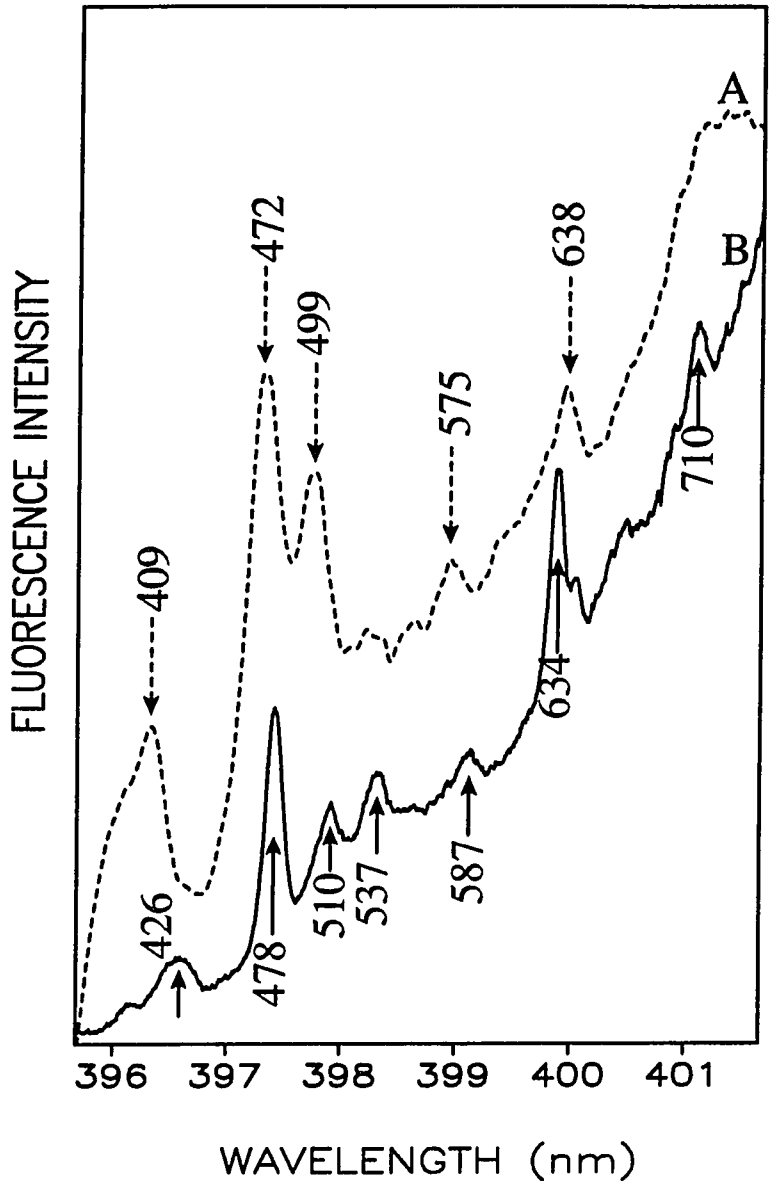

Figure 30. FLN spectra of 12-MBA-7-CH_2-N3Ade (spectrum A) and 7-MBA-12-CH_2-N7Ade (spectrum B) obtained at T = 4.2 K with λ_{ex} = 390 nm

products have been detected in urine. 7-Methylguanine was detected in the urine of rats treated with dimethylnitrosamine [163], and 2,3-dihydro(7-guanyl)-3-hydroxyaflatoxin B_1 was detected in the urine of rats treated with aflatoxin B_1 [164]. Autrup and Seremet reported the presence of the putative BPDE-N7Gua adduct in the urine of rats treated with B[a]P [165]. This is presumably the same adduct detected by Tiemey *et. al.* in mice and rats [166].

Because the BP-6-N7Gua adduct is very abundant in the binding of B[a]P to DNA catalyzed *in vitro* by horseradish peroxidase and cytochrome P-450, it is very interesting to identify BP-6-N7Gua as a one-electron oxidation adduct from rat feces and urine after treatment with B[a]P by intraperitoneal injection. The structure of the adduct is established by cochromatography with the synthesized BP-6-N7Gua adduct, UV absorbance spectrum, and fluorescence line narrowing spectrometry. A detailed description of experimental procedures are reported elsewhere [167]. Briefly, the unknown adduct coeluted with authentic BP-6-N7Gua was collected. The collected material was evaporated, redissolved in DMSO/CH_3OH (1:1), and further chromatographed on a CH_3CN/H_2O gradient by first eluting for 5 min with 20% CH_3CN in H_2O, followed by linear gradient to 100% CH_3CN at a flow rate of 0.8 mL/min. Identical procedures were employed for adducts from both excretions.

For FLNS analysis, ~5ng of each adduct obtained from the group of the groups of Drs. E. Cavalieri and E. Rogan at Eppley Institute for Research in Cancer, University of Nebraska Medical Center, was dissolved in ~10μl of DMSO followed by mixing with

~30μl of glycerol/water/ethanol (5:4:1) in quartz tube, cooled to 4.2 K, and probed with the laser in the (1,0) vibronic excitation region. The delay time for fluorescence measurement was 25 nsec, and the width of the observation window was 60 nsec. A specific region of vibronically excited FLN spectra, obtained with laser excitation at 386.5 nm, is presented in Figure 31 for (A) the synthesized BP-6-N7Gua adduct, (B) adduct from urine, and (C) adduct from feces. The structural conformation of two unknown adducts from both urine and feces is straightforward. Since the FLN spectrum of BP-6-N7Gua is very similar to that of BP-6-C8Gua and/or BP-6-C8dG (see Fig. 19), and BP-6-C8Gua is also likely depurinated (proved later in [81]), one should carefully compare those two spectra. Previously, it was shown that FLNS technique can distinguish between BP-6-N7Gua and its C8Gua analog based on a few mode differences such as 1296 cm^{-1} in the present figure. Apparently, spectra B and C from urine and feces show a relatively well resolved peak determined as 1296 cm^{-1}. Conclusively, the virtually indistinguishable spectra in Figure 31 indicate that the adduct which depurinated into the urine and feces of rat treated with B[a]P is BP-6-N7Gua. Additional support for this assignment is provided by FLN spectra obtained with other excitation wavelengths (not shown).

C. Identification of Benzo[a]pyrene-DNA Adduct Formed by Rat Liver Microsomes *in vitro*

Two DNA adducts of B[a]P have been reported to be formed *in vitro* in reactions catalyzed by cytochrome P-450. One is the stable adduct formed by reaction of the bay-

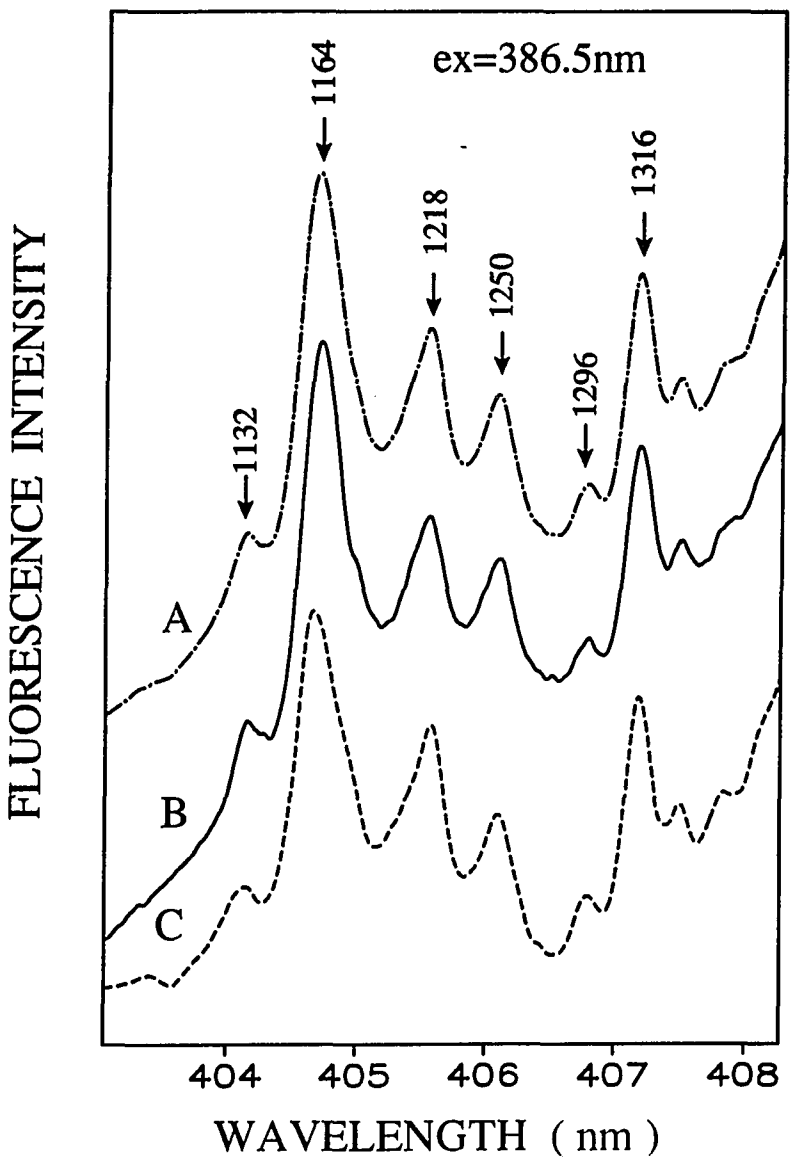

Figure 31. Comparison of the vibronically excited FLN spectra (λ_{ex} = 386.5 nm, T = 4.2 K) of (A) the synthesized BP-N7Gua adduct with adduct isolated from (B) urine and (C) feces. FLN peaks are labeled with their excited state vibrational frequencies (cm^{-1})

region diol epoxide of B[a]P at C10-position with the 2-amino of deoxyguanosine (BPDE-N_2dG) [38,168]; the second one is the adduct formed by reaction of B[a]P radical cation with the N7-position of guanine (BP-6-N7Gua), which is lost from DNA by depurination [162]. These two adducts have also been identified *in vivo*, BPDE-NHdG in mouse skin [169] and BP-6-N7Gua in the urine and feces of rats [167].

More recent experiments have revealed [81] that several new BP-DNA adducts are formed by the one-electron oxidation and the diol epoxide mechanism, namely B[a]P bound through C6-position to the C8-position of guanine (BP-6-C8Gua) and N7-position of adenine (BP-6-N7Ade) and BPDE bound through C10-position to the N7-position of adenine (BPDE-N7Ade) (see Figures 13 and 14). In addition, it is interesting to note that the BPDE-N7Gua adduct was not observed. The biological experiment was performed by Dr. E. Cavalieri's group of the Eppley Institute for Research in Cancer and Allied Diseases, University of Nebraka Medical Center, and summarized in separate [81]. The *in vitro* systems used to study DNA adduct formation were B[a]P activated by 3-methylcholanthrene (MC)-induced rat liver microsomes or horseradish peroxidase (HRP); B[a]P 7,8-dihydrodiol activated by microsomes, and direct reaction of BPDE with DNA. Authentic adducts used in these identification were synthesized and their structures were elucidated as described before [161,170].

Four depurinated B[a]P-DNA adducts formed by cytochrome P-450 in MC-induced rat liver microsomes were identified; BP-6-C8Gua, BP-6-N7Gua, BP-6-N7Ade, and BPDE-N7Ade. In the HRP system, however, only depurinated adducts from one-

electron oxidation were detected. Preliminary identification of these adducts was made by coelution with authentic adducts on high pressure liquid chromatography (HPLC) in two different solvent systems, namely CH_3OH/H_2O and CH_3CN/H_2O gradients. Proof of structure was obtained by spectroscopic comparison of their FLN spectra with those of the authentic adducts. Previously, it has been shown that FLNS possesses the selectivity to distinguish between model adducts (see section IV-A).

Identification of BP-6-N7Gua by FLN spectra was achieved with two different laser excitations, 395.7 nm (Figure 32A) and 386.5 nm (Figure 32B). The frequency ranges cover 400-700 cm^{-1} (spectrum A) and 1100-1400 cm^{-1} (spectrum B), the regions of greatest activity. In Figure 32, the FLN spectrum of the standard BP-6-N7Gua (spectrum a) is compared with that of adduct eluting at the same retention time with authentic BP-6-N7Gua from HRP-catalyzed (spectrum b) and the MC-induced microsome-catalyzed reaction (spectrum c). Spectra b and c are virtually indistinguishbale and are identical to the FLN spectra of the standard adduct (spectrum a). These FLN spectra are also identical to those of the BP-6-N7Gua adduct isolated from the urine and feces of rat treated with B[a]P (see Fig. 31) [167]. For both excitations, several strong ZPLs are observed, in which vibrational mode frequencies are significantly perturbed by the substitution of Gua at the N7-position, compare to the parent B[a]P chromophore. Each spectrum possesses vibrational frequencies at 633, 671, and 1296 cm^{-1} which are fingerprints for BP-6-N7Gua. These vibrational frequencies should be compared with those of Table 4 where a compilation of the excited state

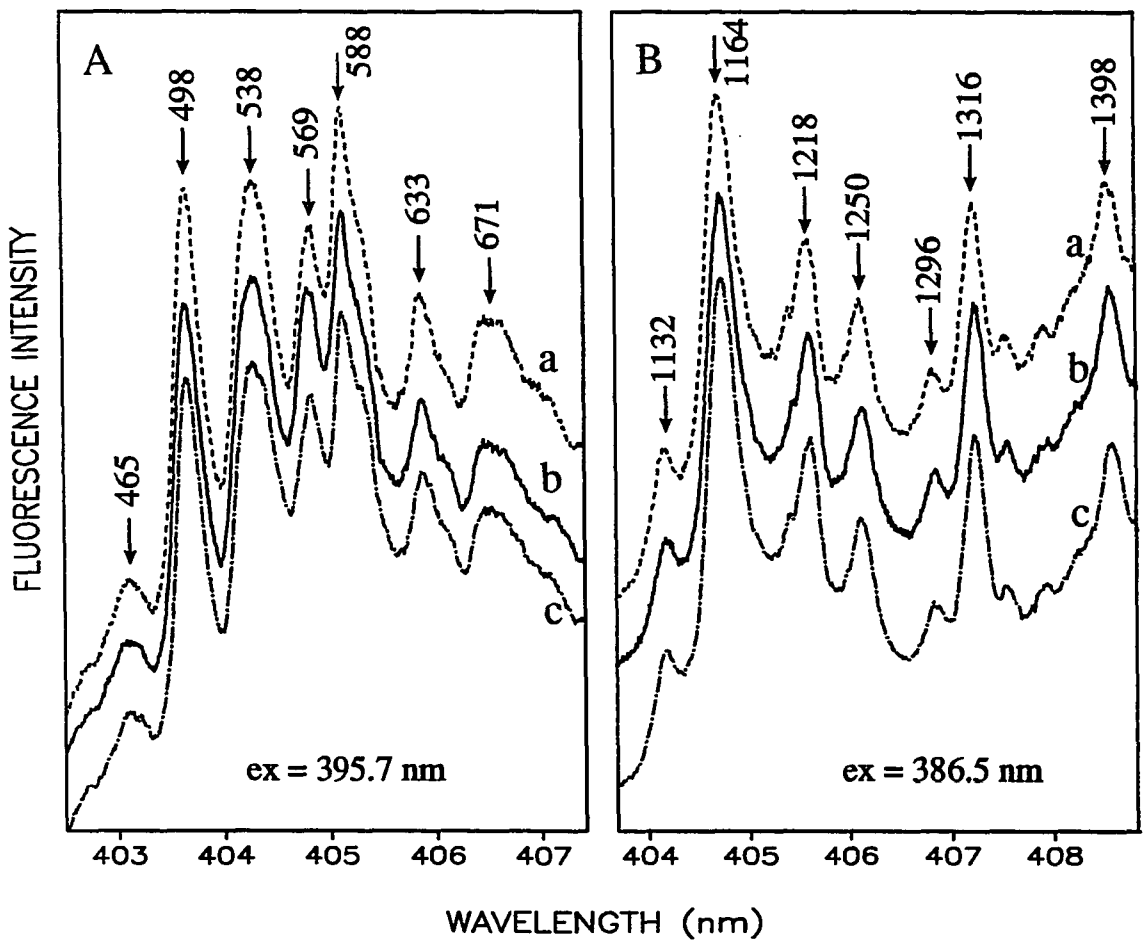

Figure 32. FLN spectrum of the synthesized BP-6-N7Gua (a) (excited with λ_{ex} = 395.7 (A) and 386.5 nm (B)) compared to the spectra of BP depurinated adducts from the HRP reaction (b) and microsomal reaction (c) which were separated by HPLC

Table 4. Excited-state (S_1) vibrational frequencies (cm^{-1}) of labile adducts from both one-electron oxidation and monooxygenation compared to vibrational frequencies of B[a]P and *anti-trans*-B[a]PT[a]

B[a]P	*anti-trans*-BPT	One-Electron Oxidation Adducts			Monooxygenation Adducts	
		BP-6-N7Gua	BP-6-C8Gua	BP-6-N7Ade	BPDE-10-N7Gua	BPDE-10-N7Ade
327 1009	450	465	469	-	394	394
376 1032	468	498	498	496	470	470
427 1063	577	538	538	-	-	495
449 1119	956	569	563	554	506	504
471 1133	1385	588	586	587	541	543
512 1179	1406	-[b]	-	612	578	580
549	1500	633	-	634	**608**[c]	**606**[c]
580	1559	671	-	-	957	957
624		1132	1126	1132	1005	1009
686		1164	1164	1164	1044	1045
750		1218	1219	1220	-	1079
789		1250	1247	1252	1110	1110
837		1296	-	-	1385	1385
912		1316	1314	1316	1442	1442
921		1398	-	1396	1464	1466
933					1504 (sh)[d]	-
954					1518	1518
973					1561	1561
					1603	1603

a. excitation wavelengths used: for one-electron oxidation adducts 386.5, 395.7 nm; for monooxygenation adducts and *anti-trans*-BPT 356.9, 363.4, 369.6 and 371.6 nm; for B[a]P 386.5, 392 and 393.8 nm.

b. not observed or very weak.

c. 608 and 606 cm^{-1} can be used to differentiate between BPDE-10-N7Gua and BPDE-10-N7Ade. The latter is pronounced while the former is weak (369.6 nm excitation).

d. pronounced shoulder which is barely discernible for BPDE-10-N7Ade. Can be used to distinguish between these two adducts.

vibrational frequencies for BP and the various adducts is presented.

Identification of BP-6-C8Gua was also obtained at excitation wavelengths of 395.7 nm (Figure 33A) and 386.5 nm (Figure 33B). As in Figure 32, these wavelengths were chosen to reveal mode structure in the 600 cm^{-1} and 1200 cm^{-1} regions. Spectra a in Figure 33A and B were chosen to reveal mode structure of the standard BP-6-C8Gua adduct and are identical to the FLN spectra reported earlier [153]. The strongest mode in spectrum A is now 498 cm^{-1} compared to 588 cm^{-1} in Figure 32A, indicating a small blue-shift as evident from Figure 19. Spectrum b, from HRP-catalyzed binding of B[a]P to DNA, and spectrum c, from MC-induced microsome-catalyzed binding, exhibit characteristic modes such as 469, 563, 586, and 1126 cm^{-1} which are exactly identical to spectrum a. These data, along with coelution with authentic adduct on HPLC, demonstrate that this adduct is BP-6-C8Gua.

The major adduct was identified as BP-6-N7Ade. A specific region of the standard FLN spectra, obtained with laser excitation at 386.5 nm is presented in Figure 34 for (a) the authentic BP-6-N7Ade standard, (b) the adduct from the HRP-catalyzed binding and (c) the adduct from the microsomal reaction. Spectra b and c which are red-shifted ~200 cm^{-1} compared to those of previous two adducts, are virtually indistinguishable from spectrum a, and it is apparent that the adduct formed by HRP or microsomes is BP-6-N7Ade. Additional support for this assignment (and others) is provided by FLN spectra obtained with other excitation wavelengths (data not shown). Conclusively, from the FLN spectra discussed above (and others obtained with different

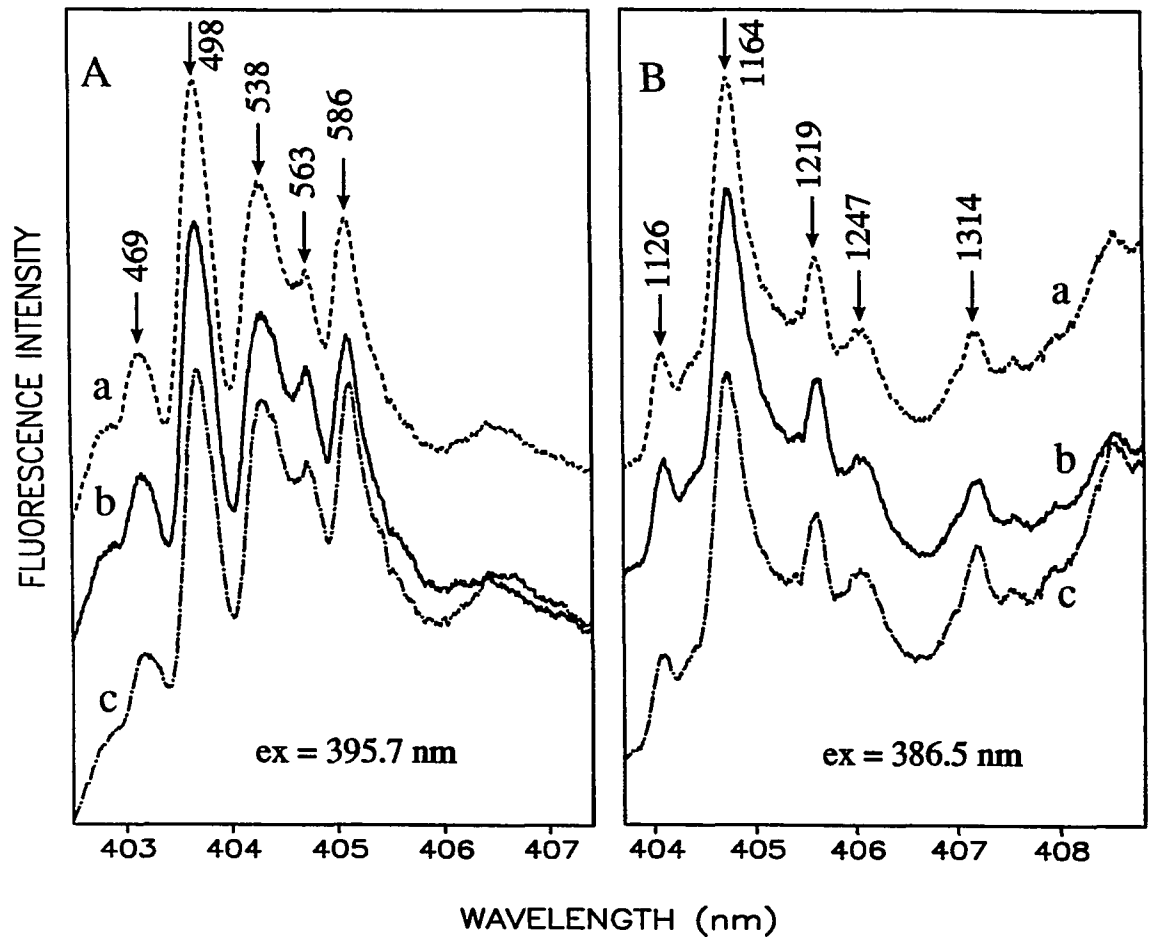

Figure 33. FLN spectrum of the synthesized BP-6-C8Gua (a) (excited with λ_{ex} = 395.7 (A) and 386.5 nm (B)) compared to the spectra of BP depurinated adducts from the HRP reaction (b) and microsomal reaction (c) which were separated by HPLC

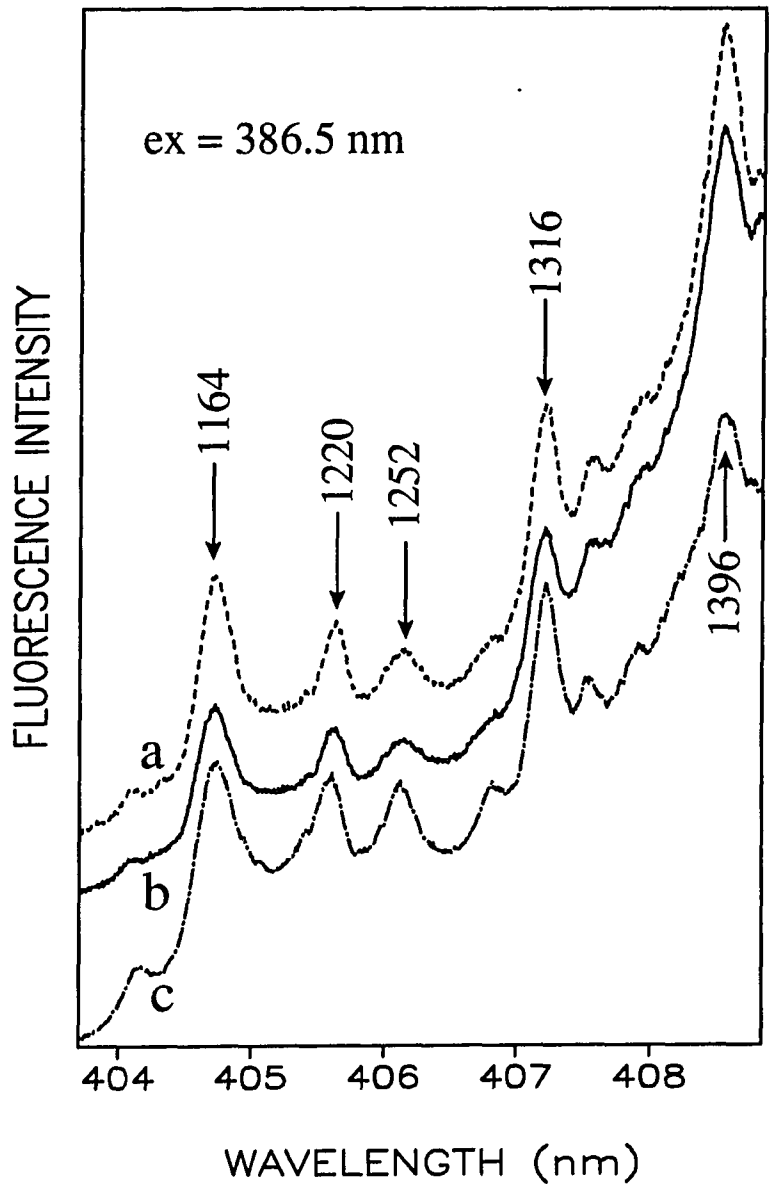

Figure 34. Comparison of the vibronically excited FLN spectra of the synthesized BP-6-N7Ade (a), BP depurinated adducts from HRP reaction (b) and microsomal reaction (c) obtained with λ_{ex} =386.5 nm

excitation wavelengths) and Table 4, it is apparent that the vast majority of the excited state mode frequencies for BP-6-N7Gua, -C8Gua and -N7Ade are identical within experimental uncertainty (± 3 cm^{-1}). There are, however, two notable exceptions: the 569 and 1132 cm^{-1} modes of BP-6-N7Gua which, for BP-6-C8Gua and BP-6-N7Ade, have the values (563, 1126) and (554, 1131) cm^{-1}, respectively.

Finally, a depurination adduct identified was BPDE-N7Ade, which are formed by monooxygenation. For this adduct four different excitation wavelengths were employed. The results for 369.6 and 356.9 nm are shown in Figure 35A and B, respectively. Spectrum a for both is for the adduct isolated from the microsome-catalyzed reaction with B[a]P while spectra b and c are for two samples of the BPDE-N7Ade standard (the sample used to obtain spectrum c was subjected to an additional purification by HPLC). One notes first that the excited state mode frequencies for the microsomal and two standard adducts are identical within experimental uncertainty. However, there are significant differences in the vibronic intensity distributions (for comparison, see the near perfect agreements in vibronic intensities for the *in vitro* and standard adducts shown in Figs. 32-34). Interestingly, Figs. 35A and B reveal a better match between the vibronic intensities of the microsomal adduct and the standard (b) presumed to be of lesser purity. Based on our library of standard FLN spectra for B[a]P tetrol stereoisomers the author is led to the conclusion that the mismatch in vibronic intensities is due, in part, to tetrol impurities present mainly in the microsomal and standard (b) samples. The tendency of BPDE adducts to undergo hydrolysis or photochemical decomposition to tetrols is well

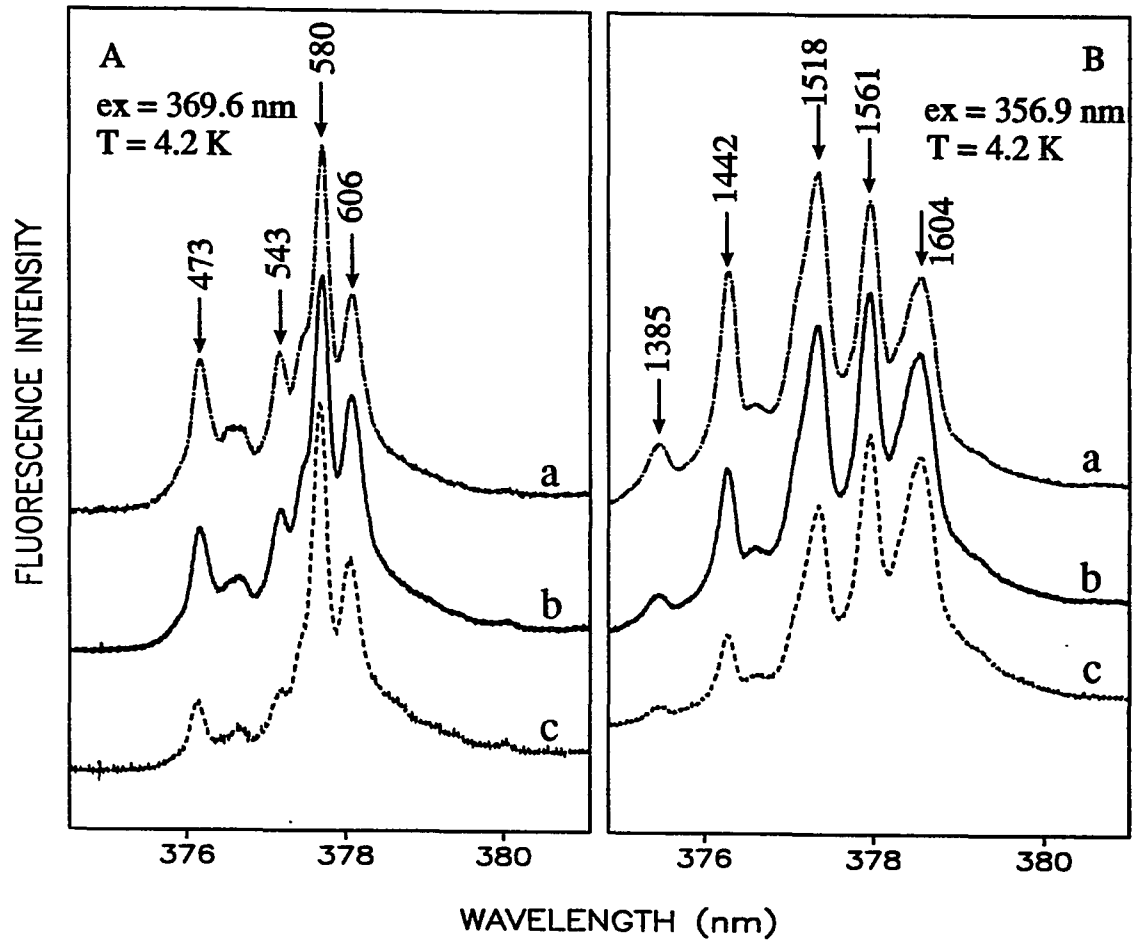

Figure 35. FLN spectra of the synthesized BPDE-10-N7Ade (b and c) compared to the spectrum of BP depurinated adduct from microsomal reaction (a). Note that the 473, 1385 and 1442 cm^{-1} bands for the highly purified adduct (c) are weaker than for standard b, see text for discussion

known. As discussed elsewhere [171], care must be exercised so as not to mistakenly assign tetrol fluorescence spectra to BPDE adducts. In support of the above conclusion vibronically excited spectra for the *cis*- and *trans*-isomers of B[a]P tetrol from (±)-*anti*-BPDE are presented in Figure 36b and c, respectively. The significant differences in vibrational frequencies and vibronic intensity distributions are comparable to those reported for *cis*- and *trans*-isomers of N2-guanine monophosphate adduct formed from (+)-*anti*-BPDE (see Figure 21) [171]. For comparison, spectrum a (microsomal adduct) from Figure 35A is shown in Figure 36 (spectrum a). It is emphasized first that BPDE-N7ade is characterized by modes at 473, 543, 580, and 606 cm^{-1}. It is only a question of what the correct relative vibronic intensities for these modes are for 369.6 nm excitation. For the reason given above, it is reasonable to assume that spectrum c of Figure 35A is minimally contaminated by tetrols. Comparison of spectra b and c with those of Fig. 35A reveals that contamination by the *trans*- isomer of B[a]P tetrol can account for the enhanced intensity of the 473 cm^{-1} band in spectra a and b of Figure 35A relative to spectrum c of Figure 35A. At the same time, the *trans*-isomer would make only a small contribution to the 580 and 606 cm^{-1} bands of BPDE-N7Ade. One cannot exclude the possibility that the *cis*-isomer of B[a]P tetrol makes a small contribution to spectra a and b of Figure 35A. The FLN spectra for the *cis*- and *trans*-tetrol isomers obtained with an excitation wavelength of 356.9 nm (not shown) show that the enhanced relative intensities of the 1385 and 1442 cm^{-1} bands of spectra a and b of Figure 35B relative to spectrum c of the same figure can also be qualitatively understood in terms of tetrol

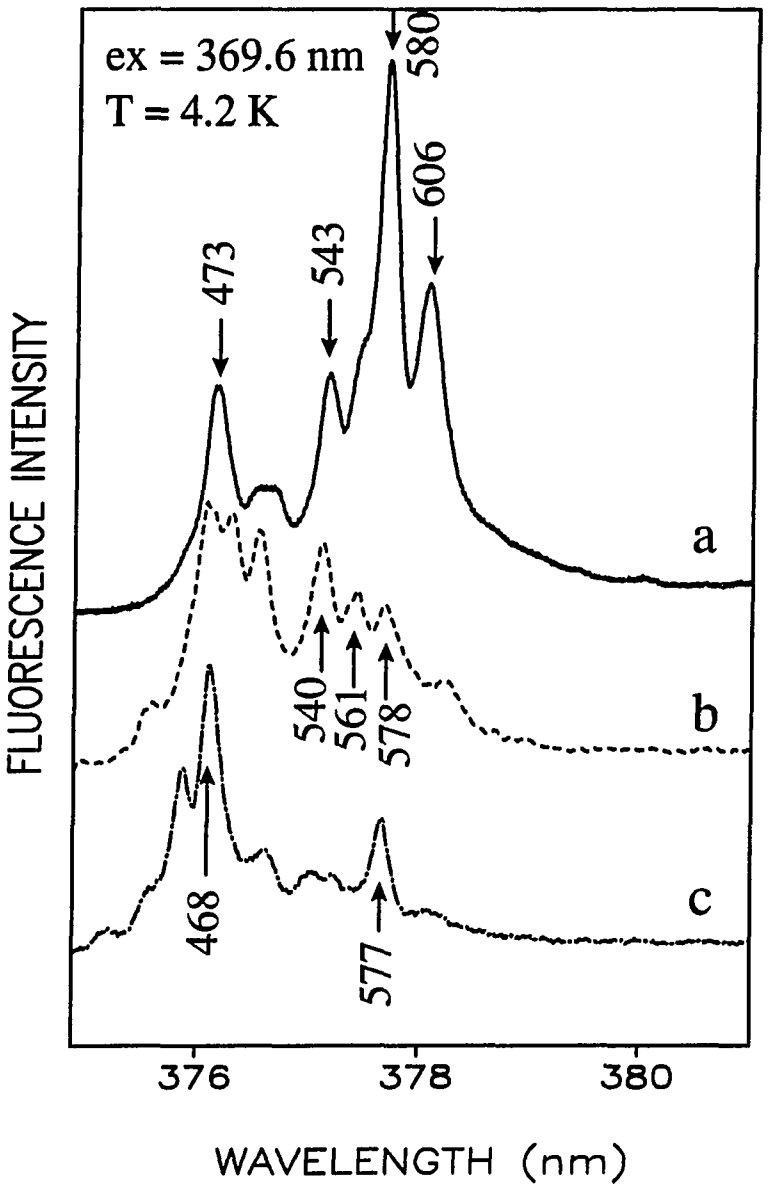

Figure 36. FLN spectrum of the microsomal adduct identified as BPDE-10-N7Ade (a), compared to the spectra of *anti-cis*-BPT (b) and *anti-trans*-BPT (c)

contamination of the samples used to obtain spectra a and b. The excited state vibrational frequencies of the *trans*-tetrol are listed in Table 4. One notes also that variations in the distribution of stereoisomers of BPDE-N7Ade could also contribute to vibronic intensity mismatches. For the current synthesized standard, only the *cis*- and *trans*-isomers from *anti*-BPDE can be present while for the microsomal reaction with BP, the *cis*- and *trans*-isomers from *syn*-BPDE could also exist. However, since standards of the stereoisomers are not available for analysis by FLNS, it is not possible to draw a conclusion as to whether or not the mismatches shown in Fig. 35A and B are due to same extent, to the presence of different stereoisomers.

On the basis of the spectra presented along with coelution with authentic standard on HPLC, it is concluded that this adduct is BPDE-N7Ade (distinguishable by FLNS from BPDE-N7Gua, see Fig. 22).

Indentified adducts were then subjected to quantification by Dr. E. Cavalieri and his group at Eppley Institute for Research in Cancer and Allied Diseases, University of Nebraska Medical Center. Quantification of stable adducts was accomplished by the ^{32}P-postlabeling method as previously described [96], whereas quantification of depurination adducts was conducted by HPLC with a radiation flow monitoring. When B[a]P was activated by rat liver microsomes, the major stable adduct was BPDE-N^{2}dG (15% of total, Table 5), whereas the other minor, unidentified stable adducts constituted only 4.4% of the total. The depurination adducts, namely, BP-6-C8Gua, BP-6-N7Gua, BP-6-N7Ade and a small amount of BPDE-N7Ade (0.5%), were, however, predominant. The three

Table 5. Quantitation of biologically-formed BP-DNA adducts[a]

Incubation system	Total adducts (mol/mol DNA)x10^6	Stable DNA adducts/(mol adduct/mol DNA)x10^6		
		BPDE-10-N^2dG	Unidentified	Stable adducts, % of total
HRP BP	21.5		6.9[b] (32)[c]	32
MC-Induced microsomes BP	18.2	2.7 (14.8)	0.8[d] (4.4)	19.2
BP 7,8-dihydrodiol	36.4	28.2 (77.5)	1.1[e] (3)	80.5
BPDE	93.4	87.6 (93.8)	4.1[f] (4.4)	98.2

a. values are the average of determinations on two preparations; the amount of each adduct varied between 10 and 25 % in the two preparations, with larger variations with the minor adducts.

b. 5 adduct spots.

c. number in parentheses is percentage of total adducts.

d. 9 adduct spots.

e. 4 adduct spots.

f. 6 adduct spots.

Table 5. (continued)

Depurination DNA adducts/(mol adduct/mol DNA)x10^6					Ratio of depurination/ stable
BPDE-10-N7Ade	BP-6-C8Gua	BP-6-N7Gua	BP-6-N7Ade	Depurination adducts, % of total	
	2.3 (10.7)	1.9 (8.8)	10.4 (48.4)	68	2.12
0.1 (0.5)	2.2 (12.1)	1.8 (9.9)	10.6 (58.2)	80.8	4.21
7.1 (19.5)				19.5	0.242
1.7 (1.8)				1.8	0.018

formed by one-electron oxidation, in an approximate molar ratio of 1:1:6, respectively, constituted 80% of the total adducts, with BP-6-N7Ade accounting for 58% by itself.

The same three depurination adducts formed by one-electron oxidation, BP-6-C8Gua, BP-6-N7Gua and BP-N7Ade, were obtained by HRP-catalyzed binding of B[a]P to DNA (Table 5). The ratio of these adducts was about 1:1:5, and they constituted 68% of all of the adducts formed. The other 32% were stable, unidentified adducts.

When B[a]P 7,8-dihydrodiol was activated by microsomes, the preponderant adduct was the stable BPDE-N_2dG, 77.5%, and the stable adducts constituted 80% of the total, with the other 20% as the depurination adduct BPDE-N7Ade. When BPDE was reacted with DNA, 98% of the adducts were stable, with 94% as BPDE-N_2dG. In this case, however, it was observed that the percentage of BPDE-N7Ade was ten times less than that obtained with B[a]P 7,8-dihydrodiol activated by microsomes.

Conclusively, activation of B[a]P by HRP or microsomes yields preponderant amounts of depurinated adducts formed by one-electron oxidation, whereas BPDE and microsome-activated B[a]P 7,8-dihydrodiol produced mainly stable adducts, in particular BPDE-N_2dG.

D. Identification of Depurinated Adducts from Mouse Skin DNA

Three depurinated adducts (temporarily named as adducts I-III) were identified from mouse skin DNA treated with B[a]P as BP-6-C8Gua, BP-6-N7Gua, and BP-6-N7Ade. Based on our library of standard FLN spectra of B[a]P adducts by one-electron,

the identification of depurinated adducts from mouse skin DNA *in vivo* experiment is straightforward. In Figure 37, FLN spectra of three adducts (adducts I-III) (spectra b) from mouse skin DNA are compared with those (spectra a) of synthetic BP-6-C8Gua (spectrum A), BP-6-N7Gua (spectrum B), and BP-6-N7Ade (spectrum C), respectively.

The FLN spectrum of authentic BP-C8Gua standard (spectrum a) is compared with that (spectrum b) of depurinated adduct I in Figure 37A. Both spectra were obtained with λ_{ex} = 395.7 nm, which yields the 400-700 cm^{-1} region of the excited state vibrational frequencies. Among the narrow ZPLs in spectrum b, the fourth peak is specially noted and determined as 563 cm^{-1}. In addition 633 and 671 cm^{-1} modes pertinent in BP-6-N7Gua (spectra in B) are not observed in current spectrum. FLN spectrum of depurinated adduct II shown as sepctrum b in Figure 37B was obtained at 4.2 K with laser excitation of λ_{ex} = 395.7 nm in glass mixture. Spectrum b shows specific 569, 633, and 671 cm^{-1} modes which are characteristics for BP-6-N7Gua adduct, what is more, the strongest mode is shifted to 588 cm^{-1} compared to the 498 cm^{-1} of BP-6-C8Gua. The third depurinated adduct from mouse skin *in vivo* experiment was identified as BP-6-N7Ade as shown in Figure 37C, where the FLN spectrum of depurinated adduct III is compared with that (λ_{ex} = 386.5 nm) of authentic BP-N7Ade. Both spectra are blue-shifted ~200cm^{-1} compared to those of BP-6-N7Gua and BP-6-C8Gua, and excited state vibrational frequencies of adduct III (spectrum b) are identical with those of standard BP-N7Ade.

From the FLN spectra discussed above (and others obtained with different

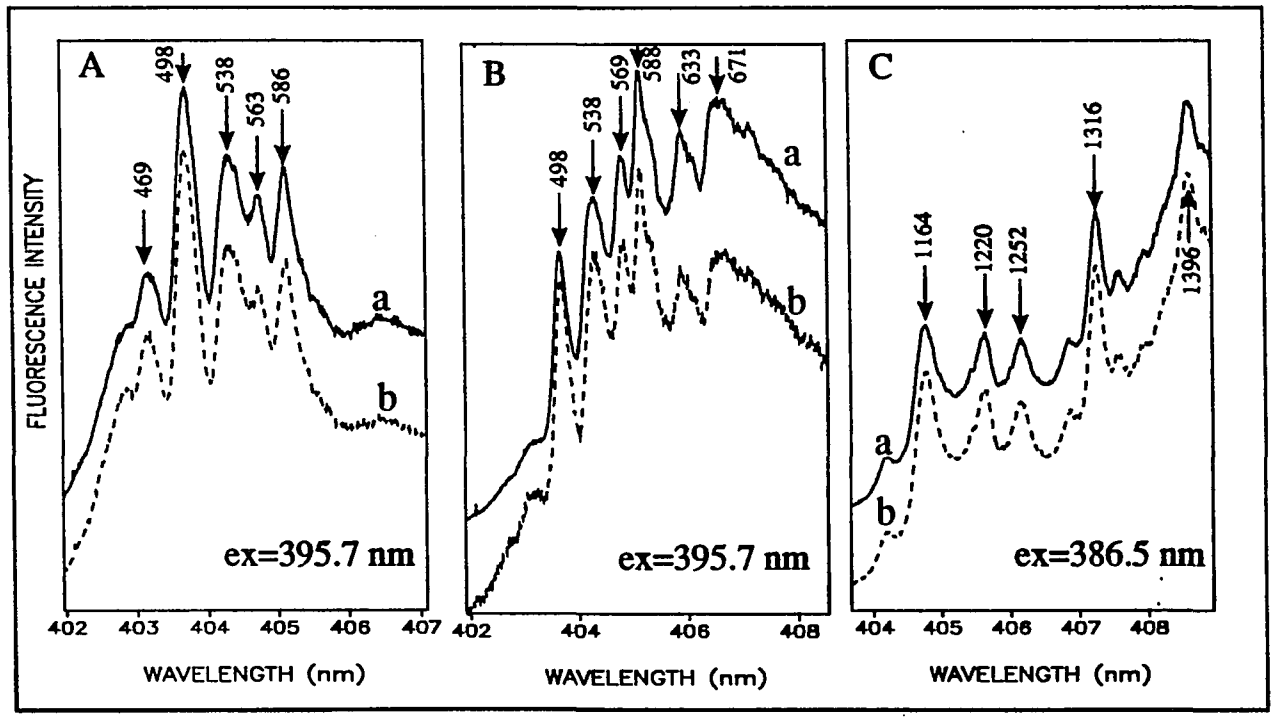

Figure 37. Comparison of the vibronically excited FLN spectra of BP depurinated adducts from *in vivo* mouse skin experiment (spectra b) to the synthesized adducts (spectra a), BP-C8Gua (A), BP-N7Gua (B) and BP-N7Ade (C). Respective λ_{ex} is denoted in each spectrum

excitation wavelengths), it is confident to conclude that three depurinated adducts from mouse skin *in vivo* experiment are BP-6-C8Gua, BP-6-N7Gua and BP-6-N7Ade. This conclusion is based on not only a few mode differencies such as 465, 569, and 1132 cm^{-1} of BP-6-N7Gua, which for BP-C8Gua and BP-6-N7Ade, have the values (469, 563, and 1126 cm^{-1}) and (no mode, 554, and 1132 cm^{-1}), respectively, and also the fact that the S_1 states of three adducts are shifted each other in such way that S_1 state of N7Ade lies about ~200 cm^{-1} lower in energy than that of the N7Gua which, in turn, lies ~50 cm^{-1} to the red of C8Gua. Indeed the true distinction among given three adducts was accomplished only after pre-separation by HPLC.

E. Identification of 7,12-DMBA-DNA Adducts Formed by Rat Liver Microsomes *in vitro*

Some evidence supports the hypothesis that the bay-region diol epoxide of 7,12-dimethylbenz[a]anthracene (7,12-DMBA) is responsible for its carcinogenic activity. 7,12-DMBA 3,4-dihydrodiol is, however, the only dihydrodiol potent in tumor initiation in mouse skin and induction of lung adenomas in newborn mice [172,173]. This proximate carcinogen is more potent than the parent 7,12-DMBA. Analysis of 7,12-DMBA-DNA adducts provides a second line of evidence. Three major adducts have previously been identified as arising from addition of the bay-region diol epoxide of 7,12-DMBA to dA and dG [57,157,158]. These adducts and several minor ones have been separated by HPLC and ^{32}P-postlabeling techniques [157,158,174,175]; however, analysis by the ^{32}P-postlabeling revealed several unidentified 7,12-DMBA-DNA adducts formed

in mouse skin [175].

It was recently proposed that one-electron oxidation is the predominant mechanism of activation for the most potent PAH, including B[a]P (see sections IV-B ~ IV-D) [81]. The DNA adducts formed when B[a]P is activated by MC-induced rat liver microsomes have recently been shown to arise primarily by one-electron oxidation; almost all of these adducts are lost from DNA by depurination (see section IV-C) [81]. A similar profile of B[a]P-DNA adducts is observed in mouse skin DNA treated with B[a]P *in vivo* (see section IV-D).

To assess the importance of one-electron oxidation in the metabolic activation of 7,12-DMBA, stable and depurination 7,12-DMBA-DNA adducts were analyzed and quantified. The adducts formed in the MC-induced rat liver microsome-catalyzed binding of DMBA to DNA were compared to the adducts formed when 7,12-DMBA was activated by HRP or 7,12-DMBA 3,4-dihydrol was activated by microsomes. Deoxyribonucleoside adducts previously synthesized by electrochemical oxidation [159] of 7,12-DMBA were used as standards in the identification of the depurination adducts by HPLC and FLNS. The stable adducts were quantitated by ^{32}P-postlabeling and the depurination adducts by radioactivity during HPLC. All biological experiments were performed by the group of Dr. E. Cavalieri at Eppley Institute for Research in Cancer and Allied Diseases, University of Nebraska Medical Center and summarized in elsewhere [80]. However, the structural identification of two depurinated adducts was accomplished by FLNS, and will now be discussed.

In the preliminary study for the stable adduct formed by one-electron oxidation, 7,12-DMBA was mixed with calf thymus DNA in the presence of HRP, and then incubated at 37 °C for one day. After removal of the supernatant, the residue was diluted with water, and kept in the dry ice prior to the FLNS experiments. Since it is well known that DNA itself may quench the fluorescence of the embedded chromophore, DNA was digested by the enzyme, DNASE I.

In Figure 38, the spectrum B of an unknown formed between 7,12-DMBA and DNA is compared with that of standard 7-MBA-12-CH_2-C8Gua (spectrum A), obtained by laser excitation at 390.0 nm. In spectrum B, relatively well resolved ZPLs are observed with an acceptable signal to noise ratio, and labeled with excited state vibrational frequencies (were determined after mathematical smoothing of the curve with commercial software, Spectra Calc). Within experimental uncertainty ($\pm$ 3 cm^{-1}), the mode frequencies of the two spectra are identical. Moreover, since 7,12-DMBA adducts which bind to the N7-position of guanine and adenine are rapidly depurinated into the supernatant, the present unknown adduct bound to the macromolecular DNA is more likely C8Gua or C8dG which are the only two adducts known to form a stable adduct by one-electron oxidation. There is a definite difference between the intensities of the 510 cm^{-1} mode of spectrum B and the 511 cm^{-1} mode of the 7-MBA-12-CH_2-C8Gua standard (spectrum A). A possible explanation for the intensity enhancement of the 510 cm^{-1} mode is that there is a contribution from 7,12-DMBA. Since unreacted 7,12-DMBA may still remain in the reaction mixture, the strongest 515 cm^{-1} mode of 7,12-DMBA (see

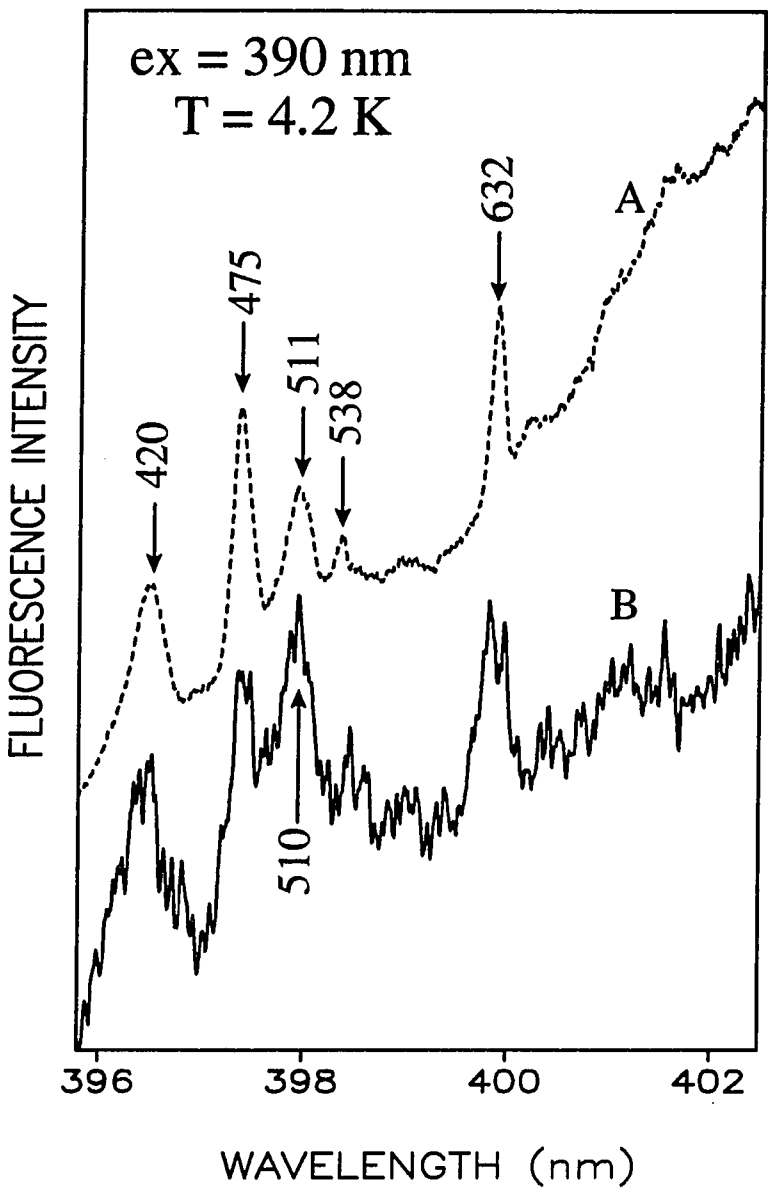

Figure 38. Comparison of the FLN spectrum of the synthesized 7-MBA-12-CH_2-C8Gua adduct (A) with FLN spectrum of DMBA bound to DNA by HRP/H_2O_2 catalyzed reaction (B)

Table 3) can contribute in the region of interest. However, since FLNS cannot distinguish between 7-MBA-12-CH_2-C8dG and its C8Gua analog, one cannot exclude the posibility that the unknown adduct is the former, not the latter or that both adducts are present. One should also note the rapid increase of fluorescence intensity of the 7-MBA-12-CH_2-C8Gua standard at ~402 nm compared to only mild, if any, increase in the spectrum of the unknown adduct (spectrum B). As discussed earlier, aggregate fluorescence of the authentic standard yields significant fluorescence at ~402 nm. However, inherently low concentration of the chromophore in the biological sample appears to reduce aggregate formation. This is an interesting aspect of the aggregate formation problem for 7,12-DMBA and its adducts.

More recently we reported that [159] FLNS, employed in the vibronic excitation mode, can differentiate between the following adducts of 7,12 DMBA formed by the one-electron oxidation pathway: 7-MBA-12-CH_2-C8Gua, 7-MBA-12-CH_2-N7Gua, 12-MBA-7-CH_2-N7Gua, 7-MBA-12-CH_2-N7Ade, and 7-MBA-12-CH_2-N3Ade. Distinction between these adducts was based on differences in vibronic intensity distributions and/or excited state (S_1) vibrational frequencies. However, it was not possible to differentiate between the first of the above adducts and its dG analogue. This could be accomplished with FAB MS/MS [159]. It was also reported that DMBA and its nucleoside adducts have a tendency to self-aggregate in solution and that very broad oligomeric fluorescence is observed from the glass at 4.2 K even for concentrations as low as 10^{-9} M. Such fluorescence, which can not be line-narrowed, is centered at ~405 nm in comparison with

the monomer fluorescence which has a maximum at ~400 nm. Interference from the broad oligomeric fluorescence to the FLN spectra of the monomers could be reduced by selective excitation and gated detection [159]. This interference is apparent in the spectra presented below.

Fluorescence line-narrowed spectra are shown in Figure 39 for the synthesized 7-MBA-12-CH_2-N7Gua standard (spectrum A) and the HPLC-isolated adducts from the HRP (spectrum B) and microsomal (spectrum C) reactions. The spectra were obtained with vibronic excitation at λ_{ex} = 390 nm and under identical gating conditions (delay = 50 ns, width = 60 ns). The prominent zero-phonon bands are labeled with their excited state vibrational frequency in cm^{-1} and appear superimposed on the high energy tail of the fluorescence band due to aggregates. Spectra obtained with λ_{ex} = 392.8 nm (not shown), which reveal excited state vibrations at 220, 273, 311 and 355 cm^{-1} [159], also show a close similarity between the FLN structures of the standard and the HRP and microsomal adducts. Therefore, we can confidently assign the strucrure of the latter two to 7-MBA-12-CH_2-N7Gua.

The FLN spectra for the 7-MBA-12-CH_2-N7Ade standard and adducts isolated from the HRP and microsomal reaction are compared in Figure 40 for λ_{ex} = 390.0 and 392.8 nm. For both excitation wavelengths the spectra are very similar. This suggests that the structure of both the HRP and microsomal adducts is 7-MBA-12-CH_2-N7Ade. However, it should be noted that the λ_{ex} = 390.0 nm spectra of Figure 40 are similar to the λ_{ex} = 390.0 nm spectra of Figure 39. There are, however, significant differences.

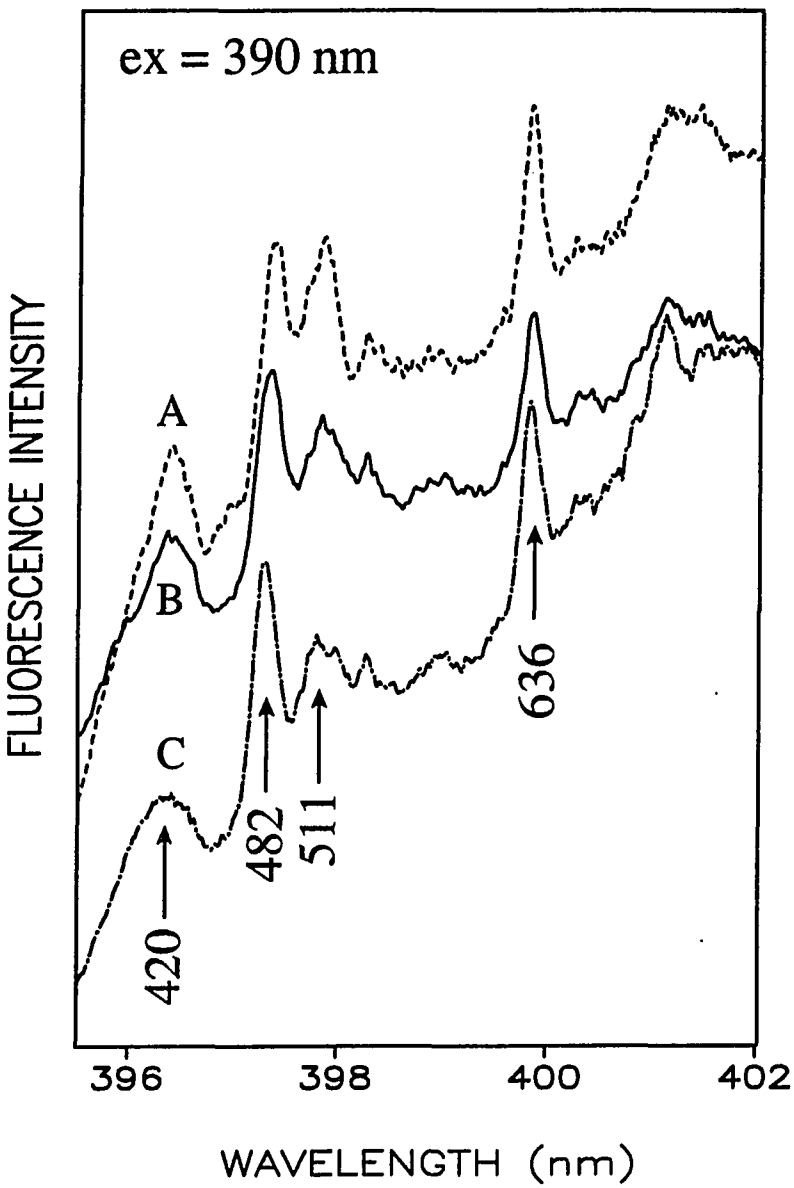

Figure 39. Segment of vibronically excited FLN spectra of the synthesized 7-MBA-12-CH_2-N7Gua standard (A), 7-MBA-12-CH_2-N7Gua from HRP reaction (B), and microsomal reaction (C) obtained with λ_{ex} = 390 nm

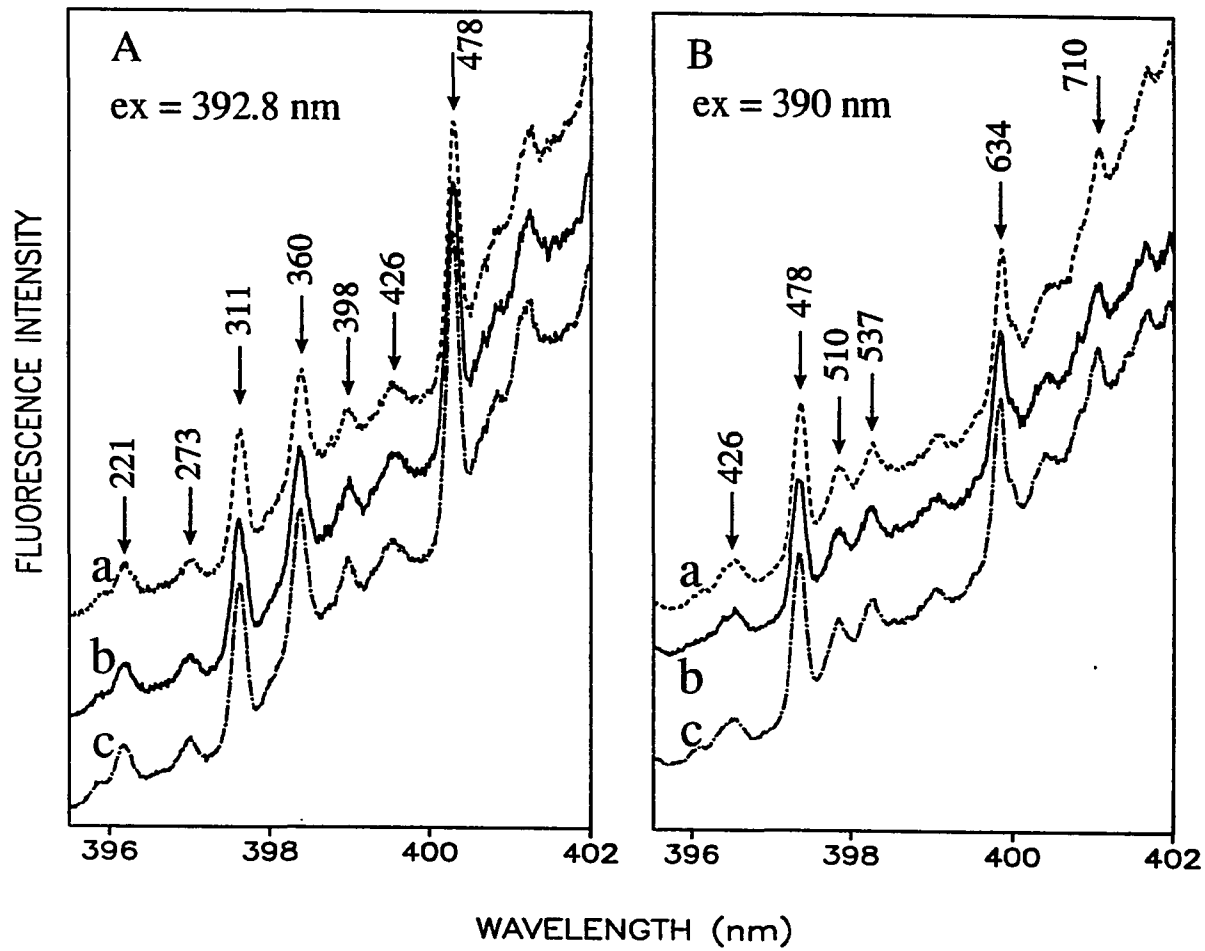

Figure 40. Comparison of vibronically excited FLN spectra of the synthesized 7-MBA-12-CH_2-N7Ade (a), 7-MBA-12-CH_2-N7Ade from HRP reaction (b), and microsomal reaction (c) obtained with λ_{ex} = 392.8 nm (A) and 390 nm (B), respectively

For example, the vibronic intensity distributions in the 400-550 cm^{-1} region are not the same and the relatively intense 420 cm^{-1} mode of N7Gua has a frequency of 426 cm^{-1} for N7Ade. In addition, the 360 cm^{-1} mode of N7Ade (left frame of Fig. 40) becomes 355 cm^{-1} for N7Gua [159]. The distinction between the N7Gua and N7Ade adducts is dealt with in greater detail in ref. 159. Thus, we can confidently assign the structures of both adducts in Figure 40 to 7-MBA-12-CH_2-N7Ade.

Quantitation of stable adducts was accomplished by the group of Dr. E. Cavalieri at Eppley Institute for Research in Cancer and Allied Diseases, University of Nebraska Medical Center using the ^{32}P-postlabeling method, whereas quantitation of depurination adducts was conducted by HPLC with a radiation flow monitoring. A sharp contrast is noted between the ratio of detectable depurination and stable adducts when binding was catalyzed by HRP or microsomes. With HRP, more than half of the analyzed adducts were stable, whereas with microsomes, depurination adducts were the overwhelmingly predominant ones detected. All these data are summarized in Table 6.

F. Interaction Between BPT and DNA in Solid Water and Glass Host

Based on a variety of experimental results, it is now well known that BPDE forms non-covalent physical complexes with double-stranded DNA within a few msec of mixing [28.155]. UV spectroscopic studies and linear dichroism measurements are consistent with an intercalation process of BPDE [155]. The intercalated diol epoxide molecules are then protonated to yield triol carbonium ions which react with water and other cellular

Table 6. Quantitation of biologically-formed DMBA-DNA adducts[a]

Incubation system	Totaladducts (mol/molDNA)x10^6	Stable adducts/(mol adduct/mol DNA)x10^6	
		Unidentified	Stable adducts, % of total
HRP DMBA	24.22	13.60[b]	56.1
MC-Induced microsomes DMBA	8.84	0.128[c]	1.4
DMBA 3,4-dihydrodiol		6.42[d]	

a. values are the average of determinations on two preparations; the amount of each adduct varied between 5 and 15 % in the two preparations; because DMBA 3,4-dihydrodiol was not radiolabeled, the depurination adducts could not be analyzed.

b. 13 adduct spots.

c. 9 adduct spots.

d. 4 adduct spots.

e. number in parentheses is percentage of total adducts.

Table 6. (continued)

Depurination adducts/(mol adduct/mol DNA)x10^6			
7-MBA-12-CH_2-N7Ade	7-MBA-12-CH_2-N7Gua	Depurination adducts, % of total	Ratio of depurination/stable
8.66 (35.8)[e]	1.96 (8.1)	43.9	0.77
7.20 (81.5)	1.51 (17.1)	98.6	70

nucleophiles. Over 90% of BPDE molecules are hydrolyzed (detoxification), while less than 10% of the molecules form biologically more important covalent bonds with nucleic acid bases. The kinetic experiments on the intercalation and reactivity of BPDE molecules in the presence of native DNA are relatively well established [176,177]. Data illustrate that both hydrolysis and covalent binding processes are accelerated upon physical complex formation with DNA, and both reactions are parallel pseudo-first order reactions charaterized by the same rate constant k [176,177].

In buffer solution, the hydrolyzed product of diol epoxide, tetrol, is also physically associated with DNA. Spectroscopic studies [171,178] show that 80% of the racemic *anti* BPTs in ~$2x10^{-3}$ M of DNA form complexes with DNA. The formation of these non-covalent physical complexes is characterized by a ~10 nm red shift of the UV absorption maxima (or ~5 nm red shift of the 0-0 origin in the fluorescence spectrum obtained at 77 K [171], and a large reduction in the molar extinction coefficient. Based on the linear dichroism results it has been suggested that these complexes are intercalative in nature. Regardless of the particular reaction conditions, however, the non-covalent binding of intercalated molecules to DNA is characterized by an association constant, K_a; the main contributions to K_a are believed to arise from intercalative stacking interactions between the aromatic regions of PAHs (or their derivatives) and the DNA bases [179].

To study the properties of BPT-DNA complexes, BPT was added to highly concentrated DNA (~$2x10^{-3}$ M) in buffer solution. Figure 41 demonstrates FLN spectra

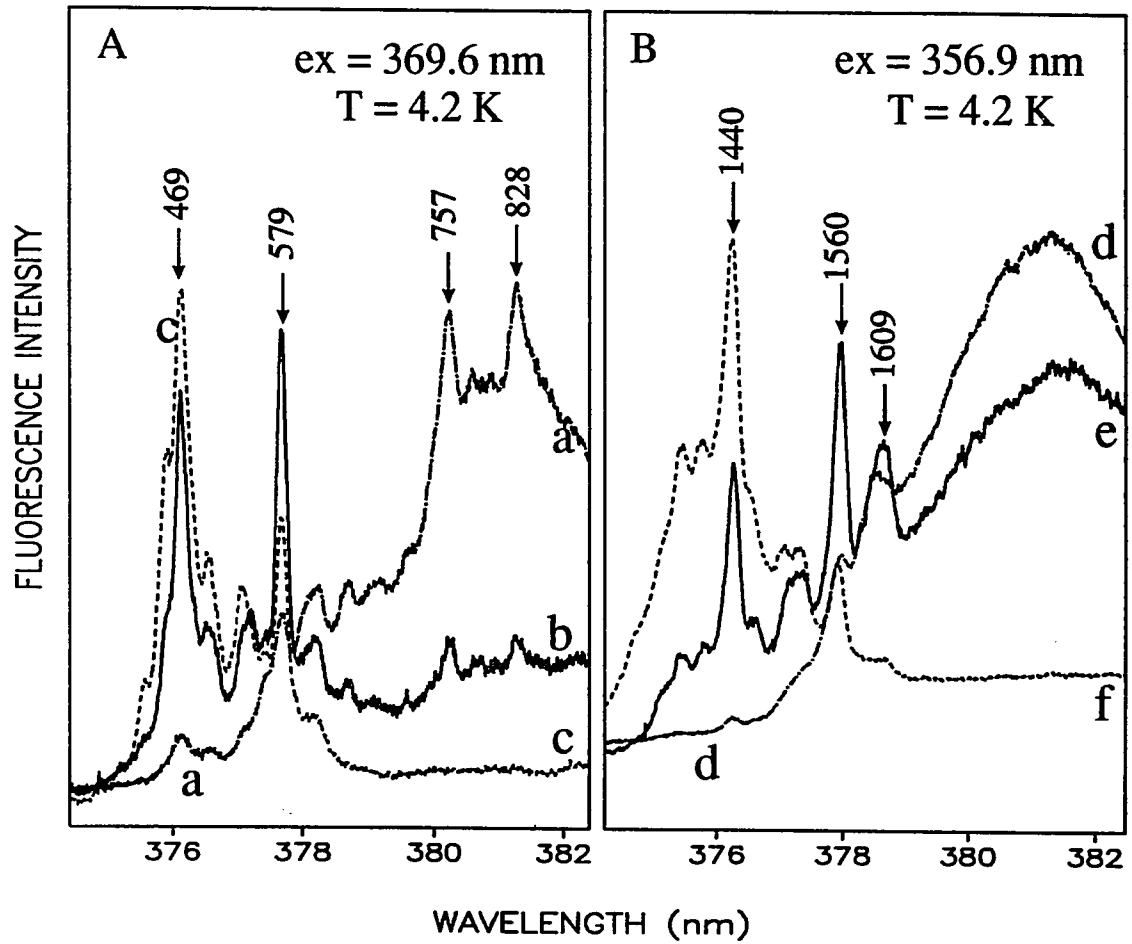

Figure 41. FLN spectra of the BPT-DNA in water (spectra a, b, d, e) and in glass mixture (spectra c and f) obtained with λ_{ex} = 369.6 nm (A) and 356.9 nm (B), respectively. Intercalated BPT shows broad tail centered ~381 nm in spectra a, d, and e

of BPT in solid water host (spectra a, b, d, e) and in the glass mixture (spectra c and f) obtained by laser excitation at λ_{ex} = 369.6 (spectrum A) and 356.9 nm (spectrum B), respectively. Only pronounced ZPLs are labeled with their excited state vibrational frequencies in cm^{-1}. Broad fluorescence spectra (data not shown) obtained under non-line narrowing conditions indicate that BPT-DNA complexes in aqueous buffer solution are characterized by relatively broad 0-0 origin band centered at ~381 nm, similar to the previous results [171]. FLN spectra of intercalated tetrol in solid water host are characterized by two relatively well resolved 757 and 828 cm^{-1} modes (spectrum a in Fig. 41A) and a very broad band at ~381 nm (spectrum d in Figure 41B).

For the glass mixture (5 glycerol: 4 water: 1 ethanol by volume), however, these two modes (757, 828 cm^{-1}) and the broad band are absent (spectra c and f). As a result, a dramatic increase of the intensities of the 469, 579, 1440, and 1560 cm^{-1} modes is observed. A broad fluorescence spectrum obtained under non-line-narrowing conditions with 355 nm excitation also confirms that the 0-0 origin band is centered at 376.5~377 nm, a blue-shift of ~4 nm relative to the band of free tetrol. However, a fluorescence quenching experiment with acrylamide (ACR) demonstrated that BPT in the glass mixture occupy at least two different configurations (*vide infra*). Similar dissociation of the non-covalent BPDE-DNA intercalation complexes has been observed upon addition of organic solvents [176], salts, or metal ions [177]. For example, the association constant of BPDE-DNA intercalation complexes is remarkably reduced in the presence of ethanol [176] and/or Mg^{+2} ion [177]. The organic solvent may influence the base-pyrene-base

interactions and reduce the physical association between BPDE and DNA bases. Mg^{+2} ion, known as a DNA stabilizer, also induces stronger base-base interactions, which, in turn, reduces base-pyrene interaction. Since the physical association of tetrols with DNA is an equilibrium phenomenon, K_a should depend on the temperature, *i. e.*, intercalation should be favored at low temperature.

To obtain spectrum b in Fig. 42A, tetrols in aqueous DNA sample were kepted at room temperature for 24 hrs and subsequently rapidly cooled to 4.2 K. Due to the rapid cooling in this process, most of the possible BPT-DNA configurations should be trapped (and have characteristic spectral properties) (cf. Figure caption). In spectrum b, the 757 and 828 cm^{-1} modes (ZPL) of the intercalated BPT are still present but the 469 and 579 cm^{-1} modes, which are relevant to other BPTs in different conformation(s), have increased in intensity. Without physical parameters such as molar absorption coefficients and fluorescence quantum yields for each BPT, however, it is not possible to determine the concentration of the intercalated BPTs relative to those of BPTs in different conformation(s) directly from the FLN spectra shown in Figure 41A. The relative fluorescence intensities of BPTs in different conformations also depend on excitation laser wavelength. This aspect is well demonstrated by the comparison between spectra a and e of Figure 41 obtained from the same sample at excitation wavelength at 369.6 and 356.9 nm, respectively. A relatively intense broad band is observed in the spectrum e compared to extremely low intensities of 757 and 828 cm^{-1} peaks in spectrum b. Based on the broad fluorescence obtained under non-line narrowing conditions, it is concluded

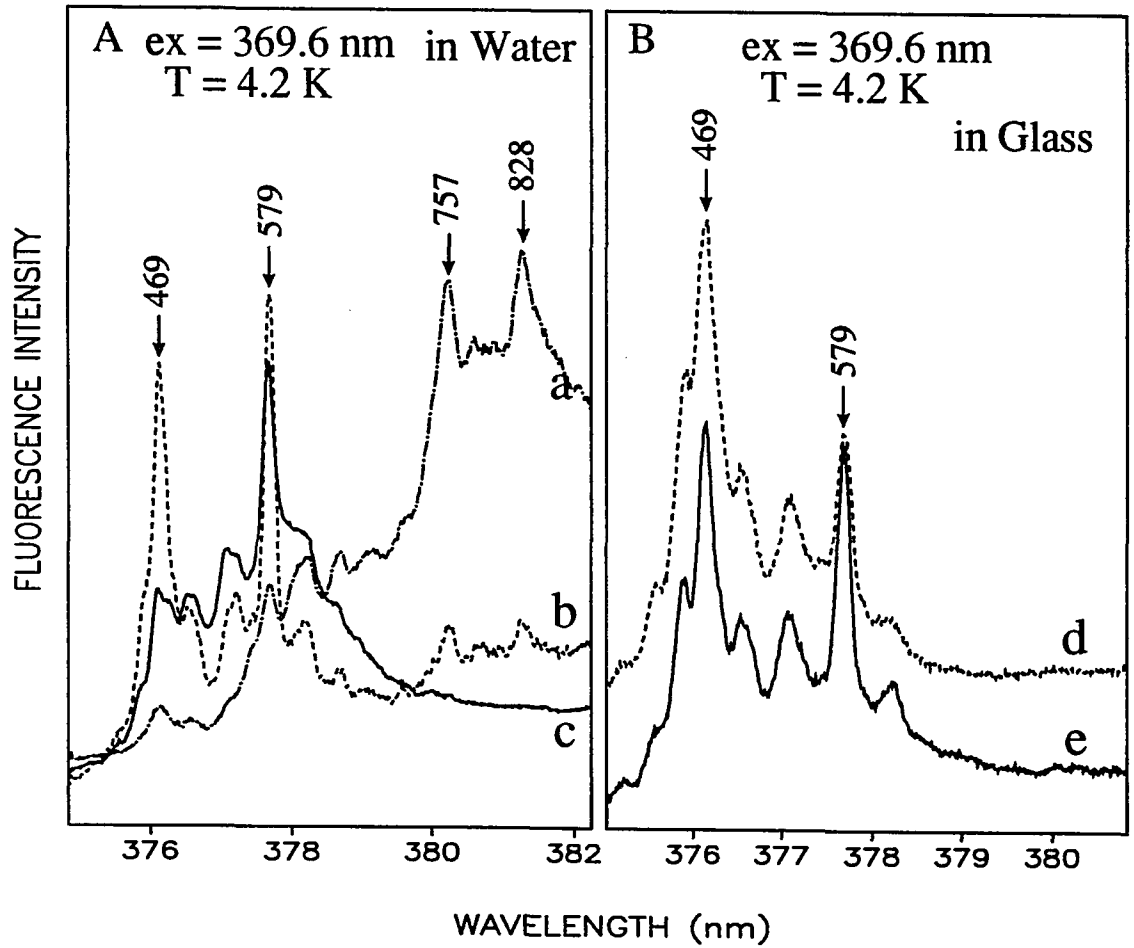

Figure 42. Comparison of the FLN spectra, in the absence (spectra a and d) and presence (spectra c and e) of ACR quencher in water (A) and glass mixture (B), respectively. Spectrum b was obtained after keeping BPT-DNA sample at room temperature for 24 hours (in the absence of quencher)

that more BPTs still reside in the base stacking intercalation.

For the study of fluorescence quenching of BPT in different configurations, 1 M of ACR was added to the aqueous and glass samples. The results are presented in Figures 42A and 42B, respectively. The FLN spectrum of tetrols in aqueous DNA with ACR obtained with 369.6 nm excitation is given as spectrum c in Figure 42A. For comparison, spectra a and b in Figure 41A are shown in Figure 42A. Two differences should be emphasized. First, no intercalated BPT contribute to spectrum c since the 757 and 828 cm^{-1} bands are absent in spectrum c. Second, the 579 cm^{-1} mode is much more intense in spectrum c than in spectrum a. Since it is difficult to understand how ACR can quench the fluorescence of intercalated chromophores in DNA, ACR may diffuse into base stacking region and replace the sites of the chromophores (pyrenes) inside the base stacking region, causing the displaced BPTs to diffuse out to more solvent-exposed regions and yield FLN spectrum b shown in Figure 42A.

Such BPTs in solvent-exposed regions appear to occupy at least two different configurations; one characterized by the 469 cm^{-1} mode, and the other by the 579 cm^{-1} mode. However, the former mode (ZPL) is also slightly contributed to by the BPT in the other configuration, and *vise versa*. The former configuration (referred to as "free" tetrol [171]) appears to be the more solvent-exposed since its fluorescence is more efficiently quenched by ACR than the latter. The tetrols in the latter configuration interact less strongly with DNA than intercalated tetrols, but more strongly than "free" tetrols. They will be referred to as physically bound tetrols.

The FLN spectrum of tetrol and DNA in the glass mixture with ACR is shown as spectrum e in Figure 42B. For comparison, spectrum c in Fig. 41A is shown again as spectrum d. As discussed earlier, the intercalated configuration for BPT is not favored in the glass matrix. The "free" tetrols are highly quenched by ACR, as was the case for the aqueous host, as indicated by the decreased intensity of the 469 cm^{-1} ZPL. On the other hand, external physical complexes of BPT-DNA are much less efficiently quenched than "free" tetrols.

These results are similar to our previous ones [171], but with a few exceptions. Special emphasis should be given to the sample preparation procedure. Since it seems that diffusion of the glass mixture (solvent molecules at room temperature) to more confined base stacking regions takes a few hours, different spectra may be generated depending on the protocol used. Therefore, the sample should be completely mixed in the glass solvent through sonification and/or shaking. In addition, to obtain reproducible spectrum, it is important to leave the sample in the liquid state for a time required to allow for complete diffusion of the solvent molecules into the base-base stacking regions of DNA. Because the ratios of tetrol configurations for the glass mixture are different from those of the aqueous sample, it may well be that utilization of aqueous solid sample can provide more realistic informations related to conformations of probe molecules in biological systems.

G. Spatial Conformations of the Stereoisomeric Oligonucleotide Adducts from (±)-*anti*-BPDE

The characterization and determination of carcinogen-modified DNA adducts is important for understanding the initial step of chemical carcinogenesis. Therefore, the distinction between BP (and/or DMBA) adducts formed with different bases, adducts formed with different nucleophilic centers of a given bases should be established. Since the base sequence specificity and subtle stereochemical effects on adduct formation are of interest, we have initiated studies of well defined oligomer-adducts. Moreover, identification of different spatial orientations of covalent adducts in DNA double helix should be heavily emphasized since this may provide information essential for clarifying biological activity-structure relationships.

The differences in the mutagenic and tumorigenic potential of the (+)- and (-)-enatiomers of *trans*-7,8-dihydroxy-*anti*-9,10-epoxy-7,8,9,10-tetrahydrobenzo[a]pyrene (*anti*-BPDE), are a well known example of carcinogenic potential-structure relationships. The (+)-*anti*-BPDE enantiomer is significantly more tumorigenic on mouse skin [172] and new born mice [180] than (-)-*anti*-BPDE. In mammalian cells, the former is extremely mutagenic [43,181,182], while in bacterial systems the relative potencies of mutagenicities of these two enantiomers are quite different [181,182]. The important questions still being investigated are: what are the relevant binding sites among the various nucleophilic centers of DNA, and how are covalent adducts spatially oriented in the DNA double helix.

Among the four different isomeric BPDEs, (+)-*anti*-BPDE is believed to be the

predominant isomer produced metabolically (~90%), but minor amounts of (-)-*anti*-BPDE and (±)-*syn*-BPDE are also formed [31]. While all four BPDE isomers are reactive toward DNA, (+)-*anti*-BPDE has strong tendency to react with exocyclic NH_2 of guanosine base in DNA, yielding ~90% N2-dG adducts [43] along with lesser amounts of N6-dA, O6-dG, and N7-dG adducts. The analogous reaction of (-)-*anti*-BPDE is less regiospecific, yielding only 50% of the N2-dG product along with substantial amounts of other adducts. Certainly, the major macromolecular adduct which accounted for about 80~85% of the alkylated product, was shown to be a guanosine derivative covalently linked between the 2-NH_2 group and the 10-position of the principal reactive metabolite of B[a]P, (+)-*anti*-BPDE.

Considerable progress on the elucidation of different spatial orientations of covalent adducts has been made by Geacintov et al. [28,155,176-179], who have used a variety of spectroscopic techniques, including linear dichroism and fluorescence quenching. The BPDE-DNA adducts have been classified as type I or II [176-179]. For the type I sites identified, the aromatic plane of pyrene appears to be nearly parallel (within ~25-30°) to the planes of the unmodified DNA bases. Such adduct sites may be viewed as interior (e. g., quasi-intercalated). Type II sites are characterized by a lower degree of interaction between the pyrenyl moiety and the bases and, therefore, may be viewed as exterior. However, the former site type is also characterized by positive linear dichroism (LD) spectrum, while the latter has negative LD spectrum. Such studies [176-179] have thus far identified only two types (site I and II types, *vide supra*) of adduct

forms each of the (+)- and (-)-*anti*-BPDE enantiomers.

Recently, Jankowiak et al. reported that FLNS in combination with fluorescence quenching and 77 K selectively excited ($S_2 \leftarrow S_0$) fluorescence spectroscopy is a more powerful methodology for DNA adduct analysis [183]. Five adducts from the reaction of (-)-*anti*-BPDE with purified DNA were identified and classified as type I or type II. The adducts were denoted as (-)-j, j = 1-5. The (+)-*anti*-BPDE enantiomer yielded three adducts, with (+)-1 being dominant (~85%). That the (-)-enantiomer yielded the more heterogeneous distribution of adducts confirmed the results of earlier work [43]. Apparently, (±)-1 adducts from both enantiomers reside in a more solvent-exposed region, *i. e.* one that leads to a weak interaction with bases. These adducts are of type II and external. Adducts (±)-3 are characteriazed by strong linear electron-phonon coupling as evidenced by an absence of line narrowing in fluorescence or fluorescence excitation. In contrast, prominent ZPLs are obtainable from (±)-1 type adducts. The strong electron-phonon coupling is presumably the result of a strong interaction between the pyrenyl chromophore and the bases, which imparts significant charge-transfer character to the S_1 state. On the basis of available data a firm classification for (±)-2 adducts could not be made. However, because (±)-2 is intermediate in energy between (±)-1 and (±)-3, one might postulate that the (±)-2 site is located more in the interior than (±)-1 but not to the same degree as (±)-3. Adducts (-)-4 and (-)-5 from (-)-*anti*-BPDE were attributed to adducts of BPDE with a bases other than guanine, e.g., adenine. Unavailability of appropriate standard adducts prevented definitive assignments for the last two adducts.

The availability of oligodeoxynucleotides with specific base sequences now makes possible the study of well-defined BPDE-DNA adducts with known sequences of nucleotides flanking the modified base. Furthermore, the biological activity-structure relationships can be illustrated by using aforementioned methodology [171,183]. Therefore, spectroscopic characterization of racemic and isomeric BPDE-oligonucleotide adducts can provide a variety of analytical data important to detailed studies of spatial conformations of carcinogen-DNA adducts formed in biological systems. With this in mind, *trans*- and *cis*-adducts formed from racemic (±)-*anti*-BPDE and synthetic oligonucleotides were prepared [178,184] and provided by Dr. N. Geacintov at Department of Chemistry, New York University. Sequences of the oligonucleotides were either d(ATATGTATA) or d(CACATGTACAC), while BPDEs are bound to the N2-position of the central guanine. Adducts formed with single-stranded (ss) and subsequently annealed double-stranded (ds) oligonucleotides were studied in both water and glass matrices. For simplicity double-stranded oligonucleotides will be denoted as $d(ATATGTATA)_2$ and $d(CACATGTACAC)_2$.

1. General remarks on adduct conformations

In order to classify different adduct conformations, we first describe the nomenclature in more detail. Compared to previous studies on BPDE-DNA adducts [171,183], oligonucleotides may induce small variations of spectroscopic characteristics including the 0-0 origin band position and excited state vibrational frequencies. Since only the distinction between different site conformations is of interest the oligomer

adducts, as in previous works [171,183], are denoted as (+)-j, j = 1-3. Therefore, (+)-1, (+)-2, and (+)-3 (for (+)-*trans*-BPDE adducts) formed with double-stranded $d(ATATGTATA)_2$ may be directly compared with adducts found in DNA adducts from the (+)-*anti*-BPDE. In general, all these adducts (with different relative concentrations) are adducted to double-stranded oligonucleotides. One should also note that the conformations found from the DNA studies for the (+)-enantiomer have their counterparts in the (-)-enantiomer, *i.e.*, (+)-1, (+)-2, (+)-3 versus (−)-1, (−)-2, and (−)-3.

FLN spectra have been obtained for single- and double-stranded (ss and ds) oligonucleotides adducts in both water and glass hosts, T = 4.2 K. Examples are shown in Figures 43 and 44. A specific region of the vibronically excited FLN spectra, obtained with laser excitation at 356.9 nm, is presented in Figure 43 for (A) (-)-*trans*-d(CACATGTACAC) and (B) (+)-*trans*-d(CACATGTACAC) in solid water host (spectra a and c) and the glass (spectra b and d). The FLN spectrum of the (-)-*trans*-adduct in water (spectrum a) is characterized by a few well-resolved but relatively weak ZPLs and a broad featureless band centered at ~380.5 nm. Based on our previous studies [171,183], the broad fluorescence originates from the chromophores in an intercalative base-base stacking conformation. Furthermore, strong electron-phonon coupling for the intercalated chromophore prevents line narrowing in fluorescence. Therefore, for the solid water host it appears that the pyrenyl chromophore in this conformation is of the base-stacked adduct type even though the oligonucleotide is ss, *i.e.*, similar to the (-)-3-DNA type, while the adduct associated with the ZPLs appears to be of the (-)-2 type.

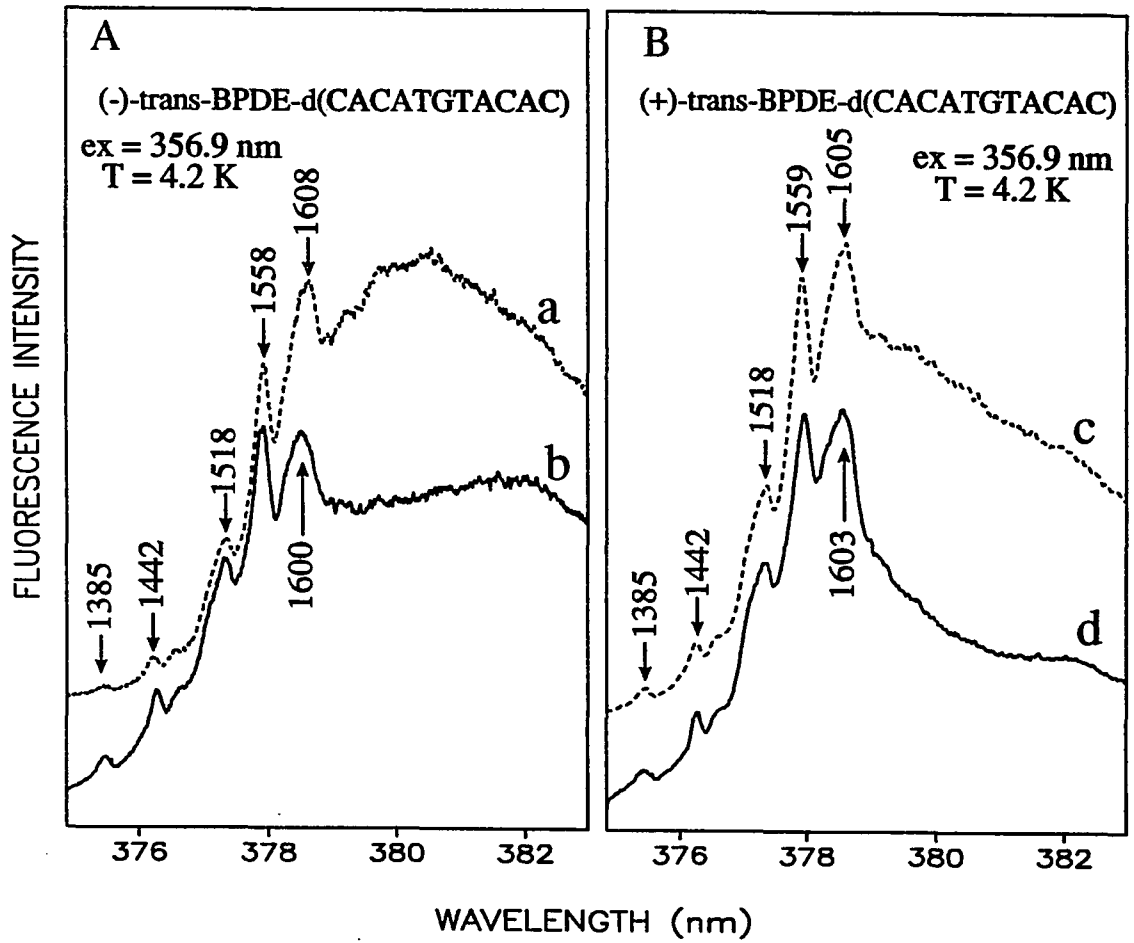

Figure 43. Comparison of FLN spectra of the (+)-*trans*- (B) and (-)-*trans*-BPDE-d(CACATGTACAC) (A) in water (spectra a and c) and glass mixture (spectra b and d)

Comparison of the spectra of Figure 43 shows that the intensity of the broad band at ~380.5 nm relative to those of the ZPL is significantly reduced in the glass host (the protocol for this experiment was to add the glass forming solvent to the water). Therefore, the glass forming solvent appears to convert the (-)-3-type conformation into the (-)-2-type, which is located in a more solvent-exposed region of the oligonucleotide. It does not seem likely that a solvent-shift is responsible for the observed spectral changes. First, the location (profile) of the broad fluorescence band in spectrum b does not depend significantly on the amount of glass forming solvent added. Second, even if adduct in base-stacked conformation is shifted due to solvent-shift induced by glass forming solvent, broad feature of the fluorescence of the base-stacked chromophore should be pertinent. However, the decreased intensity of the broad band of spectrum a in Figure 43A seems to be accompanied by an increase in the intensities of the ZPLs, *e.g.*, the 1558 and 1600 cm^{-1} modes, suggesting conversion of the base-stacked adduct to an adduct in more solvent accessible environment.

It was discussed in section IV-F that the glass mixture may disrupt base-pyrene-base interactions and cause the non-covalent binding tetrols to diffuse into the more solvent exposed region of the DNA helix, *i.e.*, to free and physically bound tetrols. Of the base stacked adducts which are covalently bound to the oligonucleotide, however, it is reasonable to suggest that only the one characterized by a weaker interaction with the base can be disrupted by the glass solvent and be converted to the (-)-2 type adduct. This postulate suggests that there may be two different adduct conformations in the base

stacking region responsible for the broad band in spectrum a of Figure 43A. Accordingly, one of them, referred to as (-)-2′ ($E_{(0,0)}$ (-)-2′ < $E_{(0,0)}$ (-)-2), is converted to (-)-2 by the glass solvent, whereas the other conformation remains unchanged. Considering the nature of the single-stranded oligonucleotide, the adduct which fluoresces broadly (~380.5 nm) in the glass should be similar, from an intercalation point of view, to the more internal (-)-3-type adduct found in BPDE-DNA. We refer to this ss adduct as (-)-3′. This suggestion is somewhat speculative since we cannot exclude the possibility that the synthetic oligomers undergo conformational transitions during formation of the glass.

One can also observe the broad fluorescence band in the FLN spectrum of (+)-*trans*-BPDE-d(CACATGTACAC) adduct in solid water host, although at diminished intensity (spectrum c in Fig.43B). To investigate whether the broad band is originates from (+)-2′ or (+)-3′, the glass forming solvent was added to and thoroughly mixed with the aqueous sample. The resulting FLN spectrum (spectrum d in Fig.43B) obtained with 356.9 nm excitation shows a marked reduction in the intensity of the featureless tail, indicating that the (+)-2′ adduct is reponsible for the broad tail in spectrum c.

For the study of adduct conformations in double-stranded $d(CACATGTACAC)_2$, the adducted oligomer was annealed by adding the natural complement of the oligonucleotide. Striking differences in the FLN spectra of the (-)- and (+)-*trans*-adduct are observed. Vibronically excited FLN spectra of (-)-*trans*-BPDE-$d(CACATGTACAC)_2$ (spectra a and c) and (+)-*trans*-BPDE-$d(CACATGTACAC)_2$ (spectra b and d) are

presented in Figure 44 for (A) solid water and (B) glass hosts, respectively. All spectra were obtained with laser excitation at 356.9 nm. First, spectrum a in Figure 44A of the (-)-*trans* adduct (ds) should be compared with spectrum a for ss in Figure 43A. The spectra are very similar. Thus, upon annealing, most of the base-stacked adduct covalently bound to the single-stranded oligonucleotide retains a similar base-stacking structure. The next question is whether this base-stacking is homogeneous in nature or not. Since the oligonucleotide is now double-stranded, the (-)-3′ type adduct should have been be converted to the truly intercalated (-)-3 type adduct, while the (-)-2′ type adduct should have been transformed to the (-)-2 and/or (-)-1 (*vide infra*) type adduct upon addition of glass forming solvent. To test this hypothesis we turn to the FLN spectra obtained for the ds oligonucleotide adducts following addition of the glass forming solvent to the water. The FLN spectrum of (-)-*trans*-d(CACATGTACAC)$_2$ in the glass matrix (spectrum c in Figure 44B) shows that the broad fluorescence band has essentially disappeared, compare with spectrum a of Figure 43A. Therefore, the base-stacked adduct found in spectrum a of Figure 43A is assigned as (-)-2′. In contrast, as can be observed in spectrum b of Figure 43A, the (+)-2′ type adduct found in single-stranded (+)-*trans*-adduct is completely converted to the (+)-2 type adduct demonstrating reorientation of the base-stacked pyrenyl chromophore by annealing. Consequently, no significant change is expected from addition of the glass forming solvent as is observed, see spectrum d of Figure 44 which shows the FLN spectrum of the predominant (+)-2 type adduct. A similar observation was reported earlier [185]; upon covalent binding of BPDE to DNA,

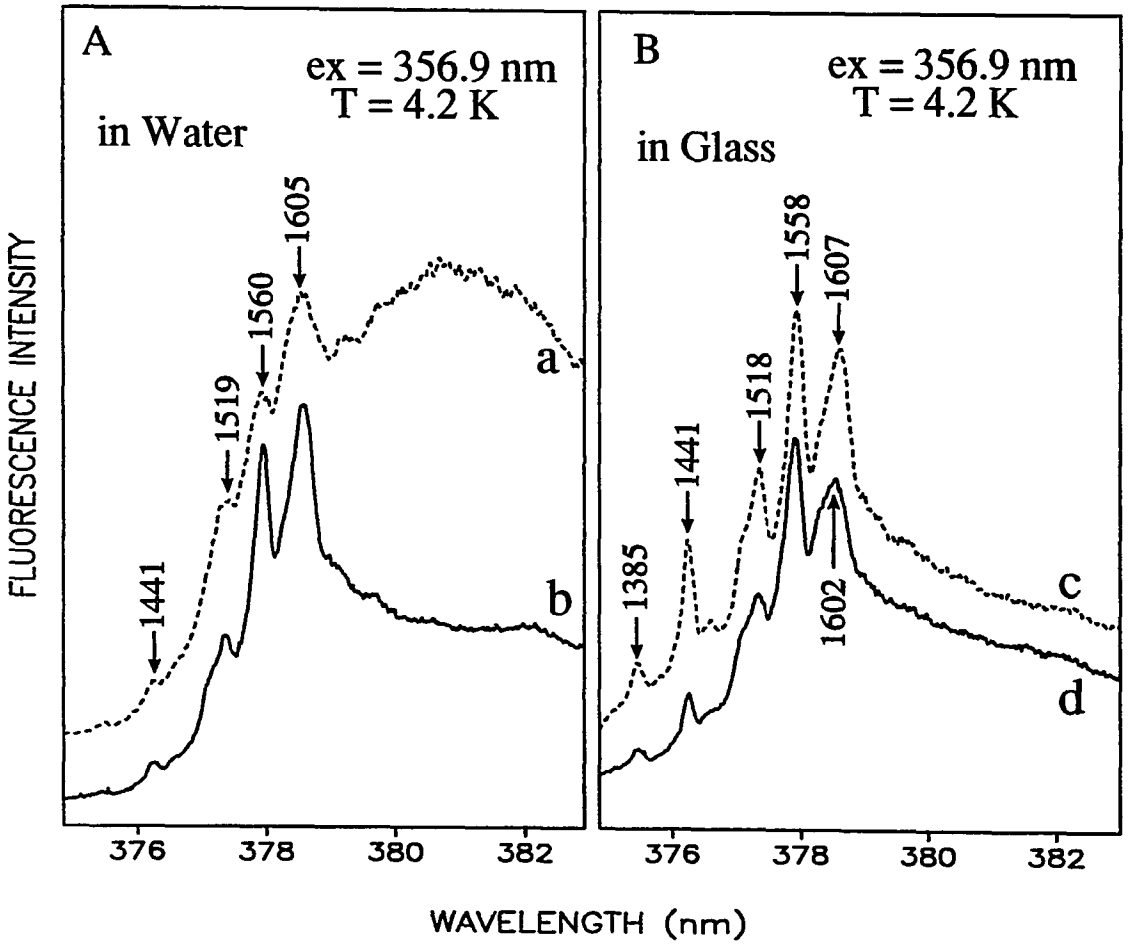

Figure 44. FLN spectra of the (+)-*trans*- (spectra b and d) and (-)-*trans*-BPDE-d(CACATGTACAC)$_2$ (spectra a and c) in water (A) and glass (B), respectively

a pronounced reorientation of the base-stacked pyrenyl ring system was observed in the case of *anti*-BPDE, where (+)-*trans*-adduction dominates. On the other hand, such reorientation does not seem to occur in the case of *syn*-BPDE for which the relative ratio of adduction from other than (+)-*trans* addition is markedly increased.

The (+)-1 and (-)-1 type adducts have been detected on the basis of selectively excited broad fluorescence spectra obtained under non-line narrowing conditions and FLN spectra obtained with suitable λ_{ex}-value (data not shown). Broad fluorescence spectra obtained with laser excitation at 355 nm (spectrum a) and 346 nm (spectrum b) for (+)-*trans*-BPDE bound to single-stranded d(ATATGTATA) is shown in Figure 45A for the glass host. The broad fluorescence spectra and FLN spectrum obtained with laser excitation at 356.9 nm (see Fig. 46) demonstrate that the (+)-2 adduct is predominant in this oligomer. However, one can observe a small shoulder on the high energy side of spectrum a (Figure 45A) which indicates that there is another emitting species (adduct). Since the latter adduct, presumably (+)-1, absorbs to higher energy than the major (+)-2 adduct type, 346 nm excitation was employed to better reveal its contribution. The resulting spectrum is presented in Figure 45A (spectrum b). This spectrum is blue-shifted by ~1 nm relative to spectrum a demonstrating significant contribution from a second adduct which we assign as (+)-1 site type. The contribution of the (+)-1 type adduct to spectrum a of Figure 45A can be approximately eliminated by subtracting spectrum b (to which the (+)-1 adduct contributes more than to the spectrum a) from spectrum a. The subtraction yields spectrum c of Figure 45B for which the contribution of the shoulder is

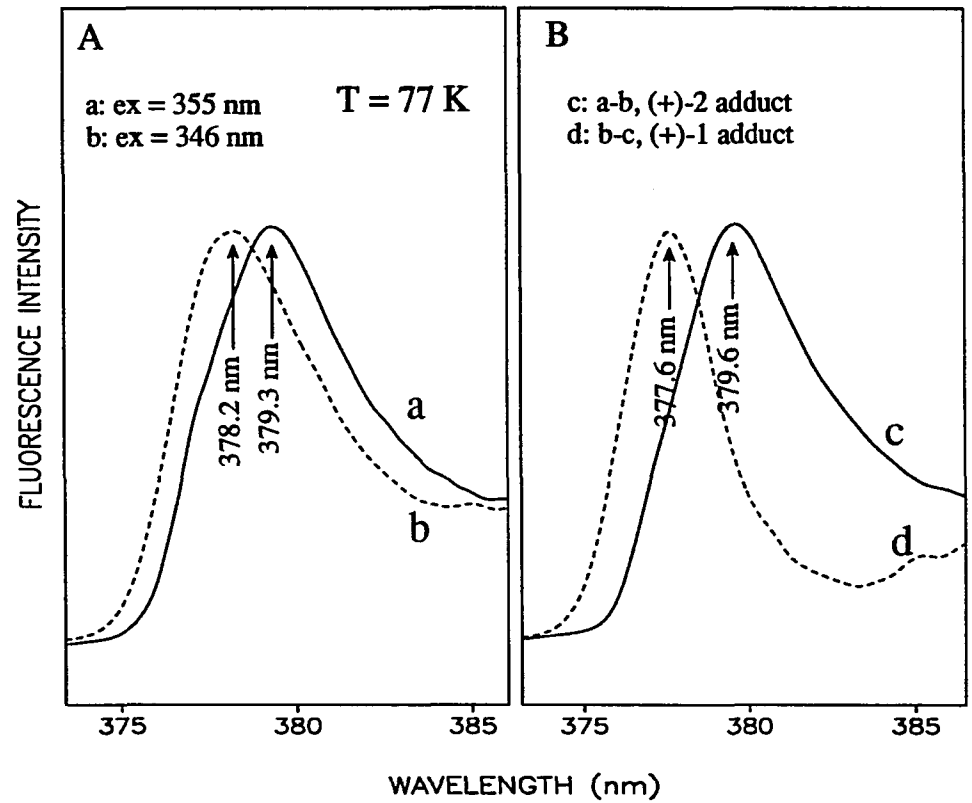

Figure 45. Laser-excited fluorescence spectra (A) of (+)-*trans*-BPDE-d(ATATGTATA) obtained with λ_{ex} = 355 nm (spectrum a) and 346 nm (spectrum b). Spectrum c was obtained by subtracting the contribution of (+)-1 type adduct (spectrum a) from spectrum b to depict the origin band of the (+)-2 type adduct, whereas spectrum d was obtained by subtracting the contribution of the (+)-2 type adduct (spectrum b) from spectrum a to reveal the origin band of the (+)-1 type adduct

markedly reduced. The contribution of the (+)-2 type adduct to spectrum b can also be eliminated by subtracting an appropriately scaled spectrum c from spectrum b. The resulting b-c spectrum is shown as spectrum d in Figure 45B, and is that of the minor (+)-1 type adduct. As can be seen in Figure 45B, the non-line narrowed fluorescence profile of the (+)-1 adduct is characterized by narrower band width (FWHM ~220 cm^{-1}) than that of the (+)-2 adduct and, furthermore, is blue-shifted by ~2 nm. This has been observed previously for DNA- and polynucleotide-BPDE adducts, where (+)-1 type (+)-*anti*-BPDE adduct has been determined as the major contribution.

Precise quantitation of the (+)-1 and (+)-2 adducts cannot be obtained from the spectra in Figure 45 (*e. g.* molar extinction coefficients and fluorescence quantum yields have not been measured). However, with essentially identical experimental conditions (*e. g.*, same laser power, same gated mode, same slit width, *etc.*) for both excitations wavelengths (355 and 346 nm), and since the (+)-1 adduct should have the higher fluorescence quantum yield due to weaker interaction with the oligonucleotide helix we conclude that the major adduct formed from (+)-*trans*-BPDE-d(ATATGTATA) is a (+)-2 type in glass host (see Table 8). Similar spectral deconvolution of the other isomeric adducts formed with single- and double-stranded oligonucleotides (and FLN spectra for other excitation wavelengths, data not shown) demonstrate that (+)-*trans*-BPDE-d(ATATGTATA) in the glass shows the largest relative contribution of the (+)-1 adduct. Furthermore, since the energy of the 0-0 origin band and FLN spectra of tetrols and the (+)-1 adduct are very similar, one cannot exclude the possibility that BPT makes a small

contribution to the spectra in Figure 45A and B. We believe that spectrum d in Fig. 45B represents the contribution from (+)-1 adduct, since (+)-*trans*-adduct is the most stable among all isomeric adducts. A summary of the above observations is given in Table 7.

2. Adducts from (+)-*trans*-BPDE

Since spectral deconvolutions (of the type just discussed) of broad fluorescence spectra for most of the olgonucleotide adducts from (±)-*anti*-BPDE studied in this dissertation were not possible, major emphasis will be given here only to the identification of the types of isomeric adducts formed with single- and double-stranded oligonucleotides. Relative ratios of the adducts of different conformation in a given sample are also determined based on broad fluorescence spectra obtained under non-line narrowing conditions as well as on FLN spectra.

Vibronically excited FLN spectra, obtained with laser excitation at 369.6 nm (spectrum A) and 356.9 nm (spectrum B) in the solid water matrix, are presented in Figure 46 for (+)-*trans*-BPDE adducts formed with d(ATATGTATA) (spectra a and e), $d(ATATGTATA)_2$ (spectra b and f), d(CACATGTACAC) (spectra c and g), and $d(CACATGTACAC)_2$ (spectra d and h), respectively. Figure 46B shows that the contribution from (+)-2′ and/or (+)-3′ ((+)-3 in double-stranded adducts) decreases from spectrum e to h, while it is comparable in spectra f and g. Excited state vibrational frequencies were labeled only for the (+)-*trans*-BPDE-d(ATATGTATA). As discussed earlier (section III-G-1), it is believed that the FLN spectrum of the (+)-*trans*-BPDE-$d(CACATGTACAC)_2$ (spectrum h) is due mainly to a (+)-2 type adduct. An important

Table 7. Nomenclature of different spatial adduct-conformations found in single- and double-stranded oligomers

Adduct[a]	Site type	Conformation
(±)-1	site II	external, weakest interaction with bases
(±)-2	site I/site II[b]	external/internal, weak interaction with bases
(±)-2′	site I	internal, moderate interaction with bases, disrupted by glass solution
(±)-3′	site I	internal, strong interaction with bases
(±)-3	site I	internal, intercalated, found in adduct formed with double-stranded oligonucleotide

a. energy level of origin band: $E_{(0,0)}$ ((±)-1) > $E_{(0,0)}$ ((±)-2) > $E_{(0,0)}$ ((±)-2′ > $E_{(0,0)}$ ((±)-3)′ > $E_{(0,0)}$ ((±)-3).

b. has more site II characteristic due to the short length of oligonucleotide.

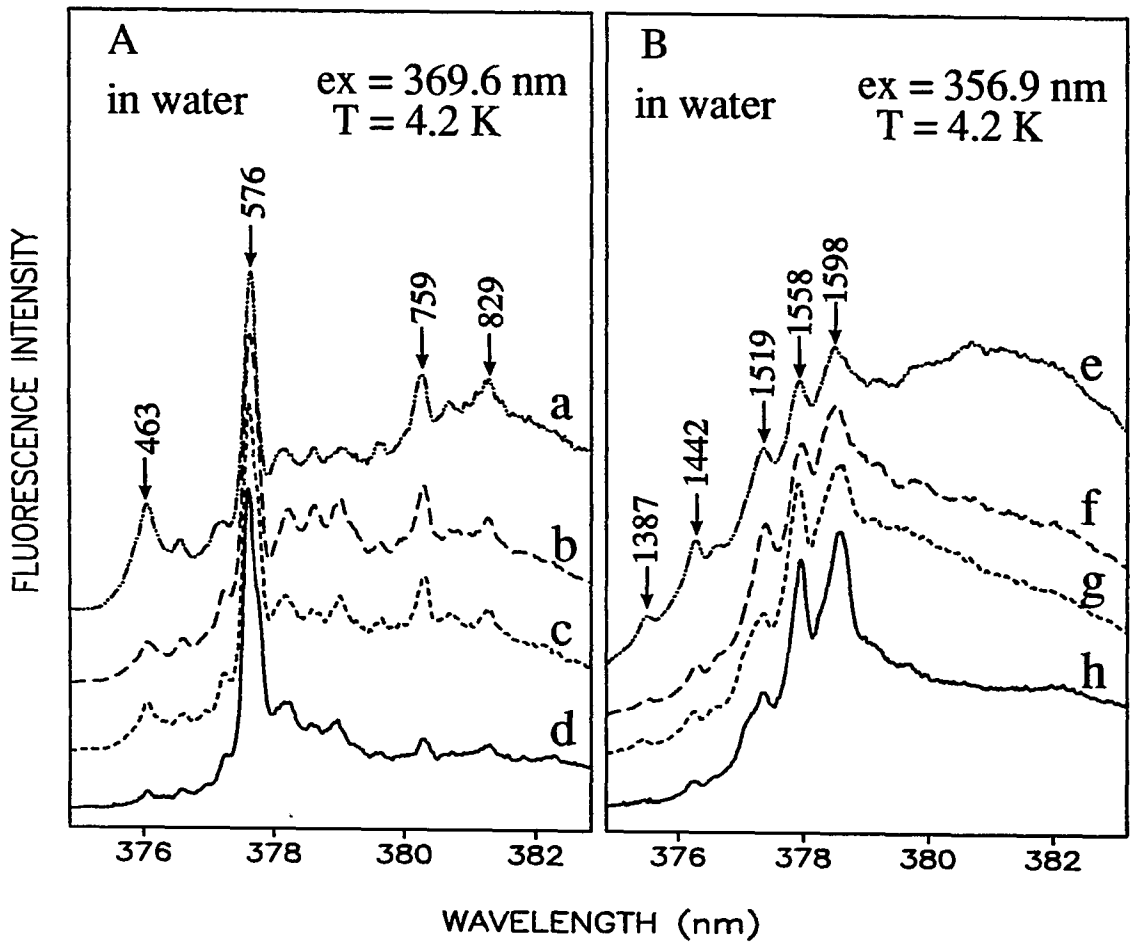

Figure 46. FLN spectra of (+)-*trans*-BPDE adducts formed with d(ATATGTATA) (spectra a and e), d(ATATGTATA)$_2$ (spectra b and f), d(CACATGTACAC) (spectra c and g), and d(CACATGTACAC)$_2$ (spectra d and h) obtained with λ_{ex} = 369.6 nm (A) and 356.9 nm (B), respectively

question is whether (+)-2′ or (+)-3′ ((+)-3 in double-stranded adducts) contributes to the broad tail in each spectrum, cf. section IV-G-1. Upon addition of the glass forming solution to the aqueous solution the broad tails in spectra e, f, and g are markedly diminished in intensities indicating that fluorescence from (+)-2′ adduct is the major contributer to the broad tails in the spectra of Figure 46B. Another aspect of the contributions from base-stacking type adducts is revealed by the FLN spectra obtained with different a laser excitation wavelength of 369.6 nm (see Figure 46A). These results show that the intensity ratio of the 576 cm^{-1} mode to either the 759 or 829 cm^{-1} mode is increased as long as more contribution of the determined (+)-2′-adducts is observed. As was observed for the (+)-*trans*-BPDE-d(ATATGTATA) adduct, see section IV-G-1, monor contributions from (+)-1 adducts are observed in all (+)-*trans*-BPDE adducts formed with single- and double-stranded oligomers upon addition of the glass solvent to the aqueous solvent (as by evidenced by a blue-shift of the fluorescence maxima for 346 nm excitation relative to the maximum for 355 nm excitation).

Broad non-line narrowed fluorescence spectra for the solid water matrix are compared in Figure 47 for two extreme cases: (+)-*trans*-d(ATATGTATA) for which the (+)-2′ contribution is maximized (spectrum b) and (+)-*trans*-d$(CACATGTACAC)_2$ for which no (+)-2′ conformation is observed (spectrum a). The fluorescence origin band of the adduct formed with the double-stranded 11-base oligonucleotide centered at ~380.5 nm is due mainly to the (+)-2 adduct, while that originating from the (+)-*trans*-d(ATATGTATA) at ~381.0 nm is due to the (+)-2′-adduct. Interestingly, the broad

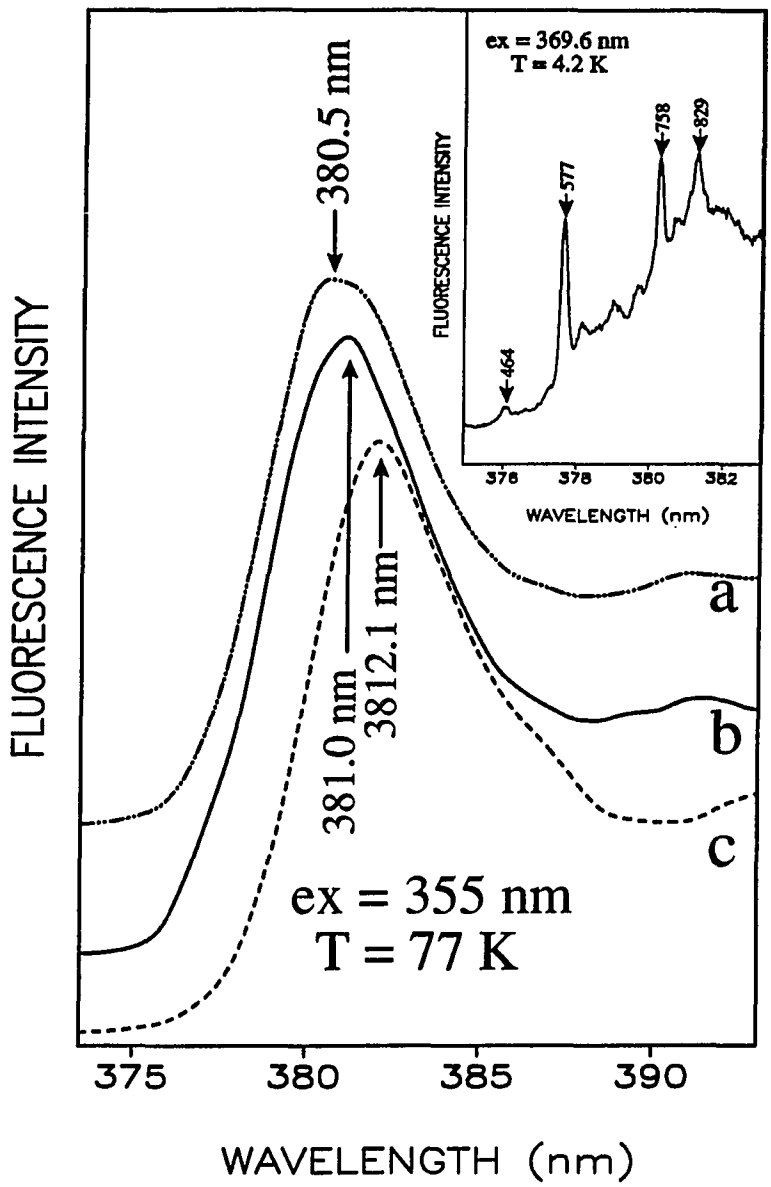

Figure 47. Laser-excited fluorescence spectra of (+)-*trans*-BPDE adducts formed with d(CACATGTACAC)$_2$ (spectrum a), d(ATATGTATA) (spectrum b), and d(CACATGTACAC)•d(GTGTAAATGTG) (spectrum c), respectively. For comparison, FLN spectrum of the (+)-*trans*-BPDE adduct formed with artificial duplex obtained with λ_{ex} = 369.6 nm is shown in the inset

fluorescence origin band (spectrum c) of the (+)-*trans*-BPDE adducts formed with the 11-base oligonucleotide annealed with the artificial complement (d(GTGTAAATGTG)), is far more red-shifted and centered at ~382.1 nm, indicating that the random sequence arising from the duplexation of two different strands, in contrast to self-complexation, forms adducts with much stronger base-stacking interactions. One expect, therefore, that the intensity ratio of the 576 cm^{-1} mode to 759 cm^{-1} mode shown (see FLN spectra of Figure 46A) should be decreased significantly in the corresponding spectrum of the artificial duplex. This is confirmed by the FLN spectrum which was obtained with a laser excitation at 369.6 nm (see the inset of Figure 47).

For reasons discussed in section III-G-1, quantitation of the nucleotide-adducts of different conformation is not as straightforward as site type identification. But again, the fluorescence quantum yields of base-stacked adducts should be lower than those of external adducts. It follows that the base-stacked adducts constitute the major contribution as long as the intensity of their broad featureless fluorescence is comparable to that of the prominent 1598 cm^{-1} mode (associated with the (+)-2-adduct) in the FLN spectra obtained with 356.9 nm excitation. With this reasoning the major adduct conformation from (+)-*trans*-d(ATATGTATA) in the solid water matrix is the (+)-2′ type, see spectrum e of Figure 46B, while the (+)-2′ type adduct for (+)-*trans*-BPDE adducts formed with $d(ATATGTATA)_2$ and d(CACATGTACAC) is minor, respectively. Our findings are summarized in Table 8.

An interesting speculation can be made based on the fluorescence spectra of (+)-

Table 8. Spatial conformations of the (+)-*anti-trans*-BPDE-oligonucleotide adducts in solid water and glass host

(+)-*trans*-BPDE-d(ATATGTATA)	in Water	(+)-2 major (+)-2′ major ~381.5 nm
	in Glass[a]	(+)-1 minor ~377.6 nm (+)-2 major ~379.6 nm
(+)-*trans*-BPDE-d(ATATGTATA)$_2$	in Water	(+)-2 major ~380.3 nm (+)-2′ minor
	in Glass	(+)-1 minor (+)-2 major ~379.9 nm
(+)-*trans*-BPDE-d(CACATGTACAC)	in Water	(+)-2 major[b] (+)-2′ minor
	in Glass	(+)-1 minor (+)-2 major ~380.0 nm
(+)-*trans*-BPDE-d(CACATGTACAC)$_2$	in Water	(+)-2 major ~380.5 nm (+)-2′ minor
	in Glass	(+)-1 minor (+)-2 major ~380.4 nm

a. mixture of glycerol 0.5: water 0.4: ethanol 0.1

b. origin band of adduct in (+)-2 conformation cannot be determined due to relatively large contribution of minor adduct in (+)-2′ conformation.

trans-BPDE adducted to single- and double-stranded 11- and 9-mers. When single-stranded aqueous (±)-*trans*-BPDE adducts of d(ATATGTATA) or d(CACATGTACAC) form complexes with their natural complements, the base-carcinogen interactions responsible for the broad tails in Figure 46B are interrupted as shown by the dramatic intensity decreases of the tails, *i.e.*, spectrum e versus f (for 9-mer) and spectrum g versus h (for 11-mer). This was confirmed by the studies of Geacintov *et al.* [186] which showed that the origin band(s) was blue-shifted and the molar absorption coefficients of (±)-*trans*-BPDE adducts with the 11-base oligonucleotide were increased upon annealing. As can be seen in Figure 46B and Table 8, for both adducts of $d(ATATGTATA)_2$ or $d(CACATGTACAC)_2$ in the solid water host, more solvent accessible but still (+)-2 type conformation is preferred over the base-stacked conformation ((+)-2′ and/or (+)-3′) in the single-stranded adduct. Similar behaviors of (+)-*trans*-BPDE adducts with native DNA and/or different synthetic polynucleotide were also observed [186].

3. Adducts from (+)-*cis*-BPDE

The characteristics of (+)-*cis*-BPDE adducts are markedly different from those of (+)-*trans*-BPDE. Compared to the dominant (+)-2 conformation of (+)-*trans*-BPDE adducts formed with single- and double-stranded oligonucleotides, the formation of adducts from (+)-*cis*-BPDE formed with the same oligonucleotides favors the more base-stacked (+)-2′ and/or (+)-3′ ((+)-3 in duplex) conformations. This finding is in agreement with our previous assignment [171] that the majority of intercalated adducts in native DNA, adopting site I configuration, have the *cis*-BPDE-dG structure. Broad 77 K non-

line narrowed fluorescence spectra are presented in Figure 48A. Spectrum a for (+)-*cis*-BPDE-d(CACATGTACAC)$_2$ with its fluorescence origin band at 381.5 nm is red-shifted ~1 nm relative to the (0,0) band of (+)-*trans*-d(CACATGTACAC)$_2$, see spectrum a of Figure 47. This large red-shift suggests that the contributions from much stronger base-stacked adduct conformations, (*e. g.*, (+)-2′ and/or (+)-3) are present. Some part of this red-shift may be due to the fact that the origin bands of adducts in the *cis*-configuration is generally located at lower energy than those of adducts of *trans*-configuration. For comparison, the broad fluorescence spectrum of (+)-*cis*-BPDE-d(CACATGTACAC) annealed with the artificial complement, d(GTGTAAATGTG), is also shown in Figure 48A (spectrum b). As in the case of the (+)-*trans*-BPDE adduct formed with an artificial duplex, the (+)-*cis*-BPDE adduct also shows tendency to form strongly base-stacked conformation in artificial duplex. As expected, spectrum b in Figure 48A is further red-shifted from spectrum a by ~0.3 nm but not to be as same degree as that observed between (+)-*trans*-BPDE-d(CACATGTACAC)$_2$ (spectrum a) and (+)-*trans*-BPDE-d(CACATGTACAC)• (GTGTAAATGTG) (spectrum c) in Figure 47.

The contribution of (+)-2′ and (+)-3′ ((+)-3 adduct in duplex) is confirmed by FLN spectra obtained with laser excitation at 356.9 nm . A specific region of vibronically excited FLN spectra is presented in Figure 48B for (+)-*cis*-BPDE adducts formed with d(CACATGTACAC)$_2$ (spectrum c), d(CACATGTACAC) (spectrum d), d(ATATGTATA)$_2$ (spectrum e), and d(ATATGTATA)$_2$ (spectrum f) in the solid water matrix. All spectra are characterized by intense broad band at ~381.5 nm and a few

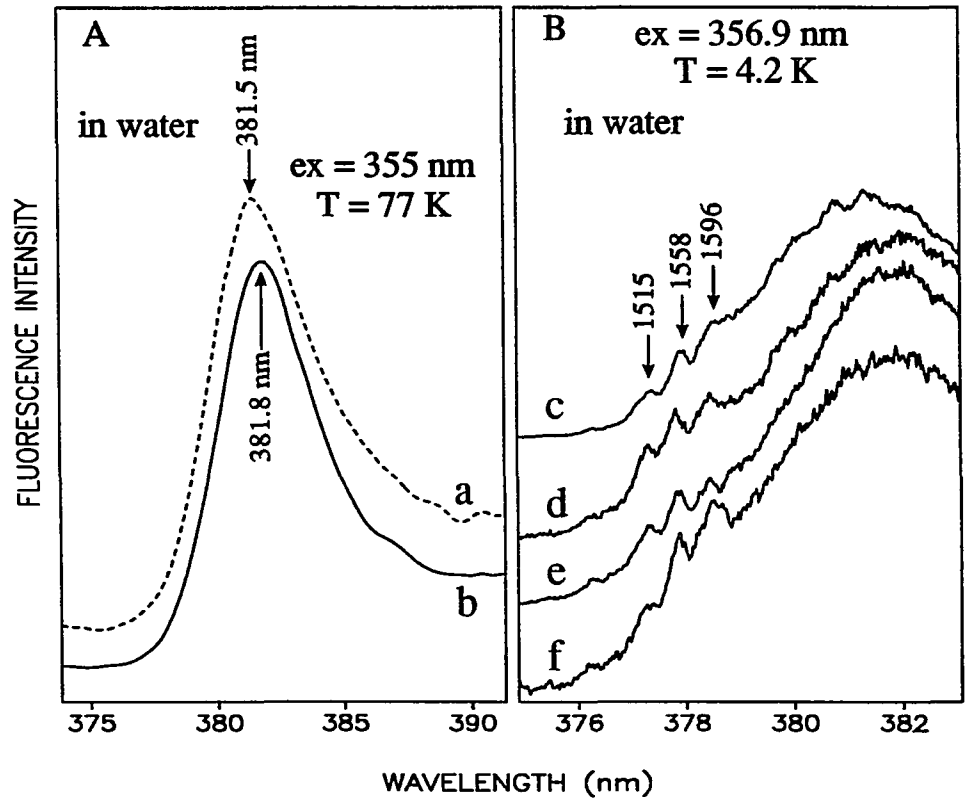

Figure 48. Laser-excited fluorescence spectra (A) of aqueous (+)-*cis*-BPDE adducts formed with d(CACATGTACAC)$_2$ (spectrum a) and d(CACATGTACAC)•d(GTGTAAATGTG) (spectrum b) obtained with λ_{ex} = 355 nm. FLN spectra (B) of aqueous (+)-*cis*-BPDE adducts formed with d(CACATGTACAC)$_2$ (spectrum c), d(CACATGTACAC) (spectrum d), d(ATATGTATA)$_2$ (spectrum e), and d(ATATGTATA) (spectrum f), respectively

weak ZPLs. In a manner consistent with the results presented in section IV-G-1, the intense broad band in each spectrum is believed to originate from adducts possessing a base-stacked conformations, *i.e.*, (+)-2′ and/or (+)-3′ ((+)-3 adduct in duplex). Minor amount of the (+)-2 adducts are indicated by the weak ZPLs in Figure 48B. The intensity ratios of the ZPL, for example that of the 1596 cm^{-1}mode, to the broad band are extremely low compared to those of (+)-*trans* analogs shown in Figure 45B. In contrast to the preference of the (+)-2 conformation for (+)-*trans* adducts formed with single- or double-stranded d(CACATGTACAC) in the solid water matrix, base-stacked (+)-*cis* adducts formed with single-stranded oligonucleotides (spectra d and f in Fig. 48B) seem to retain their conformation upon annealing (spectra c and e in Fig. 48B). Nevertheless, the broad band in each spectrum of Figure 48B is believed to be due primarily to (+)-2′ and/or (+)-3′ ((+)-3 adduct in duplex). To check this, each aqueous sample was mixed with an equal amount of the glass forming solvent and subjected to FLNS analysis.

The corresponding FLN spectra of glassy sample obtained with 356.9 nm excitation are presented in Figure 49 for (+)-*cis*-BPDE adducts formed with $d(CACATGTACAC)_2$ (spectrum a), d(CACATGTACAC) (spectrum b), $d(ATATGTATA)_2$ (spectrum c), and d(ATATGTATA) (spectrum d), respectively. Since we have postulated that only less tightly base-stacked adducts (in (+)-2′ conformation) are disrupted by the glass solvent, and converted to more external (+)-2 conformations, any contribution from the adducts in tightly stacked (+)-3′ or (+)-3 conformations should contribute as a broad fluorescence feature. This is observed in Figure 49, where one can

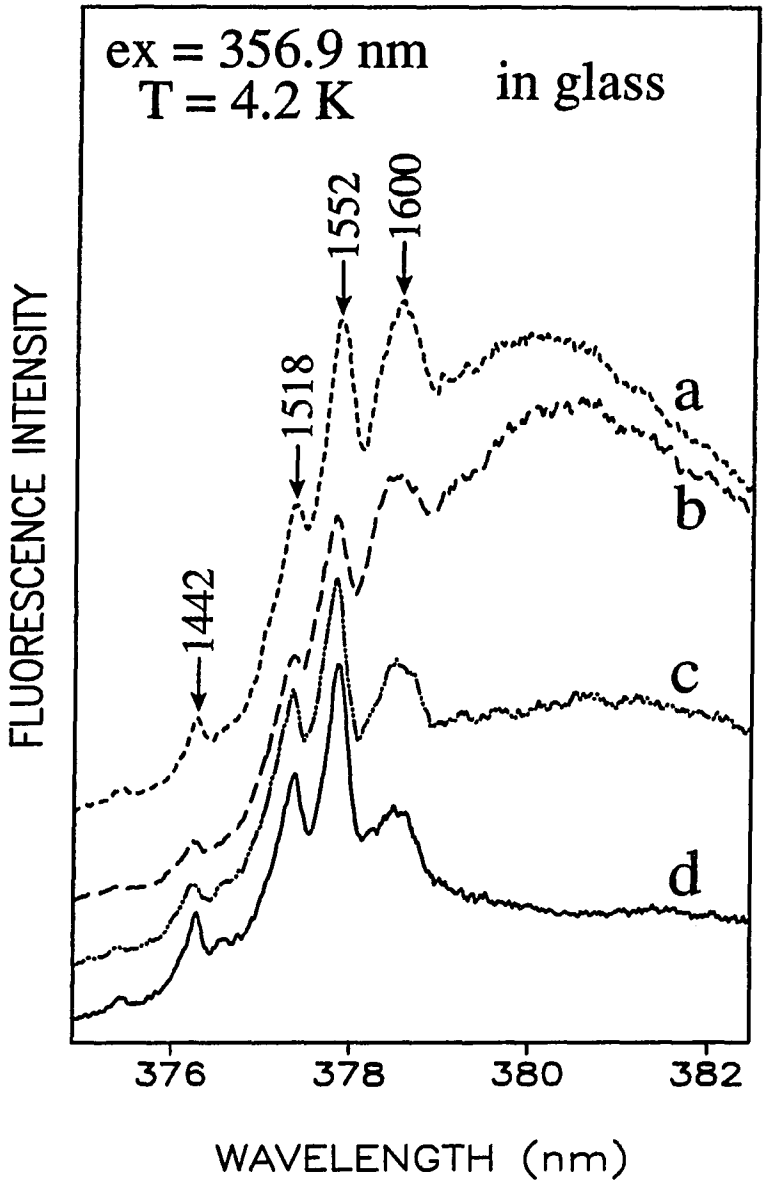

Figure 49. FLN spectra of (+)-*cis*-BPDE adducts formed with d(CACATGTACAC)$_2$ (spectrum a), d(CACATGTACAC) (spectrum b), d(ATATGTATA)$_2$ (spectrum c), and d(ATATGTATA) (spectrum d), respectively

note that intensity of broad tail is clearly decreased, while relatively well resolved ZPLs are relevant. In addition, different intensities of broad tails, believed to be originating from (+)-3′ or (+)-3, is yet noticed depending on the nature of oligonucleotides. The FLN spectrum of adduct formed with d(CACATGTACAC) (spectrum b) and $d(CACATGTACAC)_2$ (spectrum a) show a relatively high intensity for the broad fluorescence band which indicates that the adducts of those oligomers contain a larger fraction of (+)-3′ or (+)-3. Spectra a and b indicate that upon annealing, the (+)-3′ type adduct in the single-stranded structure adopts (+)-3 conformation with its stronger base-pyrene-base interaction. Using arguments presented in section IV-G-2, we conclude that (+)-3′-*cis*-BPDE and (+)-3-*cis*-BPDE are the major conformation formed with d(CACATGTACAC) and $d(CACATGTACAC)_2$, respectively, in both the solid water and glass matricies (see Table 9). The characteristics of the adduct responsible for the broad band of spectrum f in Figure 48 for (+)-*cis*-BPDE-d(ATATGTATA) is quite different. Upon mixing with the glass forming solvent, broad band is completely quenched (compare spectrum f of Fig. 48B with spectrum d of Fig. 49) indicating that only (+)-2′ conformation is present for (+)-*cis*-BPDE-d(ATATGTATA) in the solid water matrix. In addition, the 77 K non-line narrowed fluorescence spectra obtained with λ_{ex} = 346 nm (data not shown) of the above (+)-*cis* adducts are also blue-shifted relative to those obtained with 355 nm excitation proving that minor contribution from a (+)-1 type adduct located at higher energy region than the (+)-2 type is present (see Table 8). This minor adduct is assigned as (+)-1-*cis*. However, the possibility that the unique behavior of the

Table 9. Spatial conformations of the (+)-*anti-cis*-BPDE-oligonucleotide adducts in solid water and glass host

(+)-*cis*-BPDE-d(ATATGTATA)	in Water	(+)2 minor (+)2′ major ~381.8 nm
	in Glass	(+)1 minor ~377.8 nm (+)2 major ~379.8 nm
(+)-*cis*-BPDE-d(ATATGTATA)$_2$	in Water	(+)2 minor (+)2′ major (+)3 intermediate
	in Glass	(+)1 minor (+)2 major ~380.3 nm (+)3 intermediate
(+)-*cis*-BPDE-d(CACATGTACAC)	in Water	(+)2 minor (+)2′ intermediate (+)3′ major
	in Glass	(+)1 minor (+)2 intermediate (+)3′ major
(+)-*cis*-BPDE-d(CACATGTACAC)$_2$	in Water	(+)2 minor (+)2′ intermediate (+)3 major
	in Glass	(+)1 minor (+)2 intermediate (+)3 major

9-base oligomer is caused by the helix instability (due to the short length) cannot be excluded. The preference of base-stacked conformations of (+)-*cis*-BPDE-d(CACATGTACAC)$_2$ may be the reason for observed hyperchromic effect and the 20% decrease of molar extinction coefficient in the double-stranded form of carcinogen modified 11-mer compared to (+)-*cis*-BPDE-d(CACATGTACAC) [186].

4. Adducts from (-)-*trans*-BPDE

Spectroscopic data for (-)-*trans*-BPDE formed with single- and double-stranded d(CACATGTACAC) were discussed in section III-G-1. Briefly, (-)-2′ and (-)-3′ conformations are implicated in (-)-*trans*-d(CACATGTACAC) (spectrum a in Fig. 43A). The (-)-2′ adduct is converted to (-)-2 site type by addition of the glass forming solvent. This heterogeneity of (-)-*trans* adducts should be contrasted with the homogeneity (single (+)-2′ contribution) of (+)-*trans* adducts formed with single- and double-stranded 11-mers. However, virtually all of the broad fluorescence band of spectrum a in Figure 44B for (-)-*trans*-d(CACATGTACAC)$_2$ is quenchable (spectrum c in Fig. 44B) by addition of the glass forming solvent. In other words, a significant amount of (-)-*trans*-BPDE-d(CACATGTACAC)$_2$ is in the (-)-2′ base-stacked conformation for which the chromophore is less and more tightly stacked than that in the (-)-3′/(-)-3 and (-)-2 type conformations respectively.

Geacintov *et al.* have correlated site types I and II (or internal and expernal) to the configuration of adduction (*cis* and *trans*) [176-179,186]. In general,the *trans* configuration is characterized as site type II, whereas *cis* adduct is classified as site type

I. Even though the carcinogen interacts less strongly with bases of oligonuleotides in (±)-2′ than in (±)-3, which were previuosly assigned as site I [171,183], all the base-stacking properties of the (-)-2′ conformation allow this adduct to be assigned as site type I. This (-)-2′ conformation of (-)-*trans*-BPDE-d(CACATGTACAC)$_2$, identified here for the first time, may be responsible for the disagreement in configuration-conformation relationship observed by Geacintov *et al.* [186], where they observed that the ratio of *cis* to *trans* was ~1.7, whereas the ratio of site I to site II was ~9. These ratios were obtained for (-)-*anti*-BPDE-poly(dG)•(dC) adducts [186]. Therefore, the assignment of *trans*-type adducts as site II is not generally valid based on the oligomers we have studied.

Turning to the (-)-*trans*-BPDE adduct formed with single-stranded d(ATATGTATA) (data not shown), it is observed that a greater amount of adduct tends to reside in base-stacked conformations relative to the (+)-*trans* counterpart (see Table 10). However, the (-)-2′ conformation turns out to be responsible for the base-stacked conformation of an adduct formed with the single-stranded 9-mer as evidenced by FLN spectrum of glassy sample (data not shown). Accordingly, only a small contribution of (-)-3′-*trans* to the base-stacked adducts is observed. A spectroscopic study of adducts formed with double-stranded 9-mer was not accomplished due to the unavailability of proper standard material. The identified comformations and abundances of adducts for the (-)-*trans* adducts are summarized in Table 10.

Table 10. Spatial conformations of the (-)-*anti-trans*-BPDE-oligonucleotide adducts in solid water and glass host

(-)-*trans*-BPDE-d(ATATGTATA)	in Water	(-)-2 minor (-)-2′ major (-)-3′ minor
	in Glass	(-)-1 minor (-)-2 major (-)-3′ minor
(-)-*trans*-BPDE-d(ATATGTATA)$_2$	in Water	not available
	in Glass	not available
(-)-*trans*-BPDE-d(CACATGTACAC)	in Water	(-)-2 minor (-)-2′ major (-)-3′ major
	in Glass	(-)-1 minor (-)-2 major (-)-3′ intermediate
(-)-*trans*-BPDE-d(CACATGTACAC)$_2$	in Water	(-)-2 minor (-)-2′ major
	in Glass	(-)-1 minor (-)-2 major

5. Adducts from (-)-*cis*-BPDE

The behavior of (-)-*cis*-BPDE adducts formed with d(CACATGTACAC) and $d(CACATGTACAC)_2$ are remarkably similar to their (+)-*cis*-BPDE counterparts. It is the adduct covalently bound to d(ATATGTATA) that shows the stronger base-stacking for (-)-*cis*-BPDE. The type of conformation for (-)-*cis* adducts formed with the single- and double-stranded 11-mers or single-stranded 9-mer are summarized in Table 11. Figure 50 presents vibronically excited FLN spectra, obtained with laser excitation at 356.9 nm, for (-)-*cis*-BPDE-d(ATATGTATA) in solid water matrix (spectrum a) and glass (spectrum b). As found for (+)-*cis*-BPDE-d(ATATGTATA) (spectrum f in Fig. 48), (-)-*cis*-BPDE-d(ATATGTATA) in solid water is characterized by significant base-stacked conformations as evidenced by intense featureless broad band centered at ~381.5 nm. Nevertheless, the broad bands of spectrum a in Figure 50 and sepctrum f in Figure 48 are somewhat different each other. Upon mixing with the glass forming solvent, only part of the broad band in the FLN spectrum of (-)-*cis*-d(ATATGTATA) is quenched (compare spectra a and b of Fig. 50), whereas the broad band of spectrum f in Figure 48 (for (+)-*cis*) is completely quenched. These data reveal the (+)-2′ character of the base-stacked conformation for (+)-*cis* and heterogeneous nature ((-)-2′ and (-)-3′) for the base-stacked conformation of (-)-*cis*, for which (-)-3′ is assessed as the major component. The unavailability of proper standard material prevents further spectroscopic study of the (-)-*cis* adducts formed with double-stranded d(ATATGTATA).

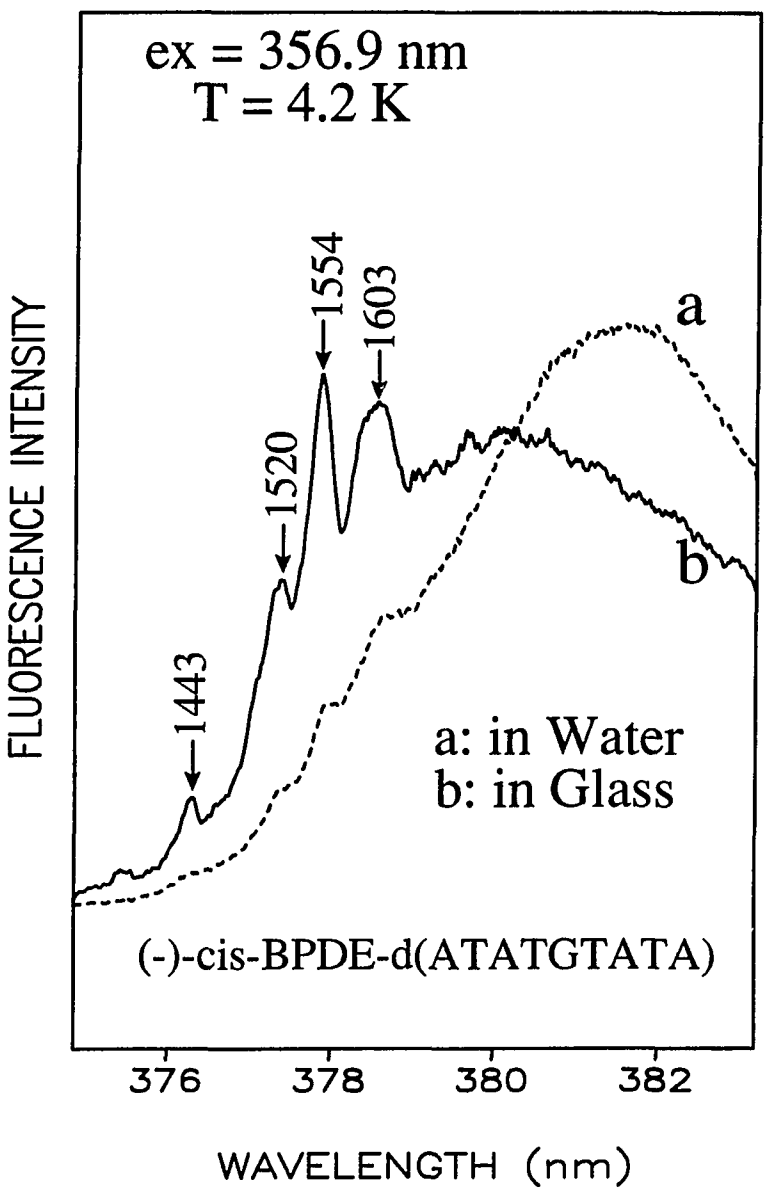

Figure 50. FLN spectra of (-)-*cis*-BPDE-d(ATATGTATA) in water (spectrum a) and in glass (spectrum b), respectively

Table 11. Spatial conformations of the (-)-*anti-cis*-BPDE-oligonucleotide adducts in solid water and glass host

(-)-*cis*-BPDE-d(ATATGTATA)	in Water	(-)2 minor (-)2′ intermediate (-)3′ major
	in Glass	(-)1 minor (-)2 intermediate (-)3′ major
(-)-*cis*-BPDE-d(ATATGTATA)$_2$	in Water	not available
	in Glass	not available
(-)-*cis*-BPDE-d(CACATGTACAC)	in Water	(-)2 minor (-)2′ major (-)3′ intermediate
	in Glass	(-)1 minor (-)2 major (-)3′ intermediate
(-)-*cis*-BPDE-d(CACATGTACAC)$_2$	in Water	(-)2 minor (-)2′ intermediate (-)3 major
	in Glass	(-)1 minor (-)2 intermediate (-)3 major

V. CONCLUSIONS

Analytical application of the superior selectivity of the laser-based solid state FLNS technique was demonstrated for the detection and identification of the PAH metabolites and adducts encountered in the metabolic pathways, one-electron oxidation mechanism and monooxygenation mechanism, of chemical carcinogenesis. Despite the fact that the thrust of this research is analytical in nature, it has been possible to generate results of pure spectroscopic interest. For example, the excited state vibrational frequencies and their intensity distributions could be obtained by taking the energy differences between excitation laser wavelength and locations of ZPLs.

The superior selectivity of FLNS methods were demonstrated by the successful resolution of B[a]P from 8 different isomeric standard B[a]P-adducts, and DMBA from 6 different isomeric standard DMBA-adducts from one-electron oxidation mechanism, and 6 different standard BPDE-adducts expected from monooxygenation mechanism. FLNS technique could also distinguish isomeric (±)-*trans*- and (±)-*cis*-tetrols from the hydrolysis of both *anti*- and *syn*-BPDE. FLN spectra of H_4DMBA were only briefly discussed to demonstrate the embeded aggregation problems encountered in FLNS study. After all, it was demonstrated that the combination of synthesis and FLNS-identification of standard adducts is a power approach to understand the process of tumor initiation and designing preventive strategies.

The isolation and FLNS-identification of depurinated BP-N7Gua adduct in urine and feces of mouse was accomplished for the first time from *in vivo* experiment in

fulfillment that one-electron oxidation is another relevant mechanism of tumor initiation step of B[a]P. This was further suppoted by subsequent *in vitro* experiment in which significant amount of B[a]P (~80%) was metabolized by one-electron oxidation in MC-induced microsomal reaction, and corresponding depurinated BP-C8Gua, BP-N7Gua, and BP-N7Ade were identified by FLNS technique. Similarly, adducts formed by one-electron oxidation mechanism were assessed as major adducts in HRP reaction condition. Other minor depurinated adduct by monooxygenation mechanism was identified as BPDE-N7Ade. Identical result from subsequent *in vivo* experiment using mouse skin demonstrated that *in vitro* experiment is legitimate for the study of biological system.

Similar experiment performed with DMBA demonstrated that one-electron oxidation is the predominant mechanism in the covanent binding of DMBA to DNA catalyzed by MC-induced rat liver microsomes. The two major DMBA-DNA adducts formed were depurinated adducts in which specifically the 12-CH_3 group is bound to the N-7 of Ade and Gua. These two adducts constitute 98.6% of the total adducts. No adducts were detected in which the 7-CH_3 group was bound to a nucleic acid base.

A methodology based on the combination of fluorescence line narrowing spectroscopy at 4.2 K with non-line narrowed ($S_2 \leftarrow S_0$ laser excitation) fluorescence spectroscopy at 77 K, and structural interuption by glass mixture, was employed to characterized (±)-*trans*- and (±)-*cis*-adducts formed with the single- and double-stranded d(ATATGTATA) or d(CACATGTACAC) oligonucleotides. Detailed comparisons of the fluorescence spectra in both aqueous and glass mediums were utilized to characterized

spacial orientations of pyrenyl moiety as (±)-1, (±)-2, (±)-2′, (±)-3′, and (±)-3, respectively. It was also demonstrated that glass solution frequently used for FLNS study may interupt spacial conformations of adducts in aqueous state. Furthermore, it was illustrated that pyrenyl chromophore of (+)-*trans*-BPDE adducts in base-stacked conformation is interupted upon annealing that a solvent-exposed (+)-2 conformation is preferred over the carcinogen-base stacked conformation in the single-stranded adduct. In concontrary, however, (±)-*cis*-BPDE adducts prefers highly interactive base-stacked conformation when these are annealed. (-)-*trans*-BPDE adducts covalently bound to, especially, d(CACATGTACAC)$_2$ seems to prefer base-stacked conformation which are different from those in (±)-*cis*-BPDE adducts bound to oligonucleotides in nature. Upon annealing, the base-stacked pyrene of (-)-*trans*-BPDE adudct formed with double-stranded 11-mer is in (-)-2′ conformation, whereas (±)-*cis* analogs are in (±)-3 conformation.

VI. LITERATURE CITED

1. Chemical and Human Cancer; International Agency for Research on Cancer Monographs, 1972; Vol. 3.
2. Bishop, J. M. Science 1987, 235, 305.
3. Pollack, R. Readings in Mammalian Cell Culture; Cold Spring Harbor: New York, 1975.
4. Heiger, I. Carcinogenesis; Academic Press: New York, 1961; pp 7-17.
5. Lynch, H. T. Cancer Genetics; Thomas: Springfield, IL, 1976.
6. Schimke, R. N. Genetics and Cancer in Man; Churchill Livingstone: New York, 1978.
7. Ponder, B. A. J. Biochim. Biophys. Acta 1980, 605, 369.
8. Rowley, J. D. Cancer Invest. 1983, 1, 267.
9. Yunis, J. J. Science 1983, 221, 227.
10. Rowley, J. D. Cancer Res. 1984, 44, 3159.
11. Lehmann, A. R. Cancer Surv. 1982, 1, 1982.
12. Hanawalt, P. C.; Sarasir, A. Trends Genet. 1986, 2, 124.
13. Ames, B. N. Science 1979, 204, 587.
14. Tooze, J. DNA Tumor Viruses. Molecular Biology of Tumor Viruses; Cold Spring Harbor: New York, 1981.
15. Weiss, R.; Teich, N.; Varmus, H.; Coffin, J. RNA Tumor Viruses. Molecular Biology of Tumor Viruses; Cold Spring Harbor: New York, 1984.

16. Upton, A. C. In Cancer Medicine; Lea and Febiger: Philadelphia, 1982; pp 96-108.

17. Baum, E. J. In Polycyclic Hydrocargons and Cancer; Harvey, R. G., Ed.; Academic Press: New York, 1978; pp 45-62.

18. Brown, R. A.; Huffman, H. L. Science 1976, 191, 847.

19. Shabad, L. M. J. Natl. Cancer Inst. 1980, 64, 405.

20. Pott, P. National Cancer Inst. Monogr. 1963, 10, 7.

21. Phillips, D. H. Nature 1983, 303, 468.

22. Cook, J. W.; Hewett, C.L.; Hieger, I. J. Chem. Soc. 1933, 395.

23. Thakker, D. R.; Yagi, H.; Levin, W.; Wood, A. W.; Conney, A. H.; Jerina, D. M. In Bioactivation of Foreign Compounds; Anders, M. W., Ed; Academic Press: New York, 1985; pp 177-242.

24. Miller, E. C.; Miller, J. A. Cancer 1981, 47, 2327.

25. Gräslund, A.; Jernström, B. Quart. Rev. Biophys. 1989, 22, 1-37.

26. Huggins, G. C. B. Experimental Leukemia and Mammary Cancer; University of Chicago Press: Chicago, 1979.

27. Harvey, R. G. In Working Group on: Molecular Mechanism of Carcinogenic and Antitumor Activity; Chagas, C.; Pullman, B., Eds, 1986.

28. Geacintov, N. E. In Polycyclic Hydrocarbon and Carcinogenesis; Harvey, R. G., Ed; Americal Chemical Sciety: Washington, D. C., 1985.

29. Jankowiak, R.; Day, B. W.; Lu, P.; Doxtader, M. M.; Skipper, P. L.; Tannenbaum, S.R.; Small, G. J. J. Am. Chem. Soc. 1990, 112, 5866-5869.

30. Calleman, C. J. Ph. D. Dissertation, University of Stockholm: Sweden, 1984.

31. Conney, A. H. Cancer Res. 1982, 42, 4875-4917.

32. Sims, P.; Grover, P. L. In Polycyclic Hydrocarbons and Cancer; Gelboin, N. V.; Ts'o, P. O. P., Ed.; Academic Press: New York, 1981; Vol. 3, pp 117-181.

33. Weinstein, I. B.; Jeffrey, A. M.; Jennette, K. W.; Blobstein, S. H.; Harvey, R. G.; Harris, C.; Autrup, H.; Kasai, H.; Nakanishi, K. Science 1976, 193, 592-595.

34. Cavalieri, E. L.; Rogan, E. G. Free Rad. Res. Comms. 1990, 11, 77-87.

35. Cavalieri, E. L.; Rogan, E. G. Environ. Health Perspect. 1985, 64, 69-84.

36. Cavalieri, E. L.; Rogan, E. G. In Polycyclic Hydrocarbons and Carcinogenesis; Harvey, R. G., Ed.; ACS Press: Washington, DC., 1985; Chapter 11.

37. Pullman, A.; Pullman, B. Adv. Cancer Res. 1955, 3, 177.

38. Sims, P.; Grover, P. L.; Swaisland, A.; Pal, K.; Hewer, A. Nature 1974, 252, 326.

39. Boyd, D. R.; Jerina, D. M. In Small Ring Heterocycles; Hassner, A., Ed.; Wiley: New York, 1984; Part 3, pp 197-282.

40. Jerina, D. M.; Daly, J. W.; Witkot, B.; Zaltzman-Nirenberg, P.; Udenfriend, S. Arch. Biochem. Biophys. 1968, 128, 176-183.

41. Lu, A. T. H.; Jerina, D. M.; Levin, W. J. Biol. Chem. 1977, 252, 3715-3723.

42. Borgen, A. O.; Dover, H.; Costagnoli, N. Crucker, T. T.; Rasmussen, R. C.; Wong, I. Y. J. Med. Chem. 1973, 16, 502-506.

43. Osborne, M. R.; Jacobs, S.; Harvey, R. G.; Brookes, P. Carcinogenesis 1981, 2, 553.

44. Holdr, G.; Yagi, H.; Dansette, P.; Jerina, D. M.; Levin, W. Lu, A. Y. H.; Conney, A. H. Proc. Natl. Acad. Sci. U.S.A. 1974, 71, 4356-4360.

45. Selkirk, J. K.; Croy, R. G.; Gelboin, H. V. Science 1974, 4, 169-171.

46. Holder, G.; Yagi, H.; Levin, W.; Lu, A. Y. H.; Jerina, D. M. Biochem. Biophys. Res. Commun. 1975, 65, 1363-1370.

47. Selkirk, J. K.; Croy, R. G.; Gelboin, H. V. Arch. Biochem. Biophys. 1975, 168, 322.

48. Selkirk, J. K.; Croy, R. G.; Gelboin, H. V. Cancer Res. 1976, 36, 922-926.

49. Cohen, G. M.; Haws, S. H.; Moore, B. P.; Bridges, J. W. Biochem. Pharmacol. 1976, 25, 2561-2570.

50. Grover, P. L.; Hewer, A.; Sims, P. Biochem. Pharmacol. 1974, 23, 323-332.

51. Stohs, S. J.; Grafström, R. C.; Burke, M. D.; Molders, P. W.; Orrenius, S. G. Arch. Biochem. Biophys. 1976, 177, 105-116.

52. Bresnick, E.; Stoming, T. A.; Vaught, J. B.; Thakker, D. R.; Jerina, D. M. Arch. Biochem. Biophys. 1977, 183, 31-37.

53. Jenstrom, B.; Vadi, H.; Orrenius, S. Cancer Res. 1976, 36, 4107-4113.

54. Pezzuto, J. M.; Yang, C. S.; Yang, S. K.; McCgwrt, D. W.; Gelboin, H. V. Cancer Res. 1978, 38, 1241-1245.

55. Baird, W. M; Diamond, L. Biochem. Biophys. Res. Commun. 1977, 77, 162-167.

56. DiGiovanni, J.; Sawyer, T. W.; Fisher, E. P. Cancer Res. 1986, 46, 4336.

57. Dipple, A.; Pigott, M. A.; Bigger, C. A. H.; Blake, D. M. Carcinogenesis 1984, 5,

1087.

58. Dipple, A.; Pigott, M.; Moschel, R. D.; Costantino, N. Cancer Res. 1983, 43, 4132.

59. Melikian, A. A.; Lesczynska, J. M.; Amin, S.; Hecht, S. S.; Hoffmann, D.; Pataki, J.; Harvey, R. G. Cancer Res. 1985, 45, 1990.

60. Perin-Roussel, O.; Barat, N.; Zajdela, F. Carcinogenesis 1985, 6, 1791.

61. Cavalieri, E. L.; Rogan, E. G.; Higginbotham, S.; Cremonesi, P.; Salmasi, S. Poly. Aromatic Comps. 1990, 1, 59-70.

62. Cavalieri, E. L.; Rogan, E. G.; Sinha, D. J. Cancer Res. and Clinic. Oncol. 1988, 114, 3-9.

63. Cavalieri, E. L.; Rogan, E. G.; Higginbotham, S.; Cremonesi, P.; Salmasi, S. J. Cancer Res. Clinic. Oncol. 1988, 114, 16-22.

64. Cavalieri, E. L.; Rogan, E. G.; Higginbotham, S.; Cremonesi, P.; Salmasi, S. J. Cancer Res. Clinic. Oncol. 1989, 115, 67-72.

65. Cavalieri, E. L.; Roth, R. J. Org. Chem. 1976, 41, 2679-2684.

66. Cavalieri, E. L.; Roth, R.; Rogan, E. G. In Polynuclear Aromatic Hydrocarbons: Chemistry and Biological Effects; Freudenthal, R. I.; Jones, P. W., Eds.; Raven Press: New York, 1976; Vol. 1, pp 181-190.

67. Rogan, E. G.; Roth, R.; Cavalieri, E. L. In Polynuclear Aromatic Hydrocarbons: Chemistry and Biological Effects; Bjorseth, A.; Dennis, A. J., Eds.; Battelle Press, Columbus, OH., 1980; pp 259-266.

68. Cremonesi, P.; Cavalieri, E. L.; Rogan, E. G. J. OrggwChem. 1989,54, 3561-3570.

69. Boyd, J. A.; Eling, T. E. J. Biol. Chem. 1984, 22, 13885-13896.

70. Josephy, P. D.; Eling, T. E.; Mason, R. P. J. Biol. Chem. 1983, 258, 5561-5569.

71. Degen, G. H.; Eling, T. E.; McLachlan, J. A. Cancer Res. 1982, 42, 919-923.

72. Cavalieri, E. L. Devanesan, P. D.; Rogan, E. G. Biochem. Pharmacol. 1988, 37, 2183-2187.

73. Potter, D. W.; Hinson, J. A. J. Biol. Chem. 1987, 262, 966-973.

74. Burka, L. T.; Guengerich, F. P.; Willard, R. J.; MacDonald, T. L. J. Am. Chem. Soc. 1985, 107, 2549-2551.

75. Stearns, R. A.; Ortiz de Montellano, P. R. J. Am. Chem. Soc. 1985, 107, 4081-4082.

76. Cavalieri, E. L.; Rogan, E. G.; Devanesan, P.; Cremonesi, P. Biochemical Pharmacol.1988, 37, 2173-2182.

77. Cavalieri, E. L.; Rogan, E. G.; Roth, R. W.; Saugier, R. K.; Hakam, A. Chem. Biol. Interact. 1983, 47, 87-109.

78. Devanesan, P; Rogan, E. G.; Cavalieri, E. L. Chem. Biol. Interact. 1987, 61, 89-95.

79. Arcos, J. C.; Argus, M. F. Chemical Induction of Cancer; Academic Press: New York, 1974; Vol. IIA, p 15-41.

80. RamaKrishna, N. V. S.; Devanesan, P. D.; Rogan, E. G.; Cavalieri, E. L.; Jeong, H.; Jankowiak, R.; Small, G. J. Chem. Res. Toxicol. 1991, submitted.2

81. Devanesan, P. D.; RamaKrishna, N. V. S.; Todorovic, R.; Rogan, E. G.; Cavalieri, E. L.; Jeong, H.; Jankowiak, R.; Small, G. J. Chem. Res. Toxicol. 1991, in preparation.

82. Jeffrey, A. M In Pocyclic Hydrocarbons and Carcinogenesis; Harvey, R. G., Ed.; ACS Press: Washington, D.C., 1985; p 187.

83. Cooper, T. G. The Tools of Biochemistry; Wiley: New York, 1977.

84. Milton, L. L; Milos, V. N.; Keith, D. B. Analytical Chemistry of Polycyclic Aromatic Compounds; Academic Press: New York, 1981.

85. Eisenstadt, E. In Pocyclic Hydrocarbons and Carcinogenesis; Harvey, R. G., Ed.; ACS Press: Washington, D.C., 1985; p 327.

86. Cooper, R. S. Ph.D. Dissertation, Iowa State University, 1987.

87. Brown, J. C. Ph.D. Dissertation, Iowa State University, 1982.

88. Yamasaki, E.; Ames, B. N. Proc. Natl. Acad. Sci. USA 1977, 74, 3555-3559.

89. McCann, J.; Choi, E.; Yamasaki, E.; Ames, B. N. Proc. Natl. Acad. Sci. USA 1975, 72, 5135-5139.

90. Ames, B. N.; McCann, J.; Yamasaki, C. Mut. Res. 1975, 31, 347-364.

91. Sugimura, T.; Sato, S.; Nagago, M.; Yahagi, T.; Matsushima, T.; Seino, Y.; Takeuchi, M. Kawachi, T. In Overlapping of Carcinogens and Mutagens; Magee, P. N., Ed.; University of Tokyo Press: Tokyl, 1976; pp 191-215.

92. Maugh, T. H., II. Science 1984, 226, 1183-1184.

93. Harris, C. C.; Yolken, R. H.; Hsu, I. C. In Methods in Cancer Research; Busch,

H.; Yoeman, L. C., Eds.; Academic Press: New York, 1982; pp 213-243.

94. Perera, F. P.; Poirier, M. C.; Yuspa, S. H.; Nakayama, J.; Jaretzki, A.; Curner, M. M.; Knowles, D. M.; Weinstein, I. B. Carcinogenesis 1982, 3, 1405-1410.

95. Santella, R. M.; Lin, C. D.; Cleveland, W. L.; Weinstein, I. B. Carcinogenesis 1984, 5, 373-377.

96. Bodell, W. J.; Devanesan, P. D.; Rogan, E. G.; Cavalieri, E. L. Chem. Res. Toxicol. 1989, 2, 312-315.

97. Reddy, M. V.; Gupta, R. C.; Randerath, E.; Randerath, K. Carcinogenesis 1984, 5, 231-243.

98. Randerath, K.; Randerath, E.; Agrawal, H. P.; Gupta, R. C.; Schurdak, M. E.; Reddy, M. V. Environ. Health, Perspect. 1985, 62, 57-65.

99. Jorgenson, J. W. Anal. Chem. 1986, 58, 743A-760A.

100. Ewing, A. G.; Wallingford, R. A.; Olefirowicz, T. M. Anal. Chem. 1989, 61. 292A-303A.

101. Devanesan, P. D.; RamaKrishna, N. V. S.; Todorovic, R.; Rogan, E. G.; Cavalieri, E. L.; Jeong, H.; Jankowiak, R.; Small, G. J. Chem. Res. Toxicol. 1991, in preparation.

102. Marsch, G. A.; Jankowiak, R. J.; Small, G. J. unpublished result.

103. Vahakangas, K.; Haugen, A.; Harris, C. C. Carcinogenesis 1985, 6, 1109-1116.

104. Vahakangas, K.; Trivers, G.; Rowe, M.; Harris, C. C. Environ. Health. Perspect. 1985, 62, 101-104.

105. Bright, F. V. Anal. Chem. 1988, 60, 1031A-1039A.

106. Maple, J. R.; Wehry, E. L. Anal. Chem. 1981, 53, 266-271.

107. Whery, E. L. Trends Anal. Chem. 1983, 2, 143-147.

108. Wehry, E. L.; Mamantov, G. Prog. Analyt. Spectrosc. 1987, 10, 507-527.

109. Hofstraat, J. W.; Gooijer, C.; Velthorst, N. H. In Molecular Luminescence Spectroscopy: Methods and Applications; Schulman, S. G., Ed.; John Wiley & Sons: New York, 1988; Part II, Chap. 4.

110. Goates, S. R.; Barker, A. J.; Zakharia, H. S.; Khoobehi, B.; Sheen, C. W. Appl. Spec. 1987, 41, 1392-1397.

111. Hayes, J. M. Chem. Rev. 1987, 87, 745-760.

112. Weeks, S.; Gilles, S.; Dobson, R.; Senne, S.; D'Silva, A. P.

113. Anderson, P. W. Phys. Rev. 1958, 109, 1492.

114. Silbey, R. In Spectroscopy and Excitation Dynamics of Condensed Molecular System; Agranovich, V.M.; Hochstrasser, R.M. Eds.; North Holland: Amsterdam, 1983; p 1.

115. Friedrich, J.; Haarer, D. Angew. Chem. Int. Ed. Engl. 1984, 23, 113, and references therein.

116. Rebane, K. K. Impurity Spectra of Solids; Plenum: New york, 1970.

117. Sapozhnikov, M. N. Phys. Stat. Sol. 1976, b75, 11.

118. O'sadko, I. S. Sov. Phys. Usp. 1979, 22, 311.

119. O'sadko, I. S. In Spectroscoy and Excitation Dynamics of Condensed Molecular

Systems; Agranovich, V. M.; Hochstrasser, R. M. Eds.; North-Holland: Amsterdam, 1983; p437.

120. Keil, T. Phys. Rev. 1965, 140, A601.

121. Davydov, A. S. Theory of Molecular Excitons; McGraw-Hill: New York, 1962.

118. Feld, M. S.; Javan, A. Phys. Rev. 1969, 177, 540.

119. Szabo, A. Phys. Rev. Lett. 1970, 25, 924.

120. Personov, R. I.; Al'Shits, E. I.; Bykovskaya, L. A. JETP Lett. 1974, 15, 431.

121. Personov, R. I.; Al'Shits, E. I.; Bykovskaya, L. A. Opt. Commun. 1972, 6, 169.

122. Wehry, E. L. *Trends. Anal. Chem.* 1983, 2, 143.

123. Personov, R. I. In Spectrscopy and Exctation Dynamics of Condensed Moleculear Systems; Agranivich, V. M.; Hochstrasser, R. M. Eds.; North-Holland: Amsterdam, 1983; p 555.

124. Selzer, P. M. Laser Spectroscopy of Solids; Springer-Verlag: Berlin, 1986; Chap. 4.

125. Hofstraat, J. W. High-Resolution Molecular Fluorescence Spectroscopy in Low Temperature Matrices: Principles and Analytical Application; Free University Press: Amsterdam, 1988.

126. Jankowiak, R.; Small, G. J. Anal. Chem. 1989, 61, 1023A.

127. Jankowiak, R.; Small, G. J. Chem. Res. Toxicol. 1991, 4, 256.

128. Warren, J. A.; Hayes, J. M.; Small, G. J. Chem. Phys. 1986, 102, 313.

129. Hayes, J. M.; Gillie, J. K.; Tang, D.; Small, G. J. Biochim. Biophys. Acta 1987,

932, 287.

130. Hayes, J. M.; Jankowiak, R.; Small, F. J. In Topics in Current Physics, Persistent Spectral Hole Burning: Science and Applications; Moerner, W. E., Ed.; Springer-Verlag: New York, 1987; Chap. 5.

131. Jankowiak, R.; Small, F. J. Science 1987, 237, 618.

132. Rebane, K. K. Impurity Spectra of Solids; Plenum Press: New York, 1970.

133. Tang, D.; Johnson, S. G.; Jankowiak, R.; Hayes, J. M.; Small, G. J.; Tiede, D. M. In Perspective in Photosysthesis; Kluwer: Dordrecht, 1990; p 99.

134. Johnson, S. G.; Tang, D.; Jankowiak, R.; Hayes, J. M.; Small, G. J.; Tiede, D. M. J. Phys. Chem. 1989, 93, 5953.

135. Jankowiak, R.; Tang, D.; Small, G. J.; Seibert, M J. Phys. Chem. 1989, 93, 1649.

136. Tang, D.; Jankowiak, R.; Yocum, C. F.; Seibert, M.; Small, G. J. J. Phys. Chem. 1990, submitted.

137. Tang, D.; Jankowiak, R.; Small, G. J.; Seibert, M. Photosynthe. Res. 1990, submitted.

138. Thijssen, H. P. H.; Dicker, A. I. M.; Völker, S. Chem. Phys. Lett. 1982, 92, 7.

139. Völker, S.; Van Der Waals, J. H. Mol. Phys. 1976, 32, 1703.

140. Thijssen, H. P. H.; Völker, S. Chem. Phys. Lett. 1985, 120, 496.

141. Völker, S; Macfarlane, R. M. J. Phys. Chem. 1980, 73, 4476.

142. Drissler, F.; Graf, F.; Haarer, D. J. Chem. Phys. 1980, 72, 4996.

143. Friedrich, J. Wolfrum, H.; Haarer, D. J. Chem. Phys. 1982, 77, 2309.

144. Thijssen, H. P. H.; Van Der Berg, R.; Völker, S. Chem. Phys. Lett. 1985, 120, 503.

145. Hayes, J. M.; Small, G. J. Chem. Phys. 1978, 27, 151.

146. Small, G. J. In Spectroscopy and Excitation Dynamics of Condensed Molecular Systems; Agranovich, V. M.; Hochstrasser, R. M., Eds.; North-Holland: Amsterdam, 1983; p 515.

147. Hayes, J. M.; Stout, R. P.; Small, G. J. J. Chem. Phys. 1981, 74, 4266.

148. Jankowiak, R; Cooper, R. S.; Zamzow, D.; Small, G. J.; doskocil, G.; Jeffrey, A. M. Chem. Res. Toxicol. 1988, 1, 60-68.

149. Sanders, M. J.; Cooper, R. S.; Jankowiak, R.; Small, G. J.; Heidig, V.; Jeffrey, A. M. Anal. Chem. 1986, 58, 816-820.

150. Zamzow, D. Ph. D. Dissertation, Iowa State University, 1988.

151. Mcglade, M. J. M. S. Thesis, Iowa State University, 1983.

152. Harvey, R.; Geacintov, N. E. Acc. Chem. Res. 1988, 21, 66-73.

153. Zamzow, D.; jankowiak, R.; Cooper, R. S.; Small, G. J.; Tibbels, S. R.; Cremonesi, P.; Devanesan, P.; Rogan, E. G.; Cavalieri, E. L. Chem. Res. Toxicol. 1989, 2, 29-34.

154. Jankowiak, R.; Small, G. J. Chem. Res. Toxicol. 1991, 4, 256-269.

155. Geacitov, N. E.; Yoshida, H.; Ibanez, V.; Jacobs, S.; Harvey, R. G. Biochem. Biophys. Res. Commun. 1984, 122, 33.

156. Newman, M. S.; Tierney, B.; Veeraraghavan, S. In The Chemistry and biology of

benz[a]anthracenes; Cambridge Monographs on Cancer Research; Cambridge University Press, 1988.

157. Cheng, S. C.; Prakash, A. S.; Pigott, M. A.; Hilton, B. D.; Roman, J. M.; Lee, H.; Harvey, R. G.; Harvey, R. G.; Dipple, A. Chem. Res. Toxicol. 1988, 1, 216-221.

158. Cheng, S. C.; Prakash, A. S.; Pigott, M. A.; Hilton, B. D.; Lee, H.; Harvey, R. G.; Dipple, A. Carcinogenesis 1988, 9, 1721-1723.

159. RamaKrishna, N. V. S.; Cavalieri, E. L.; Rogan, E. G.; Dolnikowsky, G.; Cerny, R. L.; Gross, M. L.; Jeong, H.; Jankowiak, R.; Small, G. J. J. Am. Chem. Soc. 1991, submitted.

160. Martinaud, M.; Kottis, P. J. Phys. Chem. 1978, 82, 1497-1505.

161. Rogan, E. G.; Cavalieri, E. L.; Tibbels, S. R.; Cremonesi, P.; Warner, C. D.,; Nagel, D. L.; Tomer, K. B.; Cerny, R. L.; Gross, M. L. J. Am. Chem. Soc. 1988, 110, 4023-4029.

162. Cavalieri, E. L.; Devanesan, P. D.; Cremonesi, P.; Cerny, R. L.; Gross, M. L.; Bodell, W. J. Biochemistry 1990, 29, 4820-4827.

163. Hemminiki, K. Chem.-Biol. Interact. 1982, 39, 139-148.

164. Bennett, R. A.; Essignmann, J. M.; Wogan, G. N. Cancer Res. 1981, 41, 650-654.

165. Autrup, H.; Seremet, T. Chem.-Biol. Interact. 1986, 60, 217-226.

166. Tierney, B.; Martin, C. N.; Garner, R. C. Carcinogenesis 1987, 8, 1189-1192.

167. Rogan, E. G.; RamaKrishna, N. V. S.; Higginbotham, S.; Cavalieri, E. L.; Jeong, H.; Jnakowiak, R.; Small, G. J. Chem. Res. Toxical. 1990, 3, 441-444.

168. Jeffrey, A. M.; Jennette, K. W.; Blobstein, S. H.; Weinstein, I. B.; Beland, F. A.; Harvey, R. G.; Kasai, H.; Miura, I.; Nakanishi K. J. Am. Chem. Soc. 1976, 98, 5714-5715.

169. Koreeda, M.; Moore, P. D.; Wislocki, P. G.; Levin, W.; Conney, A. H.; Yagi, H.; Jerina, d. M. Science 1978, 199, 778-781.

170. RamaKrishna, N. V. S.; Gao, F.; Yedidi, P.; Cavalieri, E. L.; Rogan, E. G.; Cerny, R. L.; Gross, M. L. chem. Res. Toxicol. 1991, submitted.

171. Lu, P.; Jeong, H.; Jankowiak, R.; Small, G. J.; Kim, S. K.; Cosman, M.; Geacintov, N. E. chem. Res. Toxicol. 1990, 4, 58-69.

172. Slaga, T. J.; Gleason, G. L.; DiGivanni, J.; Sukumaran, K. B.; Harvey, R. G. Cancer Res. 1979, 39, 1934-1936.

173. Wislocki, P. G.; Gadek, K. M.; Jukiana, M. M.; MacDold, J. S.; Chou, M. W.; Yang, S. K.; Lu, A. Y. H. In Polynuclear Aromatic Hydrocarbons: Chemical Analysis and Biological Fate; Cooke, M.; Dennis, A. J., Eds.; Battelle Press: Columbus OH, 1981, pp 675-685.

174. Schmeiser, H.; Dipple, A.; Schurdak, M. E.; Randerath, E.; Randerath, K. Carcinogenesis 1988, 9, 633-638.

175. Yang, P.-F.; Randerath, K. Carcinogenesis 1990, 11, 159-164.

176. Geacintov, N. E.; Ibanez, V.; Benjamin, M. J.; Hibshoosh, H.; Harvey, R. G. In Polynuclear Aromatic Hydrocarbons: Formation, Metabolism and Measurement; Cook, M; Dennis, A. J., Eds; Battelle Press: Columbus OH, 1983, pp554-570.

177. Geacintov, N. E.; Hibshoosh, H.; Ibanez, V.; Benjamin, M. J.; Harvey, R. G. Biophys. Chem. 1984, 20, 121-133.

178. Kim, S. K.; Geacintov, N. E.; Zinger, D.; Sutherland, J. C. Photochem. Photobiol. 1989, 3, 327-337.

179. Geacintov, N. E.; Ibanez, V.; Gagliano, A. G.; Yoshida, H.; Harvey, R. G. Biochem. Biophys. Res. Commun. 1980, 92, 1335-1345.

180. Buening, M. J.; Wislocki, P. G.; Levin, W.; Yagi, H.; Thakker, D. R.; Akagi, H.; Koreeda, M.; Jerina, D. M.; Conney, A. H. Nat'l. Acad. Sci. (USA) 1978, 75, 5358-5361.

181. Wood, A. W.; Chang, R. L.; Levin, W.; Yagi, H.; Thakker, D. R.; Jerina, D. M.; Conney, A. H. Biochem. Biophys. Res. Commun. 1977, 77, 1389-1396.

182. Stevens, C. W.; Bouck, N.; Burgess, J. A. Fahl, W. E. Mutat. Res. 1985, 152, 5-14.

183. Jankowiak, R.; Lu, P.; Small, G. J.; Geacintiv, N. E. Chem. Res. Toxicol. 1990, 3, 39-46.

184. Cosman, M.; Ibanez, V.; Geacintiv, N. E. Harvey, R. G. Carcinogensis 1990, 11, 1667-1672.

185. Shahbaz, M.; Geacintov, N. E. Biochem. 1986, 25, 3290-3296.

186. Geacintov, N. E.; Cosman, M.; Mao, B.; Alfano, A.; Ibanez, V.; Harvey, R. G. 1991, submitted.

VII. ACKNOWLEDGEMENTS

I would like to dedicate this dissertation to my parents, Hang-Ha Jeong and Sun-Kyo Han, for their encouragement, love, and support. They have sacrificed throughout their life to make what I am today. Their guidance is truly responsible for this small fruit.

I would also like to express my sincere thanks and gratitude to my research advisor, Professor Gerald J. Small, for his great help, valuable discussions, and kind guidance throughout this work. This dissertation would not have been completed without his helpful advices.

I would like to thank all members of Professor Small's group for their kindness, help, and companionships. Dr. Ryszard Jankowiak deserves much credit in this work and my special appreciation. He has helped me from the first to the last moment of this work.

I also want to acknowledge and thank my collaborators, Drs. E.L. Cavalieri and E.G. Rogan (University of Nebraska, Medical Center) and Professor N.E. Geacintov (University of New York), for providing the standards, model adducts, DNA smaples, and oligonucleotide samples.

Turning to my family, I owe my biggest appreciation and thank to my grandmother who deceased during this study. My only sister, Hyun-Ju, should receive a valuable credit of this work. Memory of her help and assistance will not be erased from my heart forever. Two invaluable persons, my mother- and father-in-law, Byung-Jung

and Kum-Whan Kim deserve special appreciation for their belief and encouragement.

Above all, I am also greatly indebted to my wife, Jihyang Kim, for her endless love, pacience, encouragement, and hard sacrifice for the past several years. To my son, Hyung-Min, I owe many hours which must be shared with him but consumed for this work.

To all people I have met and/or shared times for the past years, I should also express my thanks from the bottom of my heart. Thanks!